University of Stavanger

FACULTY OF SCIENCE AND TECHNOLOGY

MASTER'S THESIS

Study program/specialization: Petroleum Engineering/ Drilling Engineering	Spring semester, 2009 Open / ~~Confidential~~
Author: Nnaemeka, Uwaezuoke	…… (signature author)
Instructor: Merete V. Madland Supervisor(s): Edvard, Omdal Megawati, Megawati	
Title of Master's Thesis: CREEP BEHAVIOR AND LOADING RATE DEPENDENCY OF CHALKS	
ECTS: 30	
Subject headings: Creep Load rate Deformation	Pages: + attachments/other:139 Stavanger, June/2009 Date/year

Abstract:

‘‘Mechanically high porosity chalks behave as frictional materials, but with an end-cap reflecting pore collapse failure, and the mechanical properties of chalk are strongly dependent on the type of fluid in the pores’’ [Risnes, R. (2000)]. Any applied axial load would lead to a deformation of the sediments by the depletion of the pore fluids. This results in compaction which is a process in which the compressive strength of the rock is exceeded and plastic deformation occurs, resulting in irreversible reduction of porosity. Compaction is a natural consequence of pore pressure depletion. However, it has been observed that there exists another kind of deformation that takes place when the state of stress in the rock skeleton is kept constant. This is known as creep and it is a time-dependent deformation which may cause a delay in deformation response under varying load conditions.

In a producing field, creep is a result of interruption of loading. In other words, when production is interrupted in a field, strains continue to occur [creep], but this strain depends on the rate of production of the reservoir fluids. When a reservoir is taken into production, the rate of change of the effective stress exerted on the reservoir rock is suddenly increased from that imposed by the burial process over a geologic time span, to that induced by the depletion-pressure history. This change in loading rate will have a large influence on the in-situ compaction behavior if the rate effects observed at laboratory loading rates also occur at geological and depletional loading rates [de Waal, J. A., Smits, R. M. M. (1988)]. In carbonates [chalk], creep is common and how the rate of loading affects creep and creep rate is then investigated. The tests for creep in this thesis are performed under drained conditions [constant pore pressure].

Core samples were taken to overburden, confining and pore pressures. The pore pressure was then depleted from the initial state to a certain value. This reduction results in an increase in the effective stresses, which then activates a certain behavior of the chalk grains. It is believed that the behavior of the grains is affected by the rate at which the stress is increased. Hence, samples are loaded both rapidly and slowly and deformation and other parameters are thereafter compared. Intermediate loading rate between the rapid and slow loading rates is also included to investigate the behavior towards the two extremes.

A reduction from 30 MPa to 5 MPa pore pressure in 100 minutes [0.25 MPa/min] was termed rapid loading. The same pressure was depleted for about 8333 minutes [0.003 MPa/min] and

regarded as a slow loading. At the lower limit of 5 MPa, the samples were left to deform under constant stress for some time. This is known as time-dependent deformation or creep.

It was observed that when loaded rapidly, the deformation accumulated at the creep stage is more [mainly at the transient creep phase] compared to when loaded slowly.

Generally, the result of the experiments in this thesis shows that other parameters such as uniaxial compaction modulus both in the elastic and plastic regions, yield stress, creep strain and creep rate, stress path etc are all loading rate dependent. Also included are porosity versus mean effective stress [pore pressure] charts, and axial differential stress versus mean effective stress chart.

Table of Contents:

Acknowledgements:

I sincerely thank the professor in charge of rock mechanics who is also responsible for the master's thesis in the rock mechanics laboratory in the University of Stavanger, Norway, Professor Merete V. Madland for giving me the opportunity to carry out the thesis. Without her approval, it would not have been possible to realize the ambition. It is an honor to have studied under your supervision.

My thanks also goes to my supervisor who is a Ph.D student, Edvard Omdal who guided me throughout the period from designing the test, setting up the laboratory equipment, providing me with literatures and ultimately exhibiting some tolerance in providing answers to my questions even the simplest ones. I extend the same gratitude to Megawati Megawati, also for her kind advice on how to carry on and providing answers to my questions with papers etc.

I also thank Reidar Korsnes, Kim Vorland, Bizhan Zangiabadi, Tania Hildebrand-Habel and the other entire bachelor's students who made the laboratory a pleasant place to stay. And finally to all the 2007-2009 set master's degree students who shared information and knowledge that made all of us better individuals, and to the department of petroleum engineering, University of Stavanger, Norway, on whose name we are going to represent as experts as we face the challenges that lie ahead.

Chapter 1: Introduction

1.1 Objective of Study

To investigate the effects of load rate on the creep behavior of chalks [Stevns Klint], core samples are loaded both rapidly and slowly and allowed to creep. The strains and creep rates are compared at the creep stage; also parameters such as uniaxial compaction modulus, yield stresses and stress paths during loading are determined and compared and then check if the loading rate is the determining factor.

1.2 Background and Scope

Pure chalks are mainly built up of whole and fragmentary parts of calcite skeletons produced by planktonic algae. The building blocks of the skeletons are calcite tablets or platelets of typical dimension 1 $\mu m.$. These calcite grains are arranged in rings or rosettes known as coccoliths, typically of the order of 10 μm in diameter. Pure high porosity chalks consists of a mixture of intact coccoliths rings and greater and smaller fragments. This gives the chalk material a rather open structure, where the dimensions of the pore space may be considerably greater than the dimensions of the individual grains [Risnes, R. (2001)]. The mechanical properties of rocks [chalk] are functions of effective stresses as far as the following conditions are met [Handin *et al.* (1963)],

- *pore spaces are connected such that pore pressure is transmitted throughout the solid phase of the sample*
- *pore fluid is inert in relation to the mineral constituents of the sample and*
- *permeability is enough for free flow of fluid in and out during deformation so that pore pressure gradient remains constant and uniform.*

During withdrawal of fluids from hydrocarbon reservoirs, a considerable drop in the reservoir pore pressure occurs. The weight of the overlying layers [overburden] is carried partly by the reservoir fluid and partly by the rock skeleton. As the pore pressure decreases, an increasing part of the constant weight of the overlying layers has to be carried by the reservoir skeleton. This resultant increased load leads to compaction until a new equilibrium is reached. This strain that acts vertically in the direction of the maximum principal stress is called the axial *strain.* It causes a reduction in porosity. However, though one might think that there would be an associated decrease in permeability due to the closing of channels in the rock and

compaction; if the initial permeability of the rock is very low [chalk], there might be a permeability increase due to the breaking of barriers due to dilatancy behavior between pores [Thomas Lindsay Blanton III (1981)]. The effect of compaction on permeability is still a subject of study due to the presence of both matrix and fracture [crack] permeabilities. However, a considerable compaction of the reservoir can be expected when one or more of the following conditions prevail [Geertsma, J. (1973)];

- *production from large vertical interval*
- *significant reduction in reservoir pressure during the production period*
- *oil or gas, or both are contained in loose or weakly cemented rock*

Surface subsidence as a result of reservoir compaction causes technical and financial problems, as well as damage to casing, tubing and liners at reservoir level. Also, there is porosity reduction which results in permeability changes [Jones, M. E., Leddra, M. J. (1989)]. However, rock compaction can act as a very effective production mechanism [compaction drive]. A model has been used to predict the compaction of sandstone reservoirs [de Waal, J. A. (1986)], but applying the model to chalk formations has proven to be more complex [de Waal, J. A. *et al.* (1988)].

One method to determine the compaction potential is to utilize laboratory testing. By simulating conditions similar to field behavior, the response of the samples is measured. Obviously, laboratory conditions might differ from field conditions in several ways, for instance, the testing time might last for shorter time duration than the actual exposure time in the field. Also, testing equipment, assumptions and lack of knowledge of the field conditions are other possible sources of discrepancy between the field and the laboratory. But particularly, if lack of knowledge of the field is the issue, the conditions are based on assumptions or theoretical models.

The focus of this thesis is on the basic assumptions related to rock mechanical testing. In most large hydrocarbon reservoirs, there is generally considered to be present a stress regime where compactional deformation occurs under conditions of no lateral strain, i.e. the reservoir will only experience vertical strain, usually referred to as *uniaxial strain.*

Stevns Klint is a high porosity, pure outcrop chalk. Its porosity is usually above 40%, with range of values from 40 to 45 percent and an arithmetic average of about 42.71% used for the experiment. The experiment involves tests in which different loading rates are applied under the same stress conditions. Both confining and pore pressures are built up simultaneously from 1.2 MPa and 0.2 MPa respectively to the desired levels with a margin of 1MPa at confining pressure of 31MPa and pore pressure of 30MPa. The confining pressure represents

the lateral stresses (x and y directions) in a reservoir, but since the test is uniaxial, the stresses in the lateral directions are considered equal due to cylindrical cores in an hydraulic confining chamber, with only axial deformation and no [negligible] lateral deformation. That is a proper representation of the stresses acting in a reservoir since in a uniaxial test the lateral deformation is assumed to be constant. The overburden pressure of 32 MPa is provided by a piston running down from the top of the uniaxial compression test cell plus an additional effect of the confining fluid taken care of by relevant friction and area factors.

Chapter 2: Theory

The experiments were conducted with Stevns Klint chalk, which is an outcrop chalk. Outcrop [a] is a geological term referring to the appearance of bedrock or superficial deposits exposed at the surface of the Earth. In most places the bedrock or superficial deposits are covered by a mantle of soil and vegetation and cannot be seen or examined closely. However in places where the overlying cover is removed through erosion, the rock may be exposed, or *crop out*. Such exposure will happen most frequently in areas where erosion is rapid and exceeds the weathering rate such as on steep hillsides, river banks, or tectonically active areas. Bedrock and superficial deposits may also be exposed at the earth's surface due to human excavations such as quarrying and building of transport routes.

Outcrops allow direct observation and sampling of the bedrock in situ for geologic analysis and creating geologic maps. In situ measurements are critical for proper analysis of geological history and outcrops are therefore extremely important for understanding earth history. Some of the types of information that can only be obtained from bedrock outcrops, or through precise drilling and coring operations, are; structural geology features orientations (e.g. bedding planes, fold axes, foliation), depositional features orientations (e.g. paleo-current directions, grading, facies changes), paleomagnetic orientations. Outcrops are also critically important for understanding fossil assemblages, paleo-environment, and evolution as they provide a record of relative changes within geologic strata. Outcrop chalks have similar reservoir properties with reservoir chalks in terms of porosity, carbonate content and permeability. Over a long time, exposed parts of an outcrop chalk are usually chemically altered by interaction with meteoric water. Also, mineralogically, offshore chalks are more homogeneous than outcrop chalk [Hjuler, M. L. (2006)].

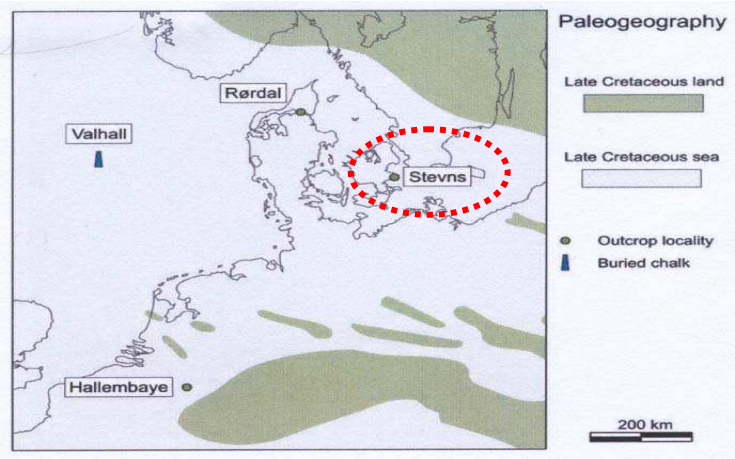

Fig.3.1 Location of Stevns Klint [after Hjuler, M. L. (2006)]

2.1 History of carbonates and chalk

2.1.1 Carbonates

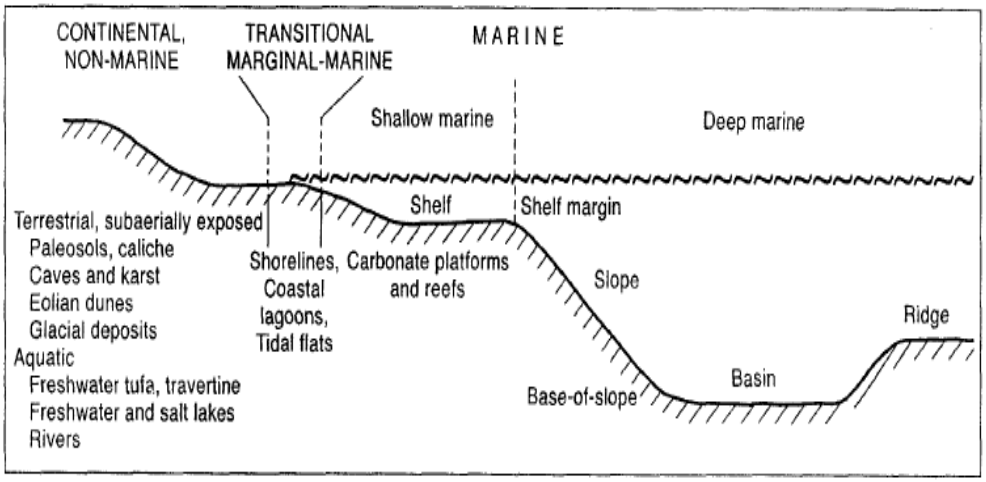

Fig.2.1 Settings of carbonate depositional environments [Erik Flugel, (2004)]

Carbonate reservoirs are principally composed of carbonate minerals, which include calcite ($CaCO_3$), dolomite (Ca, MgCO3), ankerite (Ca, Mg, FeCO3), and siderite ($FeCO_3$). Carbonate reservoirs can be sub-divided into chalk and limestone. Chalk reservoirs are composed of small spherical/plate-like particles (coccoliths) of calcium carbonate from the skeletons of marine organisms, which became compacted and cemented to form rock with a higher primary porosity. Limestone is generally formed by the deposition of fine carbonate mud with associated fragments of biogenetic material (shells, etc) which is compacted to form rock [Tucker, M.E., Leeder, M.R.]. Such a limestone reservoir would generally have a low primary porosity but a high secondary porosity owing to the dissolution of some of the rock caused by reaction of pore fluids during burial.

Carbonates originate as skeletal grains within the depositional environment while clastic sediments are formed primarily by the disintegration of parent rocks and are transported to the depositional environment. Hence, carbonates could be said to be 'born'. They originate both on land and in the sea and are formed in three major settings: on the continents, the transitional area between land and sea, and the shallow and deep sea, Fig. 2.1. Deposition of the calcite plankton in the deep sea is responsible for 90% of modern carbonate production, whereas the remaining 10% take place in the shallow seas.

The basic unit of carbonates is $(CO_3)^{2-}$, whereas the carbonate minerals are calcium trioxocarbonate (IV) or calcite (C_aCO_3), aragonite and dolomite (C_aM_g $(CO_3)_2$). Carbonate

sediments (chalk, limestone) constitute mainly of calcite, with some silica and clay minerals and cementation is mainly by precipitation of carbonate minerals.

Considering the flow of fluid in carbonate reservoirs as compared to flow in sandstone reservoirs, this generally occur as a result of fluid flow through fractures (both natural and induced), with the aim of production enhancement. This is accomplished by flow first through interconnected pores (effective porosity), and then through fracture paths to the well bore. During sediment deposition, the pores are poorly connected within carbonate reservoirs, hence has lower permeability compared to sandstone reservoirs [Seright, R.S *et al.* (1998)].

2.1.2 Chalk

Chalk particles originate as skeletons of algae that are called coccospheres, with a typical size of 30 micrometer. However, lithostatic stresses results in the crushing of these coccospheres to sizes of about (1-10) micrometer, and matrix permeabilities in micro- and milliDarcy range. Natural fracture leads to high reservoir scale permeabilities in 100 milliDarcy range.

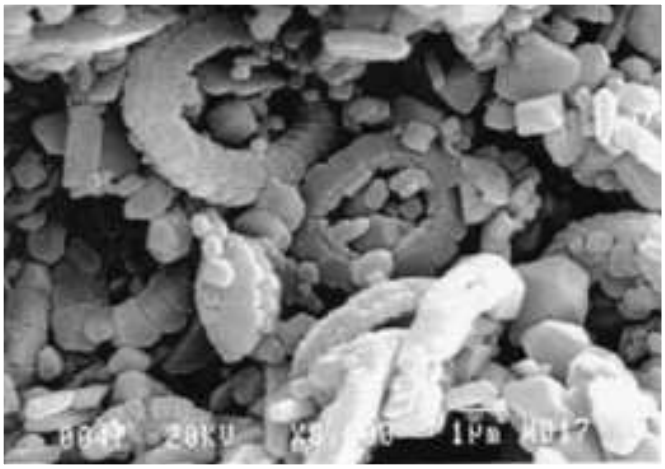

Fig.2.2a SEM image of Liege outcrop chalk [source Petroleum related rock mechanics, 2nd edition 2008]

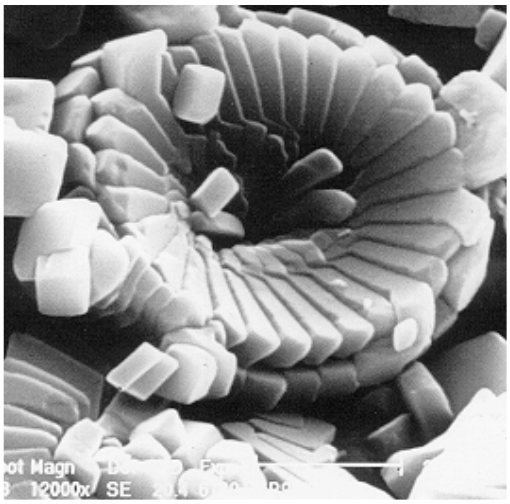

Fig.2.2b A SEM photograph of a coccoliths [Chalk facts by Harris C. S. (after singleton birch)]

Chalk reservoirs are characterized by abnormally high pore pressures, helping to maintain very high porosity. This is because cementation process which requires increased pressures or some throughput of pore water is halted. The main solid mineral in chalk is calcite with a density of 2.71 g/cm^3. Generally, chalk reservoirs are finer grained, more porous, less permeable, more uniform and widespread, and considerably more predictable in terms of petro-physical properties than reservoirs in typical shallow-water limestone.

In the North Sea, chalks are found at depths of 2500-3500 m and with 15-50 % porosity because of overpressure [low effective stress]. They have biological origins and are formed from the fossilized remains of planktonic algae. The main mineral component is calcite with small amounts of silica and clays. These fossilized algae are arranged in disk-shaped coccoliths, and the coccoliths are made up of many platelets. By weak cementing of the coccoliths, larger spherical structures are formed and are called coccospheres [Risnes, R. *et al.* (2008), Holt, R. M. (2003)]. These coccoliths and coccospheres contain large fraction of void spaces. Though the average porosity of North Sea chalks is quite high, the pore throats between the individual pores are small, typically in the range of 1-5μm, hence the permeability is low. They are of the Maastrichtian stage, named after Maastricht in SE Holland. An example is the Stevns Klint chalk with porosity of 40 to 45 %, see Table 4.1.1.

2.2 Permeability

The ability, or measurement of a rock's ability, to transmit fluids, typically measured in Darcies or millidarcies. Formations that transmit fluids readily, such as sandstones, are described as permeable and tend to have many large, well-connected pores. Impermeable formations, such as shales and siltstones, tend to be finer grained or of a mixed grain size, with smaller, fewer, or less interconnected pores. Absolute permeability is the measurement of the permeability conducted when a single fluid, or phase, is present in the rock. Effective permeability is the ability to preferentially flow or transmit a particular fluid through a rock when other immiscible fluids are present in the reservoir (for example, effective permeability of gas in a gas-water reservoir). The relative saturations of the fluids as well as the nature of the reservoir affect the effective permeability. Relative permeability is the ratio of effective permeability of a particular fluid at a particular saturation to absolute permeability of that fluid at total saturation. If a single fluid is present in a rock, its relative permeability is 1.0. Calculation of relative permeability allows for comparison of the different abilities of fluids to flow in the presence of each other, since the presence of more than one fluid generally inhibits flow.

Permeability, k, of one Darcy is defined as the permeability which gives a flowrate of one centimetre per second of a fluid with viscosity one centipoise for a pressure gradient of one atmosphere per cm, i.e.

$$k = \frac{\mu q \Delta L}{\Delta P A} \qquad \text{[Eq.2.1]}$$

where:

k -permeability [D]

q -volumetric flow rate [cm^3/s]

μ -viscosity [cP]

ΔL -length of core [cm]

A -cross-sectional area [cm^2]

ΔP -pressure drop [atm]

Permeability of chalk could be defined in terms of matrix or fracture permeability. For instance, in Ekofisk field that is a naturally-fractured chalk reservoir that has been producing hydrocarbons for over 20 years in the Norwegian sector of the North Sea, it has been suggested that shear failure process may account for the continued good producibility in spite of compaction. Ekofisk chalk which is a soft, finely textured, somewhat friable, highly porous

limestone is a high-porosity (up to 50%, much of it above 35%), low-permeability (1- to 10-md) rock that is pervasively fractured [Johnson, J. P. *et al.* (1989)]. The fractures typically are steeply dipping and show a variety of trends across the reservoir. Production data indicate that the fractures more than the matrix permeability are responsible for the high fluid production rates.

2.3 Porosity

The percentage of pore volume or void space, or that volume within the rock that can contain fluids. Hence,

$$\phi = \frac{V_p}{V_b} \qquad \text{[Eq.2.2]}$$

where:

V_p -pore volume

V_b -bulk volume

ϕ -porosity

Porosity can be a relic of deposition (primary porosity, such as space between grains that were not compacted together completely) or can develop through alteration of the rock (secondary porosity, such as when feldspar grains or fossils are preferentially dissolved from sandstones). Effective porosity is due to the interconnected pore volume in a rock that contributes to fluid flow in a reservoir. It excludes isolated pores (ineffective porosity). Total porosity is the total void space in the rock whether or not it contributes to fluid flow. Thus, effective porosity is typically less than total porosity. In this thesis, effective porosities are used and are calculated by using the pore volume of the interconnected pores and are given as:

$$V_p = \frac{W_w - W_d}{\rho_w} \qquad \text{[Eq.2.3]}$$

where:

W_w -saturated weight [with water]

W_d -dry weight

ρ_w -saturating fluid density [water]

2.4 Elasticity

2.4.1 Stress

Consider a weight resting on top of a pillar which itself is supported by the ground in Fig. 2.3. A vertical force due to the weight acts on the pillar, while the pillar reacts with an equal and opposite force. At sections (a), (b) and (c), the cross-sectional areas are (A1), (A2) and (A3) respectively. If the force acting through the cross-section at (a) is denoted as F, then the stress σ at the cross-section is defined as:

$$\sigma = \frac{F}{A1} \qquad \text{[Eq.2.4]}$$

The SI unit for stress is Pa (= Pascal = N/m^2). In rock mechanics, compressive stresses are positive.

Consider the cross-section at (b), A2 < A1, with a force acting through this section equal to the force acting through the section at (a), the weight of the pillar neglected. Hence, the stress $\sigma = F/A2$ at (b) is larger than the stress at (a), i.e. the stress depends on the position within the stressed sample.

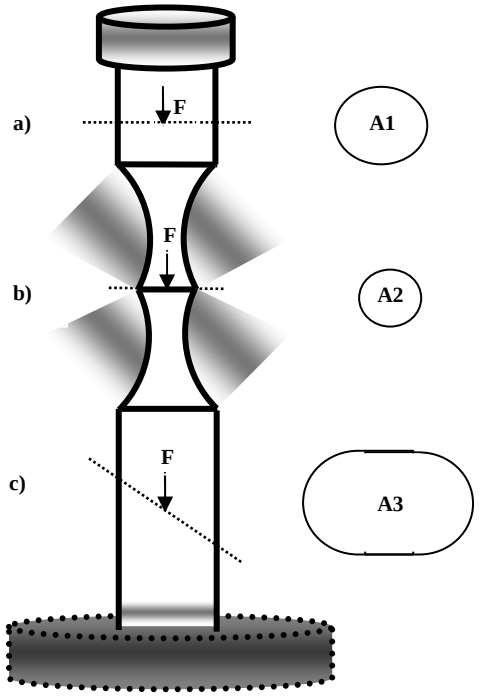

Fig.2.3 Illustration of forces and stress

If section (a) is divided into infinite number of subsections with infinitely small parts of F acting, and using a subsection i which contains a point P, then the stress at the point P is given as:

$$\sigma = \lim_{\Delta A_i \to 0} \frac{\Delta F_i}{\Delta A1_i} \qquad \text{[Eq.2.5]}$$

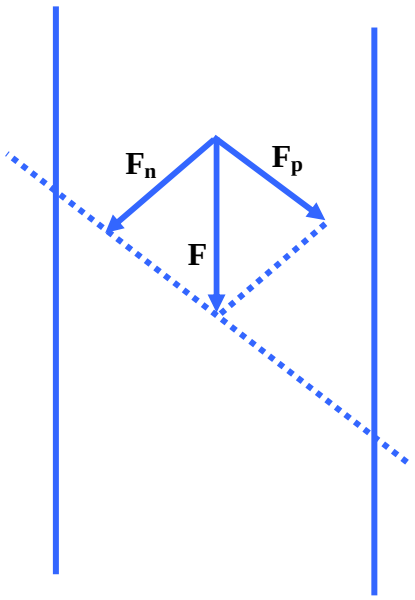

Fig.2.4 Decomposition of forces

At section (c), the force in the cross-section is decomposed into normal (F_n) and parallel (F_p) components as shown in Fig. 2.4. Subsequently, the stresses $\sigma = F_n / A3$ and $\tau = F_p / A3$ are called the normal and shear stresses respectively.

2.4.2 Strain

Consider a sample with a particle of initial position (x_i, y_i, z_i). With the application of an external force, the position of the particle is shifted by u, v and w in the x, y and z directions respectively to (x_f, y_f, z_f) as shown in Fig. 2.5.

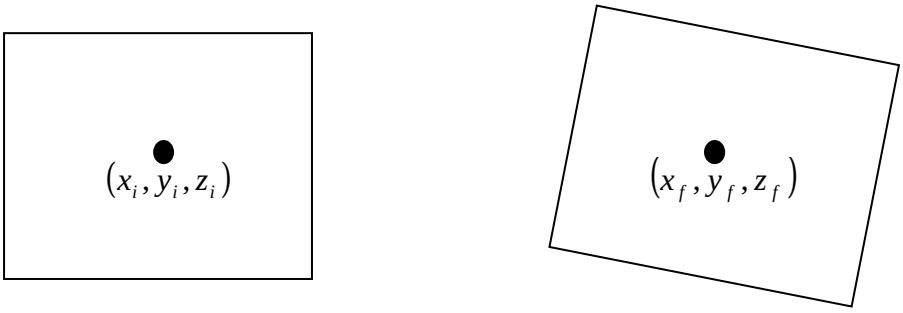

Fig.2.5 Sample deformation

Conventionally, the displacements u, v and w are positive when directed in the negative direction of the axes. Hence,

$u = x_i - x_f$

$v = y_i - y_f$ and

$w = z_i - z_f$

If the relative positions of the particles are changed, so that the new positions cannot be obtained simply by a rigid translation and/or rotation of the sample, the sample is said to be strained (Fig. 2.6). The displacements relative to the positions A and B are not equal. Elongation corresponding to point A in the direction AB is then defined as:

$$\varepsilon = \frac{L_1 - L_2}{L_1} = -\frac{\Delta L}{L} \qquad \text{[Eq.2.6]}$$

By convention, elongation is positive for contraction.

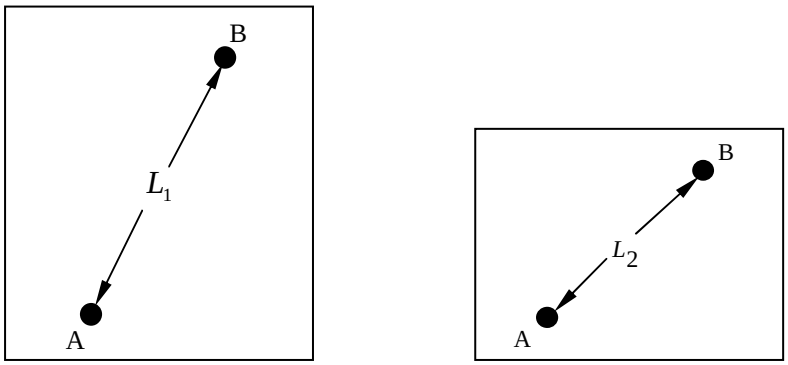

Fig.2.6 Deformation

2.4.3 Elastic Moduli

Though most rocks behave nonlinearly when subjected to large stresses, they also exhibit linear relations under small changes of stress. If a force F is applied to a sample of length L_1 and area $A = D_1^2$ as shown in Fig. 2.7, the length is reduced to L_2 .

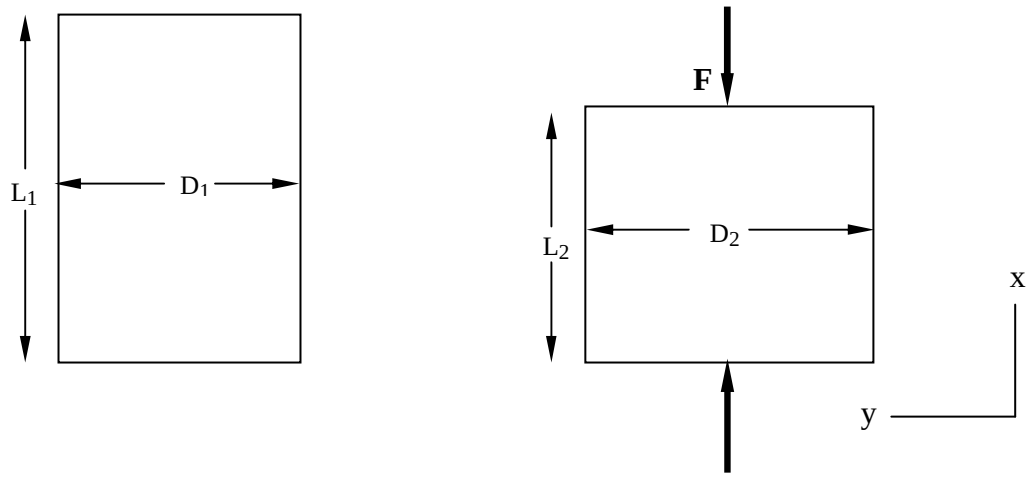

Fig.2.7 Deformation induced by uniaxial stress

The applied stress is given by:

$$\sigma_x = \frac{F}{A} \qquad \text{[Eq.2.7]}$$

and the elongation given as:

$$\varepsilon_x = \frac{L_1 - L_2}{L_1} \qquad \text{[Eq.2.8]}$$

If the sample behaves linearly, the linear relation between σ_x and ε_x is then:

$$\varepsilon_x = \frac{1}{E}\sigma_x \qquad \text{[Eq.2.9]}$$

Equation [2.9] is Hooke's law and the coefficient E is Young's modulus or E-modulus and it is the measure of the resistance of the sample to compression due to uniaxial stress. The lateral elongation is:

$$\varepsilon_y = \varepsilon_z = \frac{D_1 - D_2}{D_1} \qquad \text{[Eq.2.10]}$$

Since $D_2 > D_1$, ε_y and ε_z are negative. Also,

$$\nu = -\frac{\varepsilon_y}{\varepsilon_x} \qquad \text{[Eq.2.11]}$$

The elastic parameter ν is known as Poisson's ratio, and it is a measure of the lateral expansion relative to the longitudinal contraction.

2.4.4 Yield

There is always a constant linear relationship between the applied stress and the resulting strain regardless of their magnitudes, for a linear elastic material. The E-modulus is the slope of the curve. Conversely, any material not obeying a linear stress-strain relation is a nonlinear elastic material, and the linear stress-strain relation may be written as:

$$\sigma = E_1\varepsilon + E_2\varepsilon^2 + E_3\varepsilon^3 + ... \qquad \text{[Eq.2.12]}$$

In rocks, the stress-strain relation shown in Fig.2.8a in commonly observed, where the unloading path is different from the loading path. The reaction of the system to changes is dependent upon its past reactions to change (hysteresis). For such materials, the work done during loading is not entirely released during unloading as a part of the strain energy dissipates in the material. The E-moduli during unloading are called unloading moduli.

(a) (b)

Fig.2.8 (a) Elastic material, with hysteresis (b) Material suffering permanent deformation

If the strain vanishes when the stress returns to zero, the material is said to be elastic. But, if the strain does not vanish, the material has suffered a permanent deformation during loading/unloading cycle. Many rocks enter a phase where permanent deformation occurs and are still able to resist loading. They are said to be ductile. The point of transition from elastic to ductile behavior is called yield point.

2.5 Effective stress theory

When a material experiences stress, it compresses or elongates depending on the orientation of the applied forces, until a point of failure. In a porous and permeable material like a reservoir (chalk), a relationship is used to express the effects of stresses in the skeleton and pore fluids. Terzaghi (1923) expresses that the total overburden stress on a rock sample is shared by the rock matrix and the pore fluids, hence

$$\sigma_T = \sigma' + P_p \qquad \text{[Eq.2.13]}$$

This is also known as the effective stress concept since,

$$\sigma' = \sigma_T - P_p \qquad \text{[Eq.2.14]}$$

The equation was modified to take care of the interaction between the rock matrix and the pore fluid by introducing effective stress constant α, hence

$$\sigma_T = \sigma' + \alpha P_p \qquad \text{[Eq.2.15]}$$

For high porosity, permeable chalk, the parameter α, also known as Biot factor is approximately equal to 1. This factor is defined as a measure of the change in pore volume relative to the change in bulk volume at constant pore pressure. Generally, $0 < \alpha < 1$. Deformations are determined by the value of the effective stress. If the pore pressure is high, the effective stress is low which implies low deformation, and at low pore pressures, deformation is high. If pore pressure is increased, the material will expand and the individual grains would compress to counteract the volume expansion, hence

$$\alpha = \left(1 - \frac{c_m}{c_b}\right) \qquad \text{[Eq.2.16]}$$

But,

$$c_m = \frac{1}{K_m} \text{ and } c_b = \frac{1}{K_b} \qquad \text{[Eq.2.17]}$$

Hence,

$$\alpha = \left(1 - \frac{K_b}{K_m}\right) \qquad \text{[Eq.2.18a]}$$

For chalk, $c_m << c_b$ and $K_b << K_m$ (1 GPa and 76 GPa respectively), thus $\alpha \cong 1$. The drained [framework] bulk modulus, K_b, is obtained from a drained *hydrostatic test*, in which the pore pressure is kept constant and the sample is loaded with an external isotropic stress. The stress strain curve might not be linear but shows an increasing stiffness with increasing stress. This is as a result of closing coring-induced cracks at low stresses. The bulk modulus is then

determined as the slope of the stress-strain curve at high stress where the curve approaches linearity. Hence;

$$\varepsilon_{vol} = \frac{\Delta V}{V} = \frac{\Delta \sigma}{K_b} \qquad \text{[Eq.2.18b]}$$

The volumetric deformation of the sample is given by the bulk modulus, K_m, of the sample and is obtained from unjacketed hydrostatic test. It is a case where the sample is placed inside a pressure cell with no sleeve on, so that the confining fluid penetrates the sample and the external stress is equal to the pore pressure. Thus;

$$\varepsilon_{vol} = \frac{\Delta V}{V} = \frac{\Delta \sigma}{K_m} \qquad \text{[Eq.2.18c]}$$

The application of this overburden stress in a rock results in axial strain, and under the assumption that there is no lateral strain, the test is a uniaxial strain test.

If the material returns to its original form after the application of load, the material is said to behave elastic. Conversely, if the applied load leaves a permanent deformation on the material, it exhibits a plastic behavior. The onset of plasticity is often preceded by elasticity in chalks. For these tests, the mechanical properties of chalk are isotropic; hence Hooke's law is used to express the relationship between stress and strain in terms of the principal stresses and strains. It should be observed that the stresses used are the effective stresses [changes]. Thus,

$$\left.\begin{aligned} E\varepsilon_1 &= \Delta\sigma_1^{'} - \nu\left(\Delta\sigma_2^{'} + \Delta\sigma_3^{'}\right) \\ E\varepsilon_2 &= \Delta\sigma_2^{'} - \nu\left(\Delta\sigma_1^{'} + \Delta\sigma_3^{'}\right) \\ E\varepsilon_3 &= \Delta\sigma_3^{'} - \nu\left(\Delta\sigma_1^{'} + \Delta\sigma_2^{'}\right) \end{aligned}\right\} \qquad \text{[Eq.2.19]}$$

where:

$E =$ Young's modulus of elasticity [N/m^2]

$\varepsilon_1 =$ axial strain

$\varepsilon_2 = \varepsilon_3 =$ lateral strains

$\sigma_1^{'} =$ axial effective stress [N/m^2]

$\sigma_2^{'} = \sigma_3^{'} =$ lateral effective stresses [N/m^2]

$\nu =$ Poisson's ratio [dimensionless]

2.6 Failure Mechanics

The stress level at which a rock typically fails is commonly called the strength of the rock. *Uniaxia*l and *triaxial* tests are used to measure the strength of rock. In a uniaxial test [unconfined compression test], the confining pressure is zero, while in triaxial test, a non-zero confining pressure is used. In a uniaxial test, if the applied axial stress is plotted as a function of the axial strain as shown in Fig.2.9, several concepts could be defined:

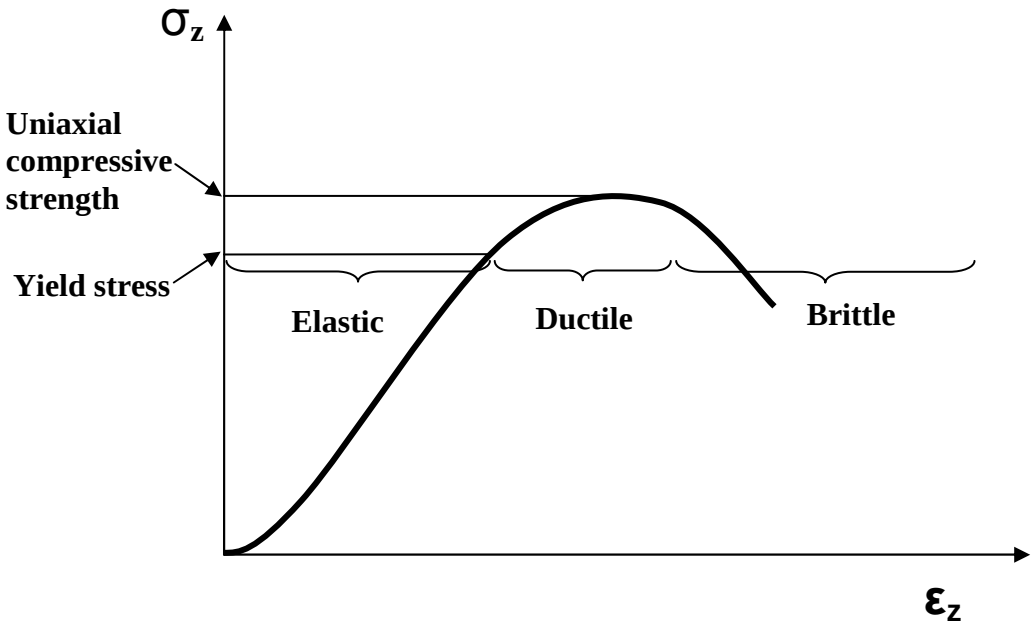

Fig.2.9 Stress versus deformation in a uniaxial compression test

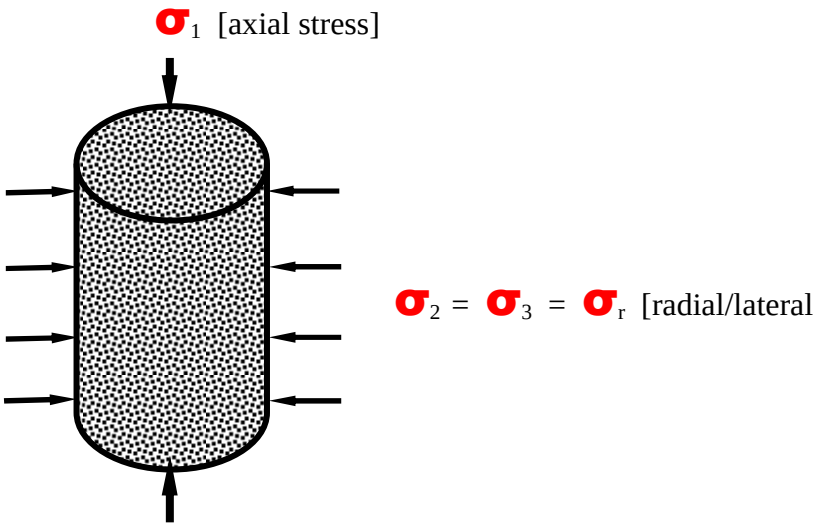

Fig.2.10 Typical core sample. In the thesis, the average length of cores used is 79.26 mm while the diameter is 38.13 mm.

Elastic region: elastic deformation. The specimen returns to its original state after the stress is released.

Yield point: permanent changes occur beyond this point. The specimen never returns to its original state when stress is removed.

Ductile region: in this region, the specimen undergoes permanent deformation without loss of the ability to support load.

Brittle region: in this region, the ability of the specimen to withstand stress decreases rapidly with increase in deformation.

2.6.1 Pore Collapse

A material subjected to stress will fail when a certain level of stress is reached. The failure mode depends on the type of material, the state of stress and the geometry of the specimen. Shear failure occurs when the shear stress along some plane in the sample is sufficiently high. Various models are used to describe the level of stress at which a material will experience failure.

In high porosity materials such as Stevns Klint chalk where the grain skeleton forms a relatively open structure, pore collapse is a failure mode that is normally observed, and it may lead to significant reduction of pore space. The $q - p'$ plot with an 'endcap' is often used to describe such materials. Failure occurs as either dilation or pore collapse for certain stress states that come in contact with the combined criterion. But when points do not come in contact with the failure line (within the envelope), the materials stress state is within the elastic region, and the material should not experience failure, Fig.2.11.

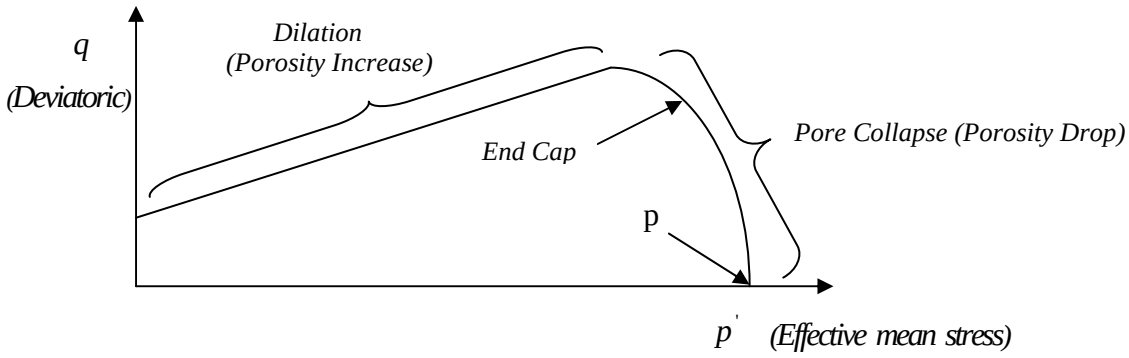

Fig.2.11 $q - p'$ plot with an end cap

$q = \left(\sigma_1^{'} - \sigma_3^{'}\right)$ is the effective differential (deviatoric) stress acting on the material, while $p^{'} = \left(\sigma_1^{'} + \sigma_2^{'} + \sigma_3^{'}\right)/3$ is the effective mean stress. When the effective stresses are equal, the material is said to be loaded hydrostatically; and up to a point p on the endcap the material yields hydrostatically.

2.7 Consolidation and Creep

Consolidation describes a transient process. It is due to pore pressure gradients induced by a change in the stress state, and the fact that it takes time to re-establish pore pressure equilibrium. Porous sediments and sedimentary rocks are two-phase systems, consisting of a skeleton of mineral grains and pore spaces filled with water, air, brine, hydrocarbons or some combination of these fluids. The load of overlying sediments (overburden) in a reservoir results in a stress that is shared between the rock matrix and the pore fluids. Thus, there exists an effective stress that acts on the rock matrix and a corresponding pore fluid pressure that acts in the pores, eqn. 2.13. Hence, an increase in stress of the rock matrix (effective stress) would occur if the total stress is increased. For a porous and permeable material, with constant total stress (overburden) acting on it, an increase in effective stress is experienced when the pore pressure is depleted. If, however, drainage of pore fluid is prevented, the pore volume of the sediment can decrease only if the pore fluid compresses in the pore space. Pore fluid pressure therefore determines the magnitude of effective stresses acting within sediment, and the resultant strain is termed ‘primary consolidation’.

Creep [Risnes, R. *et al* (2008); Johnson, J. P. (1989)] is a time-dependent deformation that originates from viscoelastic effects in the solid framework. The actual creep behavior of a rock depends on the magnitude of the applied stress. For low or moderate stresses, the material may virtually stabilize after a period of transient creep, while for high stresses; the material may rapidly run through all the three stages of creep and finally fail. Visco-elasticity [a] is a property of materials that exhibit both viscous and elastic characteristics when undergoing deformation. Viscous materials resist shear flow and strain linearly with time when a stress is applied. Elastic materials strain instantaneously when stretched and just as quickly return to their original state once the stress is removed. Viscoelastic materials have elements of both of these properties and, as such, exhibit time dependent strain. Whereas elasticity is usually the result of bond stretching along crystallographic planes in an ordered

solid, viscoelasticity is the result of the diffusion of atoms or molecules inside of an amorphous material [wikipedia definitions]

2.7.1 Pore pressure

This is the pressure of fluids within the pores of a reservoir. As stated in section 2.5, pore fluids help carry part of the total stress applied to a rock system. Both strain and failure of rock is controlled by effective rather than total stresses. Knowledge of pore pressure is essential in pore pressure prediction, wellbore stability during drilling, sand production control during production, reservoir stimulation, reservoir compaction and subsidence studies, well location and trajectory, and in fractured reservoir studies.

Pore pressure develops in a reservoir during sediment burial. If the rate of compaction is the same as the rate of fluid escape and migration to the surface, the change in pressure per unit of depth is equivalent to the hydrostatic pressure, and a normal pore pressure gradient is maintained, given by:

$$P_{fn} = \int_0^D \rho_f(z) g dz \qquad \text{[Eq.2.20]}$$

where:

P_{fn} - normal pore pressure

D - depth of interest

$\rho_f(z)$ - varying pore fluid density at depth z (pointing vertically downwards)

g - acceleration due to gravity

In a situation where the pore fluid has a pressure higher than the expected normal pressure, the zone is said to have abnormal pressure or over-pressured. Overpressure is a consequence of [Osborne, M. J., Swarbrick, R. E. (1997), Yassir, N., Addis, M. A. (2002)];

- *the rate of fluid expulsion and migration being slower than the rate of sedimentation and compaction (disequilibrium compaction, undercompaction)*
- *tectonic loading leading to undrained shear stress in association with pore pressure development.*
- *thermal and chemical processes leading to pore fluid generation or expansion.*

When the pore pressure is less than the normal or hydrostatic pressure, the zone is said to be underpressured. Underpressure, or a zone of underpressure, is common in areas or formations that have had hydrocarbon production. A typical example of pore pressure gradient curve is

shown using the Valhall field in Fig.2.12. It is a chalk reservoir (Cretaceous) in the Ekofisk area of the Norwegian sector of the North Sea.

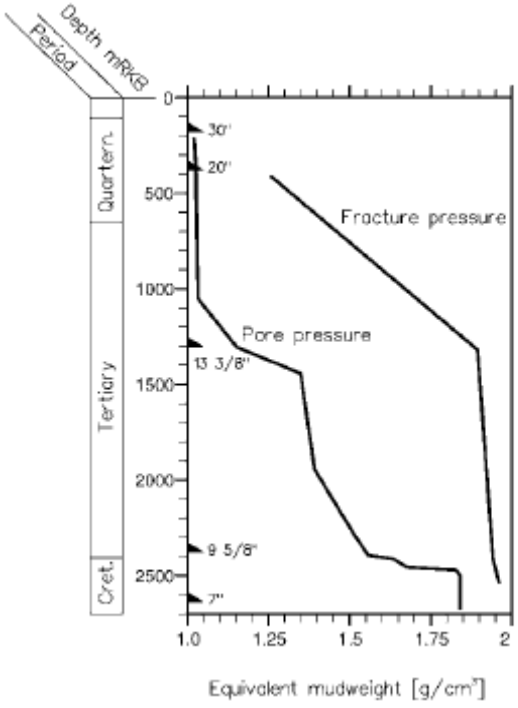

Fig.2.12 Pressure and stress gradients, given as equivalent mud weight for Valhall [source: Petroleum Related Rock Mechanics. 2nd Edition, 2008]

It is characterized by a high initial pore pressure, with about 44.7 MPa close the top of the reservoir at 2500 m. The total vertical stress is about 49 MPa which gives a low value of effective vertical stress i.e. $49 - 44.7 = 4.3\,\text{MPa}$. The net grain-to-grain stress is small, and unless the cement strength between the grains is high, particles may be mobilized. For a normally consolidated material, in which the permeability of the overlying formations is in perfectly drained conditions, the initial consolidation pressure is equal to the mean effective stress, i.e. $P'_{con} = \left(\sigma'_1 + 2\sigma'_3\right)/3$. Mineralogically, chalks are classified as carbonates, but the mechanical behavior of chalk to stresses helps to group it as a material between soil and rock.

2.7.2 Viscoelasticity [Chang, C. T., Zoback, M. D. (1998)], Cole, K. S., Cole, R. H. (1941), Gross, B. (1947), Settari, A. (2002)].

Many materials exhibit both features of elastic solids and characteristics of viscous fluids. Such materials are called visco-elastic materials and chalk is an example of such. One of the main features of elastic behavior is the capacity for materials to store mechanical energy when deformed by loading, and to set free this energy completely after removing the load. In viscous flow, however, mechanical energy is continuously and totally dissipated. Viscous materials store and dissipate energy in varying degrees during loading/unloading cycles.

Creep is time dependent deformation under constant stress. Viscoelastic theory states that if a material creeps, then it should relax given the proper boundary conditions. It is a property of chalk exhibited by its solid framework, and this behavior of chalks may cause a delay in deformation response to pressure changes. It is responsible for the creep behavior of chalks which is a time-dependent deformation. *Viscoelastic nature of chalk is related to the presence of intergranular clays.*

Both linear and nonlinear models have been used to explain the theory of viscoelasticity. Linear models consist of various combinations of linear springs (Hooke) and linear viscous dashpots (Newton), connected in series or in parallel. Such rheological models are suitable to describe the linear viscoelastic behavior of materials under *uniaxial loading*.

The Kelvin-Voigt model for solids consists of one linear spring (Hooke) and one linear dashpot (Newton) connected in parallel. The Kelvin-Voigt model depicts creep reasonably well [Liingaard, M., *et al.* (2004)]. In contrast to Kelvin model, the Maxwell model for fluids consists of one linear spring (Hooke) and one linear dashpot connected in series.

However, the BURGERS model consists of a MAXWELL and a KELVIN element coupled in series. The creep behavior of this model is described by considering the strain response under constant stress of piecewise constant stress of the single elements connected in series as shown in Fig. 2.13.

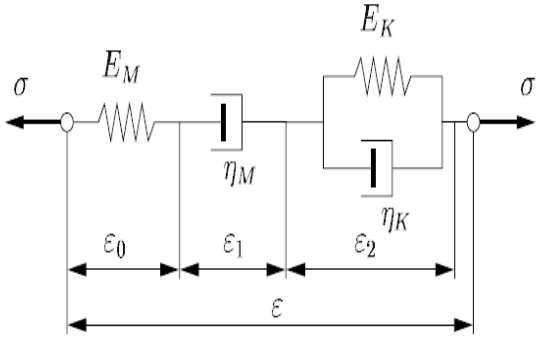

Fig.2.13 The BURGERS model; nomenclature

The total strain after some time, *t*, is decomposed into three parts,

$$\varepsilon(t) = \varepsilon_0 + \varepsilon_1 + \varepsilon_2 \qquad \text{[Eq.2.21]}$$

where the first part is the strain of HOOKE's spring, $\varepsilon_0 = \sigma / E_M$; the second part is the NEWTON's dashpot with strain rate, $\dot{\varepsilon}_1 = \sigma / \eta_M$; and the third part is the strain in the KELVIN unit which satisfies the ordinary differential equation, $\dot{\varepsilon}_2 + (E_K / \eta_K)\varepsilon_2 = \sigma / \eta_K$

where,

E -elastic modulus

σ -stress

η -shear viscosity

2.8 Stress Path

The stress path [i.e., the variation of stress state with time] depends of pressure changes and constitutive behavior of the material, as well as containment of the reservoir in terms of deformation e.g., stiffness of the surrounding rocks, [Fjaer, E. *et al.* (2008), Settari, A. (2002), and Santarelli, F. J. *et al.* (1998)]. It is the changes in the in-situ stresses in a reservoir during depletion and given as a curve of the horizontal [lateral] effective stress versus the axial [vertical] effective stress. Hence, reservoir stress path:

$$\kappa = \frac{\Delta\sigma'_{lateral}}{\Delta\sigma'_{axial}} \qquad \text{[Eq.2.22a]}$$

where:

$\Delta\sigma'_{lateral}$ - effective lateral stress [MPa]

$\Delta\sigma'_{axial}$ - effective axial stress [MPa]

The issue with the reservoir stress path is whether it could be easily predicted or modeled before the exploitation of the reservoir begins. Also, is there any possibility of getting it re-established after the reservoir has been depleted? Providing answers to these would enable prediction of other effects on the reservoir due to changes in the in-situ stresses.

For the elastic region, equation 2.22a may be written as;

$$\kappa = \frac{\Delta\sigma'_{lateral}}{\Delta\sigma'_{axial}} = \frac{\nu}{1-\nu} \qquad \text{[Eq.2.22b]}$$

where;

ν - Poisson's ratio [dimensionless]

Chapter 3: Testing Procedures

Triaxial versus uniaxial strain tests: The *triaxial test* is performed by taking the vertical and the horizontal stresses to a level (hydrostatically loading), and thereafter keeping the radial stresses at a constant value or level as the vertical or axial stress is increased, and measuring the compaction, ε_z, and the radial strain, ε_r, as the axial stress is increased. It requires fewer control variables than the uniaxial strain test, thus easier to carry out. It gives the ability to establish failure criterions, and the Young's modulus can be calculated at any desired period of interest.

The *uniaxial strain* test performed in this thesis is a standard test performed by keeping the radial displacement or deformation of the sample at a constant value $[\pm 0.01]$, allowing only the sample to compact axially or vertically. This is commonly used in the laboratory at UiS, with the assumption that it is the most suitable method of simulating field behavior. It is not unusual to combine the uniaxial strain test with a creep test; hence this study was based on such a combination. The uniaxial strain test is applied in quantifying the immediate load response of the material. By correlating the creep response in the laboratory to a depletion rate of the pore pressure, the total compaction can be calculated.

3.1 The Hydraulically Operated Triaxial Cell

The uniaxial strain assumption is achieved by a chamber where a core sample, protected by a sleeve to prevent direct contact and allow direct effect of the pressure from the confining fluid on the core, is mounted. Two draining conduits used through the lower and upper surfaces of the sample ensures that pore pressure is built to the desired level and that the loading does not induce a pore pressure change within the sample, and subsequently, overburden pressure is provided by a piston run down from the top of the triaxial cell and partly by the confining fluid. The confining fluid used is Bayol and the pore fluid is n-heptane. Another type of confining fluid that could be used is Tellus oil, but Bayol is less viscous providing less resistance to applied pressure. The choice of n-heptane [$H_3C(CH_2)_5CH_3$ or C_7H_{16}], a non-polar fluid, is to minimize the effect of use of water [seawater] considered to weaken the chalk. An extensometer measures the diameter, and also helps to monitor the fluctuations in the radial deformation of the core sample as a result of variations in pore pressure, axial and lateral stresses. An LVDT (Linear Voltage Displacement Transducer), section 3.1.3, which

operates on a magnetic induction principle resulting from axial movement of the piston gives an indirect measure of the axial deformation.

3.1.1 Diagram

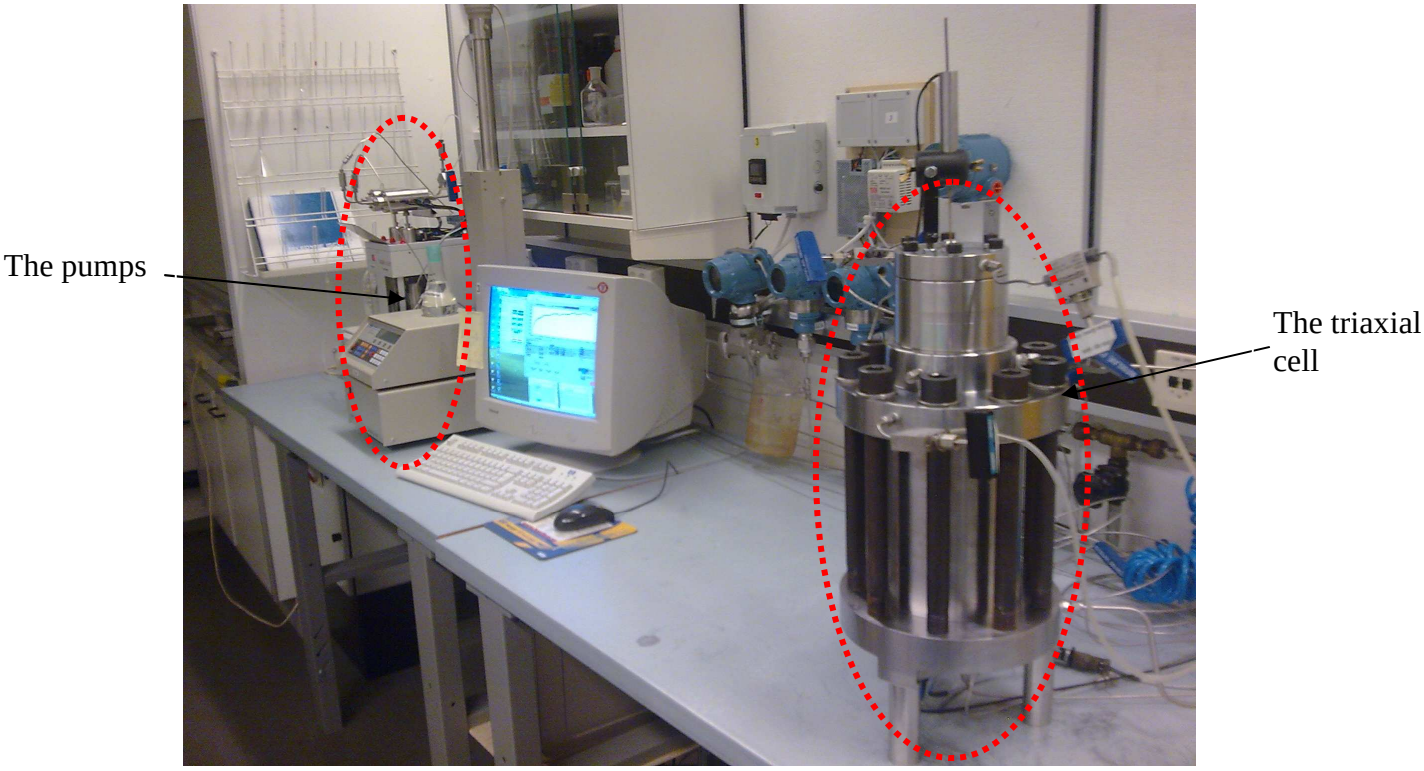

Fig.3.2a The laboratory setup

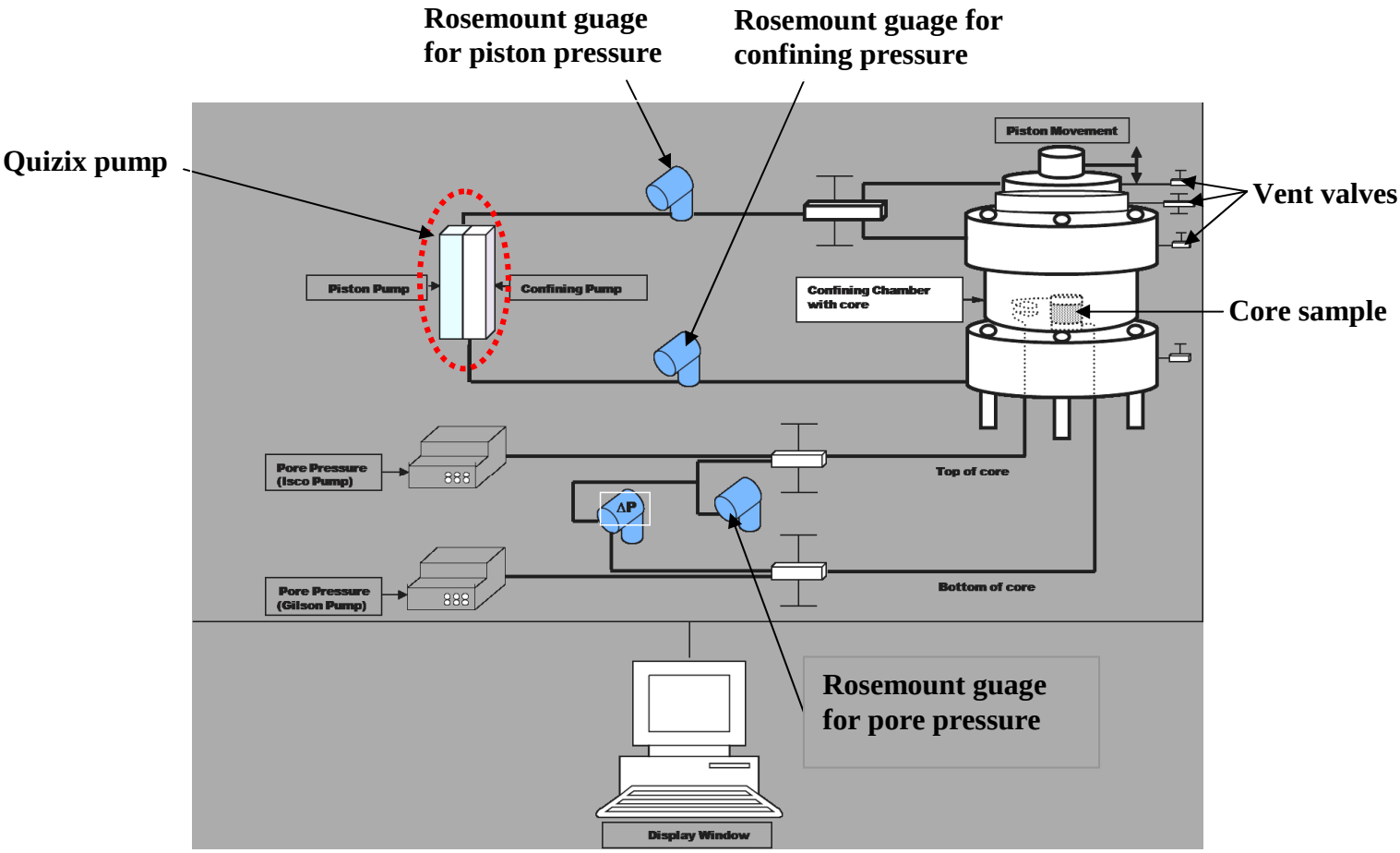

Fig.3.2b The lab setup [schematic]

Figs.3.2a and b above are the general view of the cell used to perform the experiment. It consists of an arrangement of pumps with lines and chambers capable of withstanding the required pressure to achieve the test objectives. However, a safety pressure of 60 MPa is often set whenever the test is about to run. The labview program makes use of these to provide a safety limit should the pressure be exceeded.

3.1.2 Pumps

The cell runs on four pumps to provide the confining, pore and piston pressures. Two out of the four pumps, the GILSON (Fig.3.3a) and the ISCO (Fig.3.3b) pumps are used to pump heptane as the pore fluid and to build the pore pressure to the desired limit. A flowline runs from the GILSON pump to the bottom of the core; whereas another flowline runs from the ISCO pump to the top of the core, forming a closed circuit which could be regulated by the manipulation of the ISCO pump by changing the operating mode.

The pressure gradient could be programmed to pump or receive fluid at any desired rate. An initial established pressure is input and the final desired pressure is input as well, followed by the desired time to achieve the final pressure. The program outputs the pressure gradient automatically. Conversely, a pressure gradient could be input and then the time automatically estimated.

This kind of arrangement enables pore pressure to be built by pumping through the GILSON and receiving with the ISCO at specified pressure limits. During the pumping, the ISCO pump is set at constant pressure. That enables the pump to provide a back pressure by regulating the rate of flow, hence the variation of flow rate from negative to positive. Also, during the pore pressure depletion stage of the experiment, the ISCO pump is used to reduce the pore pressure at specified pressure gradients depending on the objective of the test. A pressure differential (ΔP) that exists as fluid flows through the core is also recorded by a Rosemount gauge as shown in section 3.1.4.

Fig.3.3a GILSON pump

Fig.3.3b ISCO pump

Fig.3.3c Quizix pump

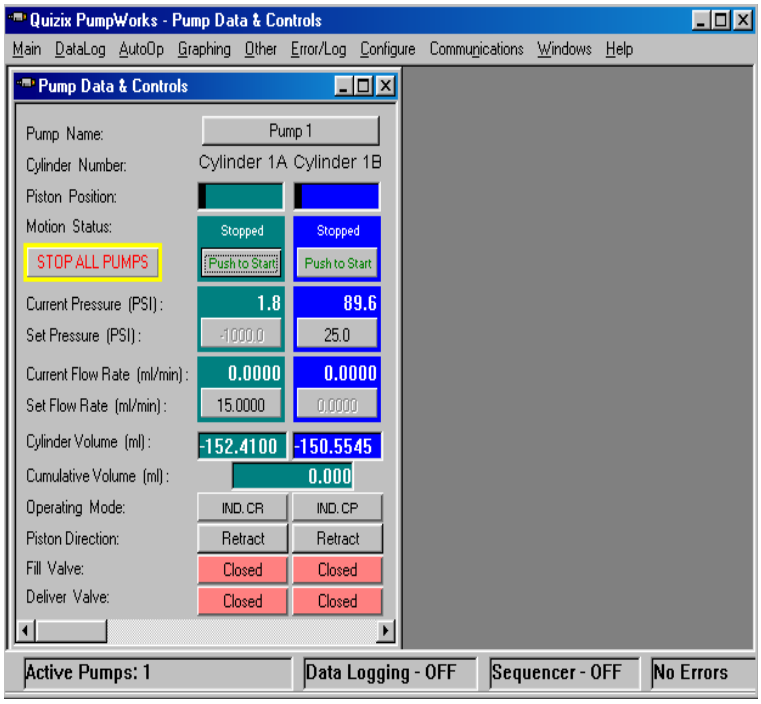

Fig.3.3d Quizix pump works

The Quizix pump (Fig.3.3c) provides the pressure on the confining chamber by pumping of Bayol to the chamber already filled with the same fluid, thus pressurizing it; and also it is used to run up and down the piston which helps to provide the most part of the overburden pressure and also where the LVTD is mounted that provides the axial movement of the piston thus the strain on the core. The piston pump makes use of Bayol for the hydraulic lifting and lowering of the piston. But, other fluids could also be used. For instance, heptane has been used in the piston chamber. The Quizix pump could be used in up to 15 different operating modes during testing [Quizix pump-works user's manual], but in the tests, independent constant rate cycles [1C] and independent constant pressure cycled [2C] were used. Independent constant rate cycled mode enables the pressure to vary while keeping the flow rate constant during operation, while independent constant pressure cycled enables the pressure to be held constant while the flow rate varies. For instance, while running down the piston, the mode is set at 1C enabling the piston to be lowered down to the top of the core at a constant flow rate with varying [increase] pressure at it moves down. But once the piston lands on the core and the pressure increases sharply to the desired level, the mode is changed to 2C to keep it at that pressure while the flow rate adjusts automatically to keep the constant pressure value. Also, while building the confining pressure, the mode is kept at 1C until the

final desired confining pressure where it is automatically changed to 2C. This is achieved by setting the cylinder 1B at auto-operation mode at constant pressure, with the desired final confining pressure and the time to achieve that input as required by the program. It would be recalled that this confining pressure build up is done concurrently with pore pressure buildup [ramping], with a 1MPa [10 bar in the Rosemount gauge] window between the two.

The Quizix pump (Fig.3.3c) has a cylinder and syringe arrangement. At every point in time, the position of the piston is seen on the Quizix pump works window as the black part while the blue part is the fluid level, see Fig.3.3d.The syringe sucks and discharges fluid with the aid of a piston through an open/close system where movement in a particular direction enables fluid to be sucked from a container of Bayol into a cylinder. Then, movement in an opposite direction results in the discharge of the fluid through a flowline and through a valve [where flow is directed] into the piston chamber, where it is pressurized to enable lifting and lowering of the piston. This is seen as retract/extend as piston direction in the Quizix pump works window. Refer to section 3.1.5.

3.1.3 The Linear Voltage Displacement Transducer [LVDT][c]

Fig.3.4 An LVDT mounted

This is used to measure the axial movement of the piston, hence the axial strain in the core. It is based on a magnetic induction principle. An LVDT comprises 3 coils; a primary and two secondaries. The transfer of current between the primary and the secondaries of the LVDT

displacement transducer is controlled by the position of a magnetic core called an armature. On the position measurement LVDTs, the two transducer secondaries are connected in opposition. At the centre of the position measurement stroke, the two secondary voltages of the displacement transducer are equal but because they are connected in opposition, hence the resulting output from the sensor is zero. As the LVDTs armature moves away from centre, the result is an increase in one of the position sensor secondaries and a decrease in the other. This results in an output from the measurement sensor. With LVDTs, the phase of the output (compared with the excitation phase) enables the electronics to know which half of the coil the armature is in.

The strength of the LVDT sensor's principle is that there is no electrical contact across the transducer position sensing element which for the user of the sensor means clean data, infinite resolution and a very long life.

3.1.4 The Rosemount gauges

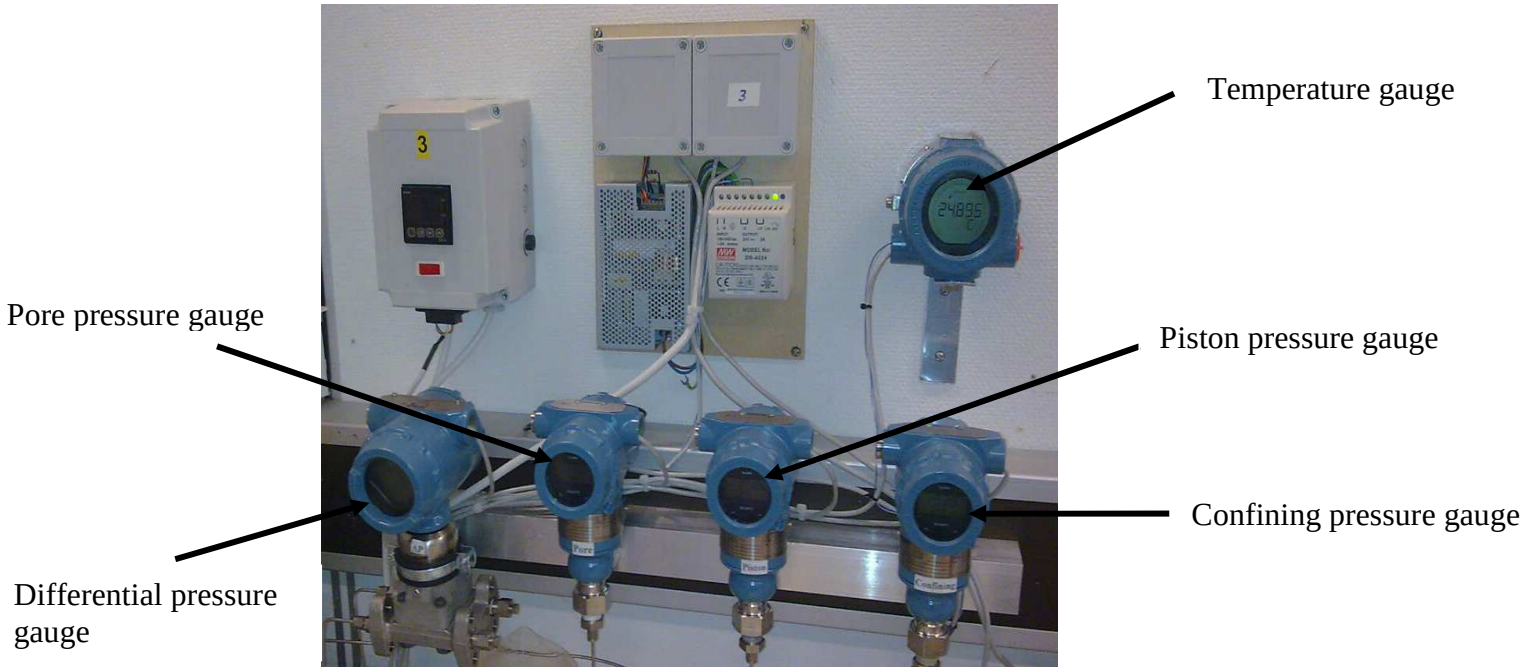

Fig.3.5 The Rosemount gauges

These gauges are used to display the pressure readings from the test, Fig.3.5. They display the pressure in bars which include the confining, pore and piston pressures in *process* conditions.

It also measures the pressure differential ΔP across the core sample in kilopascals. The ambient temperature is also displayed by one of the gauges in degrees Celsius.

3.1.5 Piston [up/down movement]

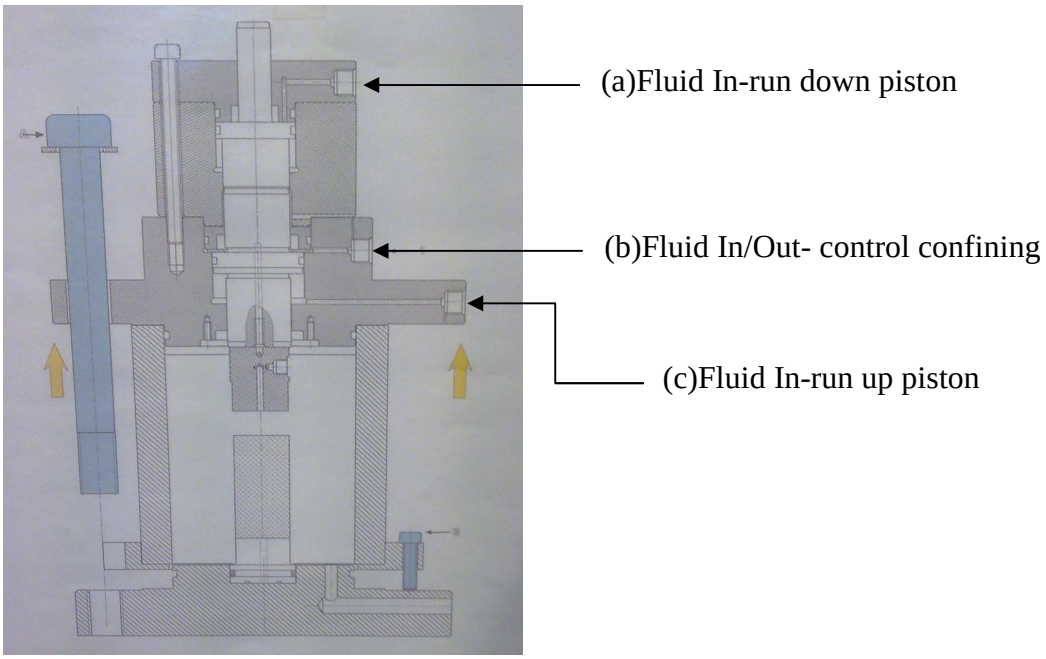

Fig.3.6 The piston chamber

Fig.3.6 shows the piston control arrangement. To run down the piston to enable it serve the purpose of overburden pressure supply, fluid is allowed into the upper chamber through a flowline connected at point (a) with flowline to point (c) shut-in, while fluid is let out through another flowline [vent line], otherwise there would not be any piston movement and an excessive pressure buildup is also observed.

Conversely, to run up the piston, fluid flows in through point (c) with flowline to point (a) shut-in, with an outlet valve allowed open to discharge the pressurized fluid in the upper chamber. The control of the fluid entrance through points (a) and (c) is done with a common valve that redirects the flow path upon manipulation.

The point (b) has a link direct to the confining chamber, hence fluid (Bayol) could be let in/out through it. It has a two-way-control valve that enables fluid in and out the confining chamber. It serves to bleed out air before pressure buildup prior to start of the test. It is also used to let in compressed air to empty the confining chamber at the completion of an experiment. This time, the confining fluid is let out through a flowline at the base of the skirt.

The open/close positions of the valves should be properly observed, otherwise there might not be any responses.

3.1.6 Extensometer

The extensometer is an instrument that is wrapped round the sleeve that holds the core sample, and enables the direct measure of radial variations of the diameter of the core sample. It is usually installed after mounting the core sample and checked to make sure the reading of the core diameter from the instrument represents the minimum possible reading as the diameter of the core, since slight changes do occur with changes in the position of the extensometer. The reading is transmitted to labview program, with +/- 0.01 mm allowable variations during test. This is because since the test is expected to be conducted with no lateral deformations, the extensometer should give values within acceptable ranges; otherwise it would be assumed that the core has extended or contracted radialy to make the test a failure.

3.1.7 Core position and Forces

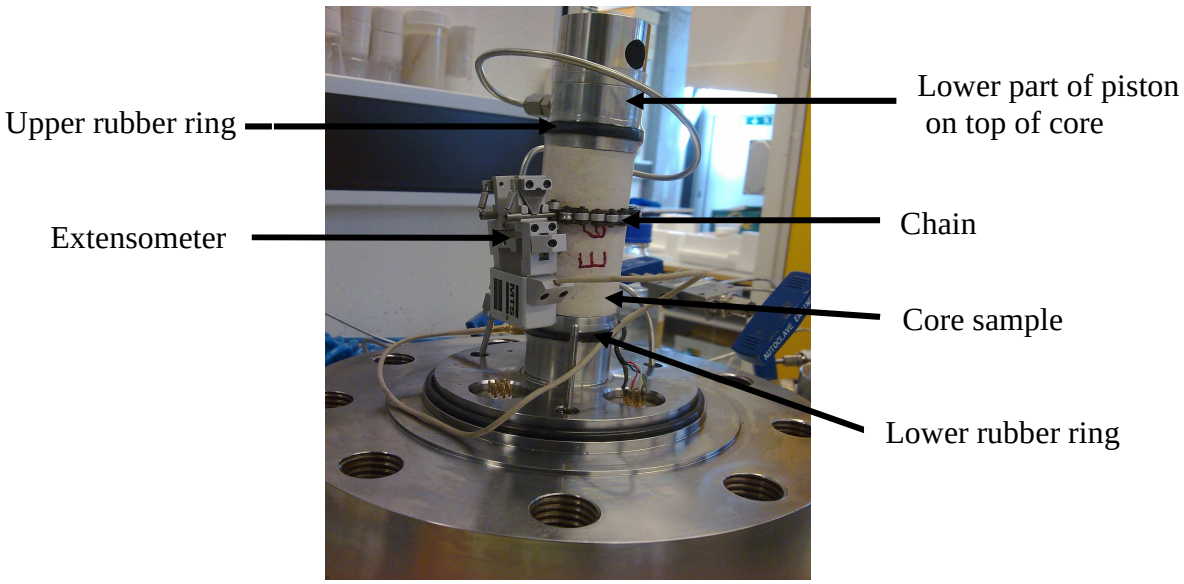

Fig.3.7 Position of core in the confining chamber

The core is embedded in an impermeable plastic sleeve, and mounted on a pore fluid supply base, at the center of the confining skirt as shown in the Fig.3.7. Rubber rings worn on the inner parts of the top and bottom sides of the sleeve prevents direct communication of the pore and confining fluids after the sleeve is welded round the core by the use of a heat gun set

at appropriate heat supply value. The position of the core enables the piston to land on top of it axially. It also enables part of the confining pressure to be used to supply the overburden. Hence, one might say that the overburden stress on the core sample is a function of both the piston pressure and the confining pressure. Laterally, the confining fluid provides equal pressures in both the x and y directions, and helps keep the core in steady position and allowing no uneven expansions.

3.1.8 The confining chamber

This is where the core is mounted and other stresses/pressures interplay to give the desired load on the core sample. The confining pressure is applied through an oil bath [Bayol] outside the sleeve, whereas the axial stress is provided by a piston attached to the axial load actuator of the load frame. Bayol has some special properties in that it offers less resistance to flow compared to Tellus oil, in addition to its water white colour, non-staining, odour free, non reactive, low aromatic contents and it is also suitable for direct and indirect contact applications. However, parts of the pressure from the piston is usually lost due to the resistance of the confining pressure in this chamber as the piston runs to hit the top of the core. This is usually taken care of by a friction factor used to remove the effect of the confining pressure on the piston. The pressure supply is achieved by the quizix pump that pumps Bayol and builds up the pressure at any desired value. The confining pressure is usually the first to be initiated at the beginning of the pressure build-up process in a uniaxial strain test, otherwise oil will invade the core and flow goes violently.

3.1.9 Display screen

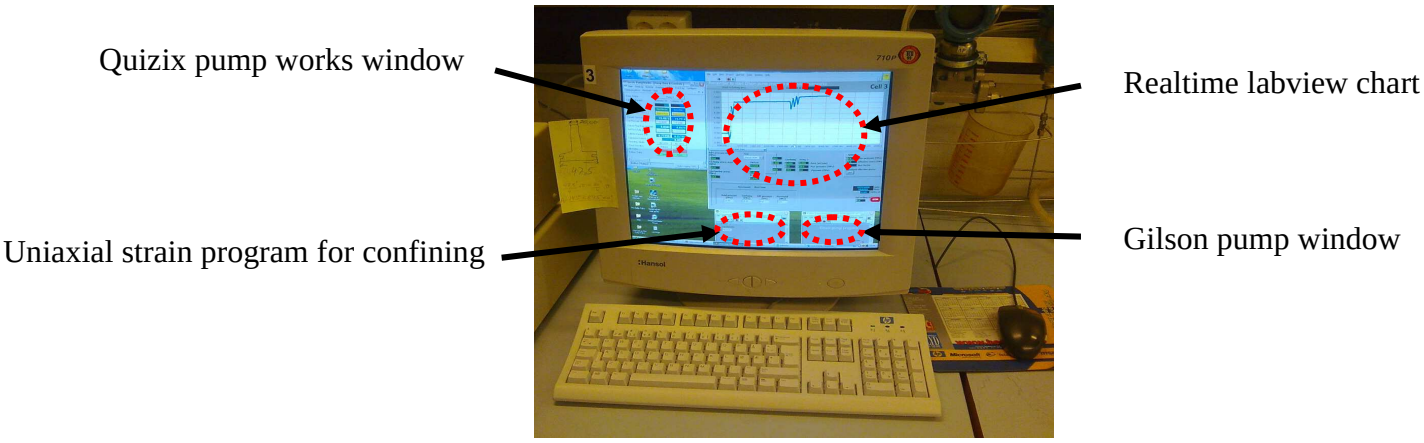

Fig.3.8 Display screen

This is a desktop screen where the quizix pump screen, labview program etc are manipulated. The response of the core to pressure variations, the pore pressure, confining pressure, extensometer readings, axial movement of the piston with respect to time etc could be observed in the screen. Hence, test progress is monitored and adjustments made when necessary. It could be said to be an eye through which one sees the actions in the cell. A typical display is shown in Fig.3.8 with piston axial movement and quizix pump data.

3.1.10 Overburden stress

Overburden stress is the axial stress exerted on the core to give axial deformation. It is analogous to the stress exerted in a reservoir rock by the overlying rock masses from the top of the reservoir to the earth's surface or the seabed. It is the summation of both the piston pressure and a part of the confining pressure that acts on the top of the core axially since the core is usually covered by the confining fluid. Factors are usually applied to account for the difference in the cross sectional area between the core sample and the piston and the effect of confining fluid resistance to piston movement and were used in the calculations on the data.

It has been shown that the overburden pressure is;

$$\sigma_T = P_C + (A_F * P_P) - (F_F * P_C) \qquad \text{[Eq.3.1a]}$$

where,

σ_T -overburden stress [MPa]

P_C -confining pressure [MPa]

A_F -area factor [dimensionless]

P_P -piston pressure [MPa]

F_F -friction factor [dimensionless]

Typical values of area and friction factors are 1.2788 and 0.0258 respectively. For a confining pressure of 31 MPa, the friction is approximately 0.8 MPa. Hence, if the desired overburden is 32 MPa,

$$32 = 31 + (1.2788 * P_P) - (0.0258 * 31) \qquad \text{[Eq.3.1b]}$$

Equation 3.1b gives a piston pressure of approximately 1.6 MPa for a desired overburden pressure of 32 MPa. That accounts for the starting value of the piston pressure on cylinder 1A.

3.2 Test program

Checklist 1- preparation for ramping

- Make sure the pore fluid circuit tubes are filled with n-heptane. This is to avoid air traps in the circuit which could introduce air pockets into the core sample, changing its form and altering the core response to pressure supplies.
- Install the core sample on the lower base, with the seals between the steel and the sleeve and the coffee filter, Fig.3.7. The seals would help prevent direct communication between the pore fluid and the confining fluid when the pressures are built up to their desired levels. Also, when the piston lands on top of the core sample and deforms it axially, the seals help to secure the pore fluid in place and balance the sleeve expansion and to prevent leakages.
- Cut a sleeve and shrink it with a heating gun to the lower console and the lower half of the sample. The sleeve is a thin plastic material that shrinks unto the core when heat is applied to it, helping to maintain a constant core diameter and serving as a barrier between the confining and pore fluids. Proper sleeve mounting ensures that equal lateral pressures are applied to the core sample.
- Install the upper part/piston with the spiral. It is at the top of this that the piston lands, hence it must lap properly to the top of the core and centered vertical, otherwise, the pressure from the piston would not deform the core uniformly. Carefully seal and cut and shrink the sleeve properly.
- Fasten the extensometer. The extensometer helps measure lateral deformations of the core sample. Position the extensometer properly so that the reading is as small as possible. Start the labview program and the GILSON pump program and monitor the development of the diameter while installing the extensometer. Keep the logging rate at 0.1 or 0 minutes between logging points. This ensures that instant readings of diameter are logged and adjustments made as desired.
- Install the steel skirt, and make sure that the upper and lower o-rings are present. These rings help ensure proper metal-to-metal seal. Check the outlet valve for confining fluid drainage. Then, fill-in the confining chamber with Bayol (hydraulic/confining fluid).

- Make sure the confining bleed valve is open to drain out any excess oil. Place the upper part of the cell carefully on top of the steel skirt. Check that the o-ring is properly fitted. Adjust the upper part to fit properly.
- Build up confining pressure by pumping piston 1B on Quizix pump. Cylinder/piston 1B applies oil to the confining chamber to build pressure. Let the bleed valve for the confining be open and let the oil flood into the chamber and out in the top for about 5 minutes. Then the air should be gone. Then close the confining valve and build up to 0.7 MPa confining pressure.
- Install the axial Linear Voltage Displacement Transducer (LVDT) while building the initial confining pressure. Ensure that the metal rod inside the LVDT cylinder has an unrestricted axial movement. Alternatively, one might stop the Labview program and the GILSON pump programs after making sure the extensometer is properly installed and restart them after installing the LVDT. That ensures that the axial movement of the piston display on the Labview program starts from zero and moves positive upwards for easier reading and understanding.
- Since 1 MPa window between confining and pore pressure is desired; when the confining pressure is starting to increase (0.2 – 0.4 MPa), start to flood pore fluid from the inlet GILSON pump with 0.25 - 0.5 ml/minute in rate. Use a maximum pressure of 0.2 MPa on the Gilson pump to ensure that the pore pressure never exceed the confining pressure.
- Let the ISCO pump receive the pore fluid at zero pressure (zero is probably not 0.0 at the ISCO pump, but probably -0.1 MPa or 0.7 bar (-1.2 to -1.4 bar). 2 bar has been used before at constant pressure. When flooding with the GILSON pump and receiving with the Isco pump, should get good values [1-2 KPa] from the differential pressure gauge.

Checklist 2- ramping

- When the confining pressure is 12 bar [1.2 MPa] and the pore pressure is 2 bar [0.2 MPa] on the Rosemount gauges, then ramping process is initiated.
- Set ‘‘autoramp’’ operation for cylinder 1B at ‘‘constant pressure’’, and ramp time of say 200 minutes as used in this study and set pressure of 31 MPa
- Program ISCO pump at program gradient [PGa] from initial pressure of 2 bars to final pressure of 301 bar as would be normally observed on the Rosemount gauges and duration of same 200 minutes.

- Enable the ‘on button’ on the autoramp operation mode first and then immediately press ‘run’ twice on the ISCO pump. That would ensure that the ramping of confining pressure to 31 MPa and the pore pressure to 301 bar [30.1 MPa] are achieved at the same time of 200 minutes.
- Immediately change the flow rate and the maximum pressure for pump 3 on the computer screen to 0.075 ml/minute [typical value] and 30.1 MPa respectively

Checklist 3- procedure for running down the piston

- To run down the piston, open up the valve at the upper chamber to let in fluid that would exert downward pressure on the piston while the lower outlet vent valve is set open to allow outflow of the fluid in the lower chamber as piston is run down.
- One may now run down the piston with pump 1A set on constant rate cycled [mode 1C] and flow rate of say 0.1 ml/min. The piston would normally travel for about 5.5-6.0 mm before hitting the core sample at the top, though the distance is a function of core length.
- One might change the flow rate to 0.01 ml/minute to allow a gentle landing on the core and to avoid damage when the piston might have travelled for about 5 mm from the start.
- Wait until ramping is done, i.e. confining pressure of 31 MPa and pore pressure of 30 MPa. Those are the desired pressures used to run the uniaxial strain test.

Checklist 4- procedure for running uniaxial strain program

- Stop flooding with GILSON pump (pump 3) by changing the flow rate from 0.075 ml/minute to zero on the computer display screen and wait for about 5 minutes.
- Ensure that the uniaxial strain mode is off. Increase the piston pressure to 1.6 MPa slowly using constant rate cycled [mode IC] with flow rate of say 0.1 ml/minute and then change the cylinder 1A to mode 2C i.e. constant pressure mode. When the pressure is 1.6, then switch to uniaxial strain mode.
- The uniaxial strain in ‘main program’ will control cylinder 1A
- Start additional uniaxial program. Choose ‘uniaxial strain 2’. This ‘uniaxial strain 2’ program controls cylinder 1B. Make sure that cylinder 1B is off the first 15 seconds to avoid the pressure jump always happening.

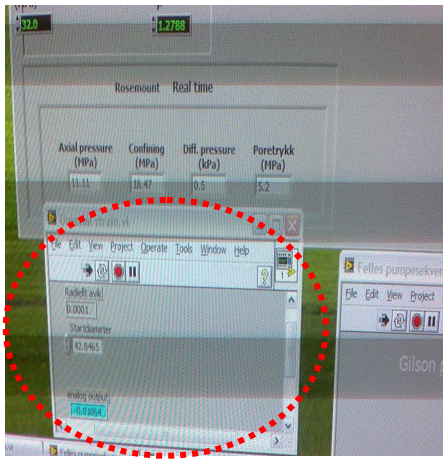

Fig.3.9 Uniaxial strain program for cylinder 1B

- Press ‘stop’ on the ISCO pump
- Program new gradient [PGa] on the ISCO pump, for example 301 bar [30 MPa] to 51 bar [5 MPa] in 1000 minutes for an intermediate loading test. This is equivalent to a pressure gradient of 0.025 MPa/minutes during depletion of the pore pressure.
- Press ‘run’ and start the cylinder 1B.
- Monitor the development of the extensometer. If the radial diameter is within +/- 0.01 mm which is the acceptable deformation in this study, the test should be allowed to progress.

3.3 Porosity Determination

20 core samples from Stevns Klint chalk block were prepared by cutting them to proper size with average length [L] of 79.26 mm and diameter [D] of 38.13 mm respectively, satisfying the condition that $(L \geq 2D)$. This was achieved by the use of lathe machine for the length while the diameters were verified with a caliper. They were randomly named E1 to E20.They were oven-dried for about 36 hours at a temperature of $130^{o}C$ and weighed thereafter, giving the dry weight.

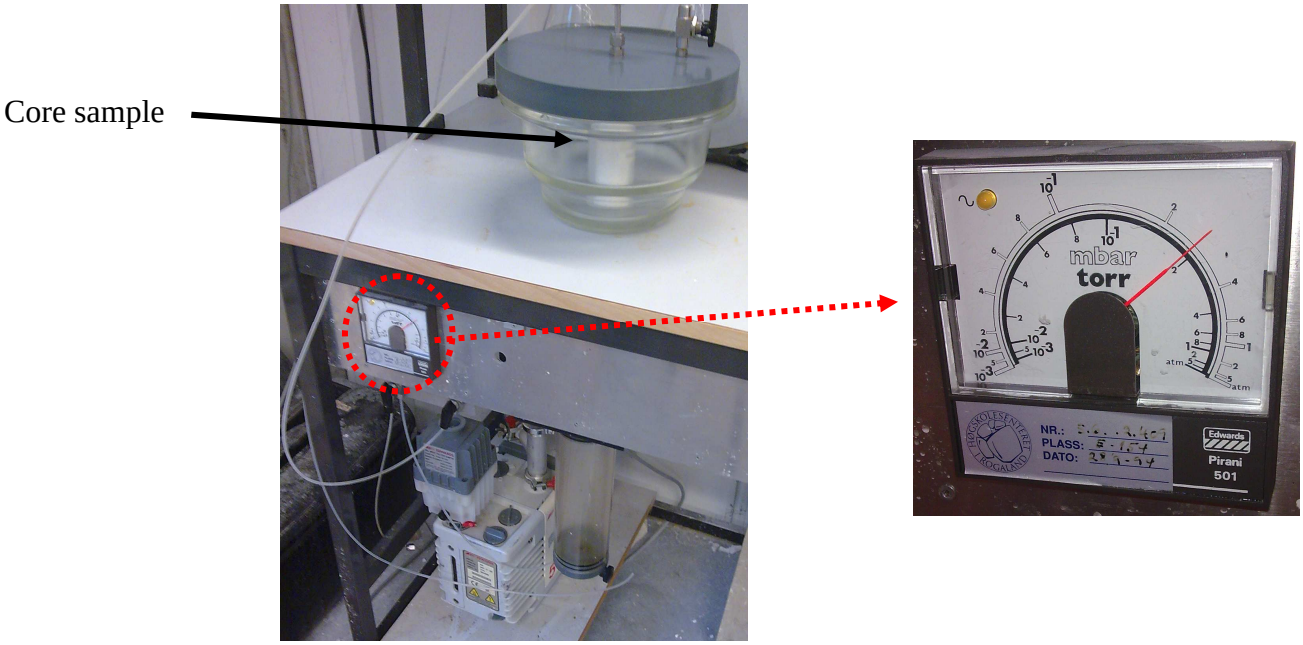

Fig.3.10 The Vacuum pump

The vacuum machine was used to suck out the air in the pore spaces, and were later flooded with water to saturate the pores to give the wet weight. The difference between the wet and the dry weights gives the weight of water contained in the pore spaces. Since there is a direct relationship between weight, density and volume $V_p = mass/density$, the volume of water gives a direct estimate of the pore volume of each sample. Also, since the length and diameter of each sample is known, the bulk volumes $V_b = (\pi * diameter^2 * length)/4$ are calculated, hence, a ratio of the pore and the bulk volumes gives the porosity of each sample.

Example using core E1:

Length [L]: 80 mm

Diameter [D]: 38.10 mm

Dry weight: 141.16 g

Wet weight: 180.58 g

Therefore, weight of water; 180.58-141.16 = 39.42 g

Using density of water of $1\,g/cc$, pore volume $[V_P] = 39.42 g/(1 g/cc) = 39.42\ \text{cm}^3$

Bulk volume $[V_b] = (\pi * 38.10^2\, mm^2 * 80 mm)/(4 * 1000) = 91.79\ \text{cm}^3$

Thus,

Porosity $[\phi] = \dfrac{V_p}{V_b} * 100 = \dfrac{39.42}{91.79} * 100 = 42.95\%$

The porosity of the samples range from $(40 - 45\%)$ with an arithmetic average of 42.71% since core is isotropic, please see Table 4.1.1

The real-time estimate of the porosities during the test was calculated based on the initial porosities on the table above. That is because the reduction in porosity due to compaction is a function of the initial porosity of each core sample. Hence, real-time porosity is given as;

$$\phi_{\text{realtime}} = \phi_{\text{initial}} + [(\varepsilon_{\text{volumetric}} * (\phi_{\text{initial}} - 1))/(1 - \varepsilon_{\text{axial}})] \qquad \text{[Eq.3.2]}$$

where:

$\phi_{realtime}$ - realtime porosity [fraction]

$\phi_{initial}$ - initial calculated porosity [fraction]

$\varepsilon_{\text{volumetric}}$ - realtime volumetric strain [fraction]

But since the test is uniaxial strain,

$\varepsilon_{\text{volumetric}} = \varepsilon_{\text{axial}}$ - realtime axial strain [fraction]

The realtime bulk volumes and pore volumes were also calculated from the changes in the lengths and porosities as the pore pressure is depleted. Plots of the observed changes are as shown in the subsequent sections where porosities are plotted as functions mean effective stress.

3.4 Failed Tests

Several failures were recorded during the test period. As would be observed in the Table 3.4.1 below, the earliest recorded failures were due to human error. They occurred at the stage when I was not too perfect in the use of the programs and pumps. Hence, they could be said to be learning process instigated. Few failures were also observed due to failure of the pumps that supplied compressed air to run the systems. New pumps were installed later in the period of the test. Also, there was one recorded failure for investigation because I wanted to find out the response of the core and the uniaxial strain program with confining pump off. Noteworthy is the fact that throughout the tests, there were no recorded failures due to leakage in the

circuits, or communication between the pore and confining pressures which shows that that part of the system was under control throughout the test. As a result, none or part of the failed test is presented in the report.

Table 3.4.1 Causes of failures

Sample	**Cause of Failure**				
	Human Error	Power	Pump Program	Investigation	Leakage
E5	*				NONE
E6	*		*		
E7		*			
E8		*			
E9		*			
E10				*	

Chapter 4: Results/Discussion [Part A]

4.1 Initial Porosity Table/Calculation

Table 4.1.1 Porosity of core samples used in the experiments

START DATE:	21.01.2009		WEIGHT (g)					
CORE NAME	LENGTH [mm]	DIAMETER [mm]	DRY	WET	ΔWT.[g]	BULK VOL. [cm3]	PORE VOLUME [cm3]	POROSITY [%]
E1	80.50	38.10	141.16	180.58	39.42	91.79	39.42	42.95
E2	79.65	38.15	139.36	178.44	39.08	91.06	39.08	42.92
E3	78.95	38.10	139.56	176.81	37.25	90.02	37.25	41.38
E4	80.00	38.10	140.01	179.45	39.44	91.22	39.44	43.24
E5	80.50	38.10	140.09	180.03	39.94	91.79	39.94	43.51
E6	79.15	38.15	145.49	182.07	36.58	90.49	36.58	40.43
E7	80.00	38.15	141.01	180.66	39.65	91.46	39.65	43.35
E8	78.30	38.10	137.25	175.5	38.25	89.28	38.25	42.84
E9	79.50	38.10	140.75	179.42	38.67	90.65	38.67	42.66
E10	79.00	38.15	139.49	178.19	38.7	90.32	38.7	42.85
E11	79.95	38.15	134.88	174.62	39.74	91.40	39.74	43.48
E12	80.00	38.20	141.19	180.8	39.61	91.70	39.61	43.20
E13	73.65	38.15	134.35	168.48	34.13	84.20	34.13	40.53
E14	79.95	38.10	138.27	177.29	39.02	91.16	39.02	42.80
E15	80.00	38.15	139.23	178.77	39.54	91.46	39.54	43.23
E16	79.65	38.15	141.77	179.26	37.49	91.06	37.49	41.17
E17	79.85	38.10	138.36	177.77	39.41	91.05	39.41	43.28
E18	79.65	38.10	138.3	177.7	39.4	90.82	39.4	43.38
E19	80.00	38.15	138.95	178.6	39.81	91.46	39.81	43.53
E20	76.90	38.10	132.59	170.67	38.08	87.68	38.08	43.43
Average	79.26	38.13						42.71

As shown in Table 4.1.1, the lengths and diameters of the core samples were measured and used together with the other parameters in the table to calculate the porosities of the core samples used in the experiments, using the method of the example for core E1 in the section 3.3. The porosity used in this experiment is the effective porosity, as explained in equation [Eq.2.3].

Also, due to the small variation in the lengths, the strains calculated in the data generated from the test utilized the individual lengths of the core samples. In other words, the strains in the respective core samples were calculated with their core lengths.

4.2 Pressure/Stress History

The pressure history describes the test procedure. Due to the ramping, loading, creep and cycles, the pressure history of the different scenarios follow the same trend pictorially though physically, the response of the materials are different. Thus, the differentiating factor in the tests is the time within which the materials were loaded, given similar stress states. Since a

window of 1 MPa between the pore pressure and confining pressure is maintained during ramping, with the same window between confining and overburden pressure, and a reduction of 25 MPa in the pore pressure is used in all the tests, it follows that the time to deplete the pore pressure differentiates the tests from one another.

4.2.1 Rapid Loading

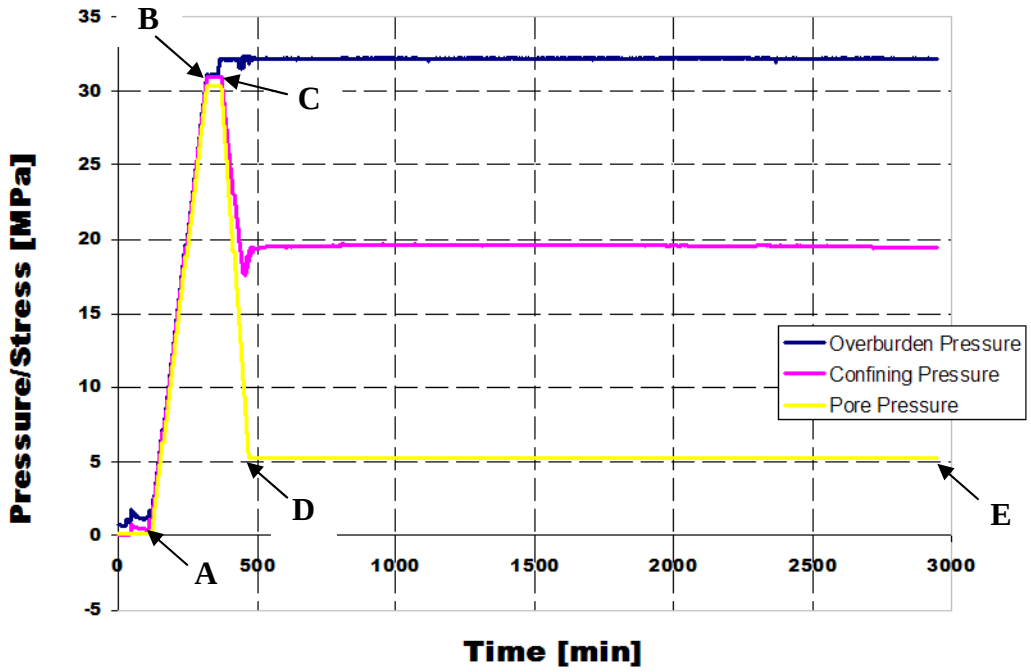

Fig.4.1 Pressure history for core E2 used for rapid loading at a gradient of 0.25 MPa/min

From Fig.4.1, part A-B represents ramping period, while C-D is the loading phase where the pore pressure is depleted thereby increasing the effective stress. The pore pressure was reduced from 300 bar [30 MPa] to 50 bar [5 MPa] within 100 minutes [1 hour + 40 minutes], and the core sample was allowed to creep in part D-E. This loading is more representative of the real life situation since geologically, formation of reservoirs takes millions of years with production only lasting for several decades.

4.2.2 Intermediate Loading

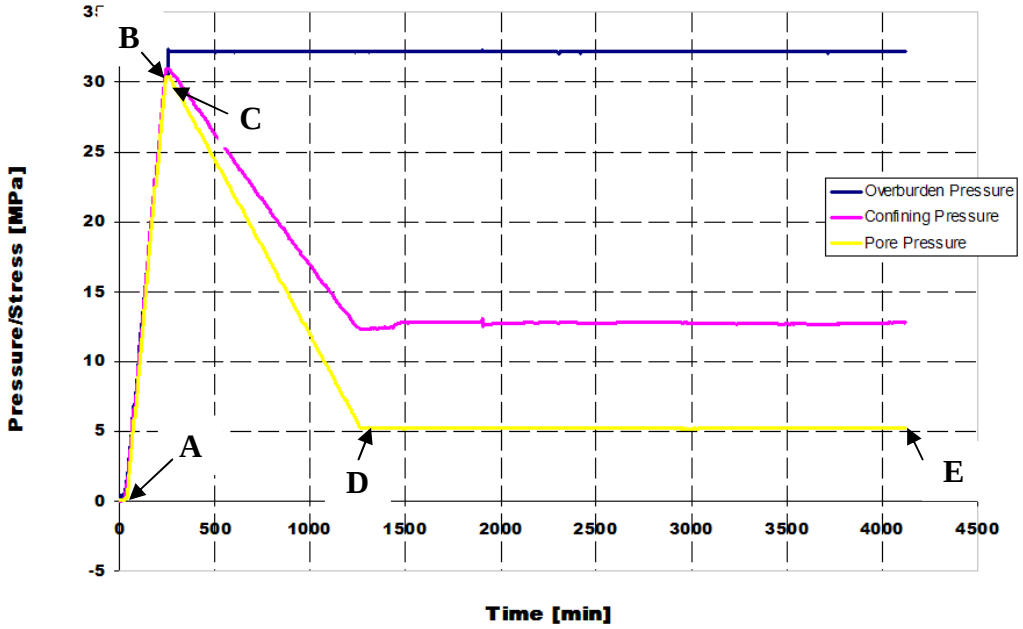

Fig.4.2 Pressure history for core E16 used for intermediate loading at a gradient of 0.025 MPa/min

In Fig.4.2, from point A, the confining and pore pressures were increased with a 1 MPa difference, up to 31 MPa and 30 MPa respectively at point B. Those are the desired pressures used in the experiment. It was allowed to stabilize at the stress state for at least 5 minutes in part B-C. The reduction in pore pressure by 25 MPa was accomplished at a constant overburden from point C to D from 30 MPa to 5 MPa, in a time of 1000 minutes [16 hours + 40 minutes]. Part D-E is the creep stage where the pore and overburden pressures are kept constant [5 MPa and 32 MPa respectively] and the core sample observed to deform axially. It is expected that the parameters estimated from this test should fall between rapid and slow loading cases.

4.2.3 Slow Loading

In Fig.4.3, the reduction in pore pressure by 25 MPa was accomplished at a constant overburden and the total time of 8333 minutes [138 hours + 51 minutes +50 seconds]. Relative to rapid loading as described in section 4.2.1, this depletion time is slow; however, it cannot be compared with real life field production of a reservoir which could last for several years. Some pore pressure load cycles were introduced in the later stages of the creep and the

responses thereafter plotted to get a trend in the creep strains and creep rates as described later in the subsequent sections.

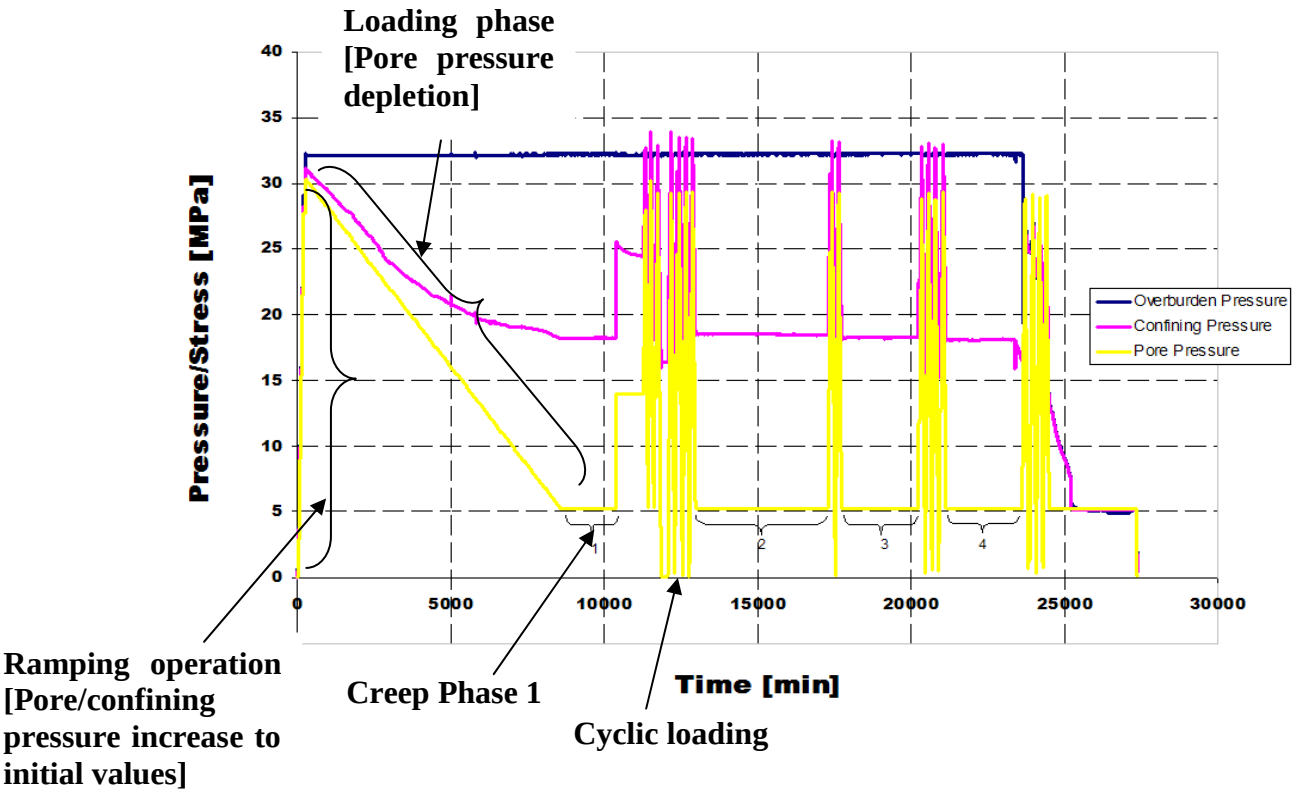

Fig.4.3 Pressure history for core E3 used for slow loading at a gradient of 0.003 MPa/min

4.3 Stress-Strain curves

This is a plot of effective axial stress [MPa] and the axial strain [%] during consolidation [load dependent deformation] or during the depletion of the pore pressure as shown in example Fig.4.4 for sample E2. Several parameters such as the yield stress and uniaxial compaction modulus [H] both in the elastic and plastic regions are estimated from such curves. There are marked differences in the parameters due to the loading scenarios. The yield stress is highest for rapid loading and least for slow loading. The H for the elastic region is higher for rapid loading compared with slow loading for the range of values of 2-3 GPa considered to be the range for chalk though 3.1 GPa was the calculated value for the rapid loading case as shown in Table 4.3.1. The H values for the intermediate loading falls between the rapid and slow loading.

Table 4.3.1 Uniaxial compaction modulus for elastic and plastic regions

Uniaxial compaction modulus, H [GPa] for the materials		
Core name	**Elastic region**	**Plastic region**
E2 [R]	**3.10**	**0.160**
E3 [S]	**2.50**	**0.063**
E4 [R]	**3.38**	**0.097**
E8 [I]	**3.76**	**0.052**
E11 [I]	**2.76**	**0.324**
E12 [I]	**2.87**	**0.340**
E13 [R]	**X**	**X**
E14 [S]	**4.02**	**0.490**
E16 [I]	**5.37**	**0.571**

Samples E4, E14 and E16 exhibited abnormal H values in the elastic range, and one can observe that they are the materials that have the highest values of yield stress as shown in Table 4.8.4. Thus, it follows that since the yield stress is higher for rapid loading, the material is able to withstand more stress before yield [sign of higher tendency to deform elastically]; whereas in slow loading, the material withstands less stress before start of yield. Also, the higher H [uniaxial compaction modulus] for rapid loading implies that there is less strain during loading but the material has a higher tendency to deform elastically in the loaded direction [axially] than for slow loading. That partly explains the more strain experienced at the beginning of creep in the transient stage compared with slow loading. Thus, a rapid increase in stress does not result in a rapid increase in strain, though there is a tendency for deformation. This is shown in a subsequent section as a marked high strain in the curve of creep strain. Please refer to section 4.8 for yield stresses from the tests as compared with the yield stress from the formula.

4.3.1 Rapid Loading

Table 4.3.2 Uniaxial compaction modulus for rapid loading

Uniaxial compaction modulus, H [GPa] for rapid loading		
Core name	**Elastic region**	**Plastic region**
E2	3.10	0.160
E4	3.38	0.097
E13	5.46	1.150

From the start of the depletion at point A, the stress-strain curve was linear, Fig.4.4. It continued up to a point where it departs from the linear trend at point B. This marks the beginning of yield and the curve is no longer linear and the transition region leads to plastic region where any applied load leaves a permanent deformation on the sample starting from point B. The yield stress is the point where the curve deviates from the linear trend. After yield, the material tends to be stiffened as shown by a marked increase in the slope of the curve from C to D .The material has become stronger and requires an increasing stress to enact more deformation.

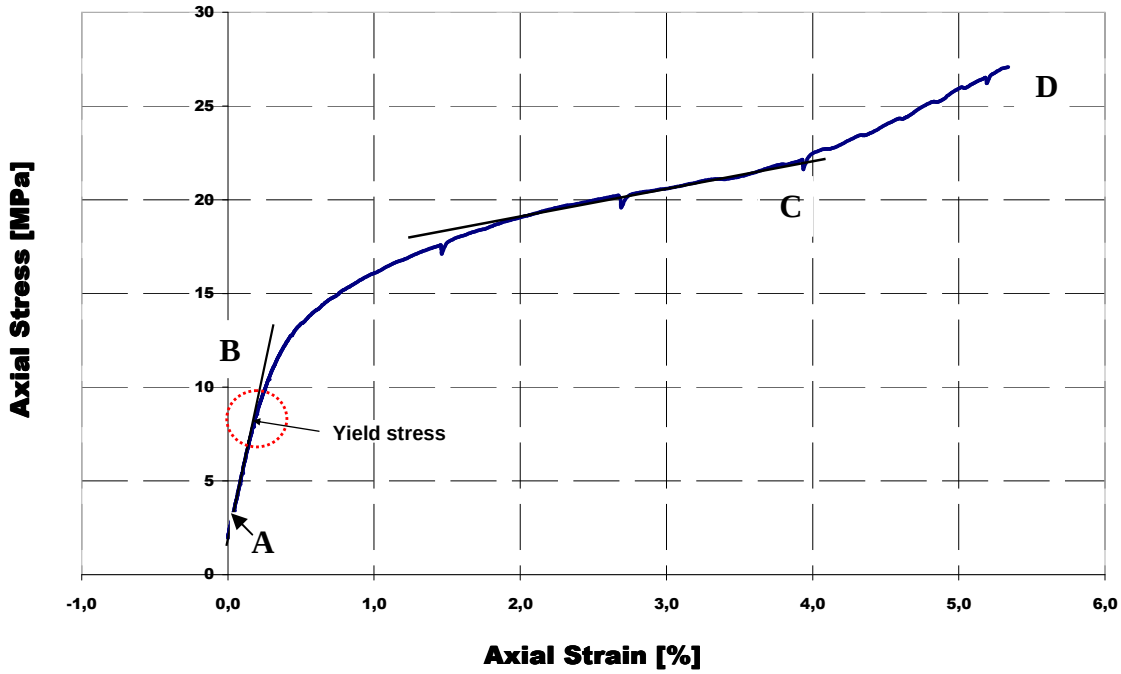

Fig.4.4 Yield curve for rapid loading using core E2

4.3.2 Intermediate Loading

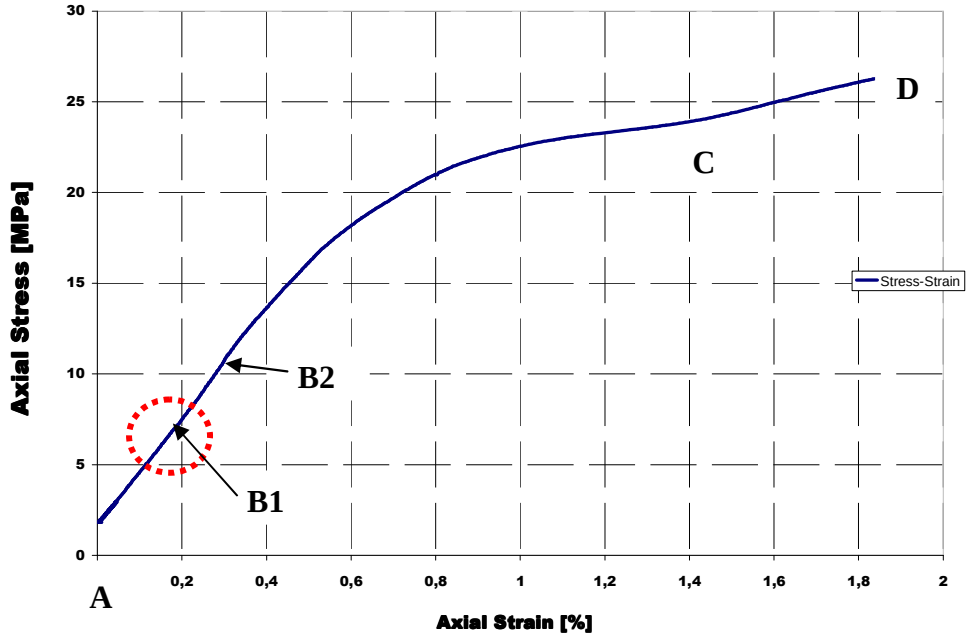

Fig.4.5 Yield curve for intermediate loading with core E12

The curve in Fig.4.5 is clearly linear from A to B1. From point B1 there is a deviation from linearity sloping a bit upwards before dropping gradually to point C. One might not easily recognize the point of deviation from linearity from B1 to B2 as can be seen from the plot since the upward shift seems be abnormal based on the observations from the other curves. Also, the zone from B1 to C has a very slow curve. The part C-D show a bit of hardening as there is a change of slope as shown.

Table 4.3.3 Uniaxial compaction modulus for intermediate loading

Uniaxial compaction modulus, H [GPa] for intermediate loading		
Core name	**Elastic region**	**Plastic region**
E8	3.76	0.058
E11	2.76	0.720
E12	2.87	0.340
E16	5.37	0.571

4.3.3 Slow Loading

Table 4.3.4 Uniaxial compaction modulus for slow loading

Uniaxial compaction modulus, H [GPa] for slow loading		
Core name	**Elastic region**	**Plastic region**
E3	2.50	0.063
E14	4.02	0.490

The same trend is recorded in this test as the curve in Fig.4.6 is linear from A-B which marks the onset of yield. From point B, the material undergoes plastic deformation; but there appears to be little variation of stress with increase in strain after yield in part C-D. That is followed by an increase in the slope which means that the material becomes hardened as more load is applied to enable more deformation to be achieved as shown in part D-E.

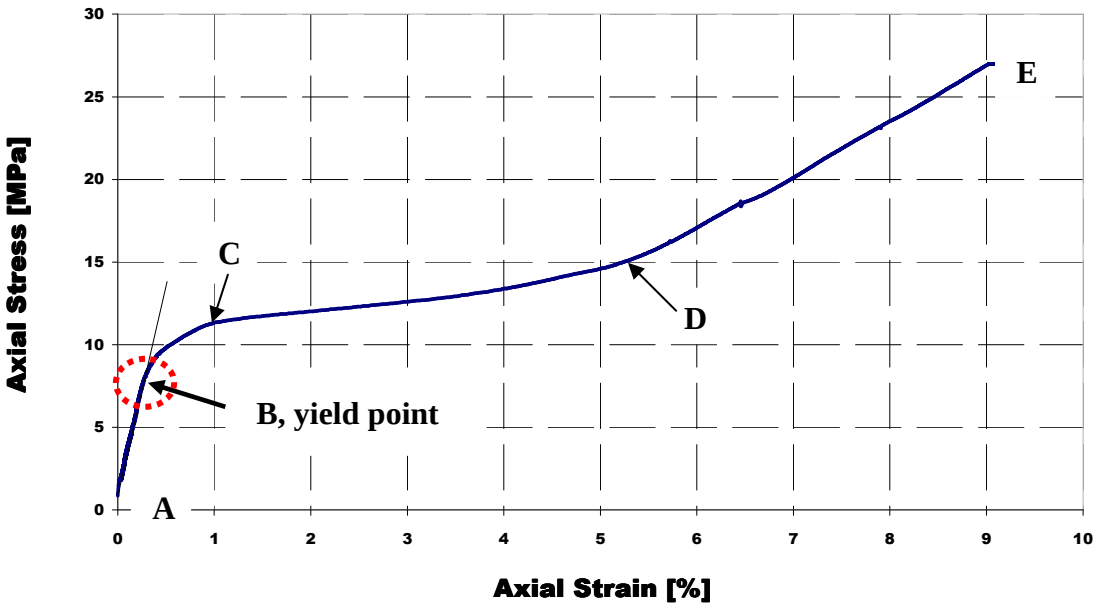

Fig.4.6 Yield curve for slow loading with core E3

4.3.4 Comparison of rapid and slow loading

As seen in the Fig.4.7, the yield stress is higher for the rapid loading compared with the slow loading.

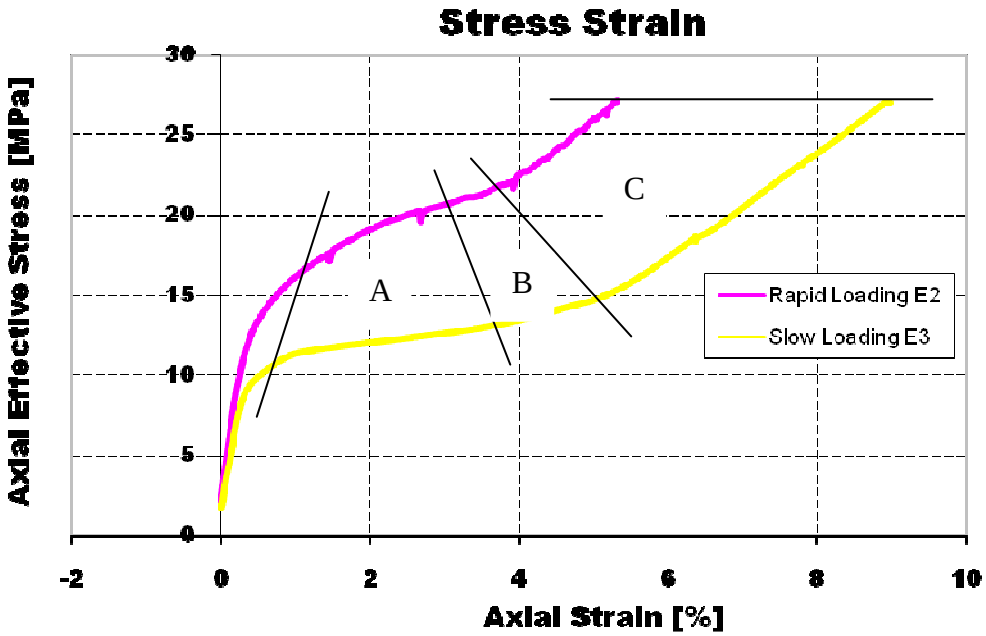

Fig.4.7 Comparison of curves for rapid and slow loading

The curves are similar in shape and there are two distinct regions A and C which are linear after yield. The regions are separated by a transition zone B since the hardening process is not an instant one but builds up gradually. Region A may be described as where most strain is seen for any change in the axial stress and not much amount of increasing stress is required to achieve additional strain; whereas in the C region, the material tends to harden as the grains are re-packed and gets more compacted and the slope increases signifying that an increasing stress is required to achieve some additional plastic deformation.

4.4 q-p Plot

This is a curve of the axial differential stress versus the mean effective stress during the pore pressure depletion. The axial differential stress is the difference between the effective axial stress [$\sigma_1^{'}$] and the effective lateral stress [$\sigma_2^{'} = \sigma_3^{'}$] while the mean effective stress is the average of the effective axial stress and the lateral stresses. The lateral stresses in these tests are equal since the confining fluid exerts the same amount of stress in the lateral directions due to the cylindrical nature of the cores. If an 'end cap' is placed on a Mohr-Coulomb diagram and this plot projected on it, the curve is expected to pass though the pore collapse

side of the diagram. In other words, pore collapse starts when the stress state reaches the 'cap' part of the failure envelope [refer to Fig.2.11]. This compaction results in an irreversible reduction in the porosity of the sample as a consequence of pore collapse. As plastic deformation occurs, the compaction cap shifts to the right as a function of the accumulated plastic strain.

4.4.1 Rapid Loading

From Fig.4.8, the differential stress varies linearly with the mean effective stress from point A. At point B there is a deviation and that marks the start of yield and there seems to be a slight deviation from linearity up to point C, beyond which the differential stress seems to vary less with increase in the mean effective stress. That is the start of strain hardening.

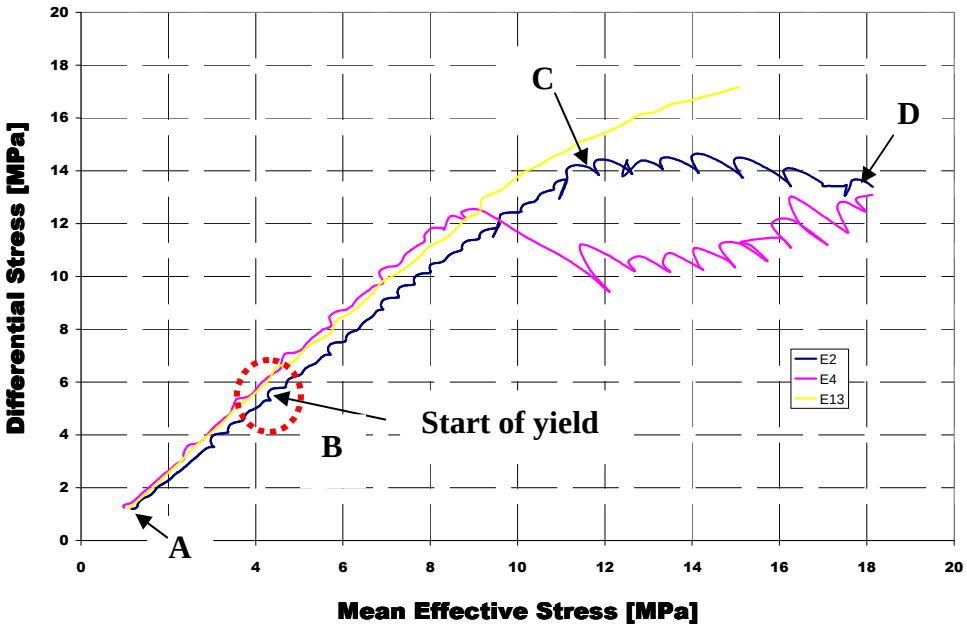

Fig.4.8 q-p' plot of rapid loading with cores E2, E4 and E13 using E2 to illustrate

4.4.2 Intermediate Loading

In **F**ig.4.9, using E16, the material yielded in pore collapse in point B and there is a deviation from the linear curve observed from point A. From point B, less additional stress is required to strain the sample up to point C after which the material hardens and more stress is required to produce additional strain. Evidently, from the curves, there seems to be two sets that behave alike; [E8, E16] and [E11, E12].

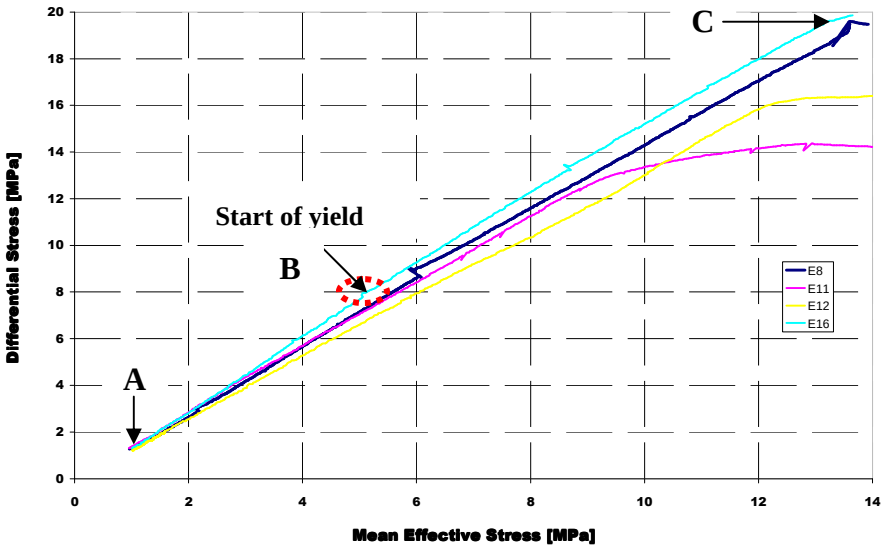

Fig.4.9 q-p' plot of Intermediate loading of E8, E11, E12 and E16 using E16 as example

4.4.3 Slow Loading

In Fig.4.10, from point A, the material deforms linearly up to point B where it yielded and plastic deformation is started. Point B on the q-p plot corresponds to a point on the 'cap' part of a Mohr-Coulomb diagram where pore collapse starts. If the curve is followed up from the behavior observed in the curves of stress-strain, then at point C, the material becomes stiffened and then the slope increases gradually and this should be happening outside the cap envelope.

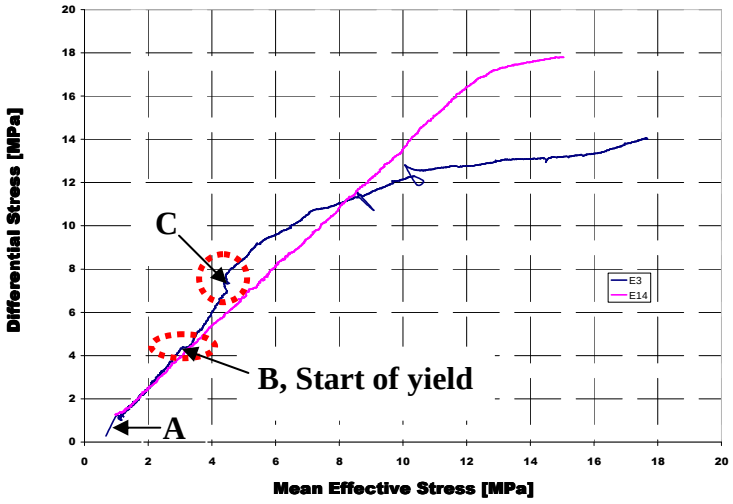

Fig.4.10 q-p' plot of slow loading of cores E3 and E14 with E3 used to explain

4.4.4 Comparison of q-p' plots at different loading rates

From Fig.4.11, the curves compare very well before yield at the different load rates as they are linear and are quite close to one another. The variation in behavior seems to come after yield where the curves begin to deviate as the stress state changes. On might say that the response of chalk samples to variation in stress state is similar before yield [pore collapse]. It is after then that the grains begin to react differently. The stress response of the core samples due to rapid loading tend to be less compared to slow and even intermediate loading, but that is only so up till point C, thereafter the differential stress seems to be constant with increase in mean effective stress for both rapid and slow loading. The ''cross-point'' C seems to be the point when the stress response of rapid loading equalizes with that of slow loading and as the pore pressure continues to be depleted, the differential stress increases for sometime before becoming constant.

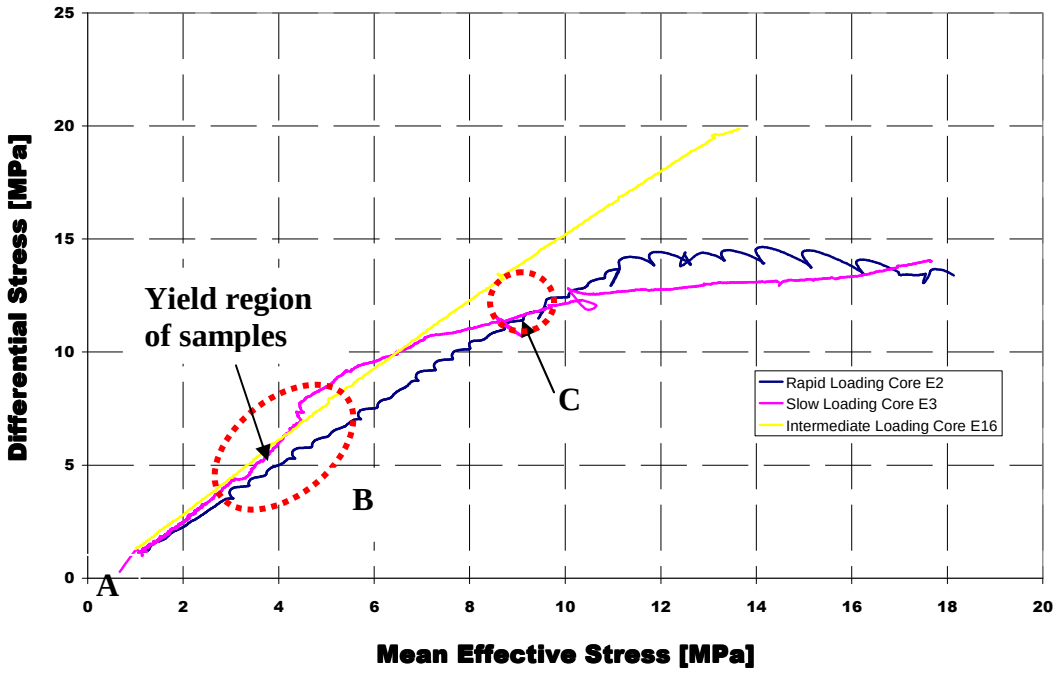

Fig.4.11 Comparison of the q-p' plots at different loading rates

4.5 Stress Path

It was observed in the tests as shown in Table 4.5.1 that for rapid loading, the values of the stress path range from 0.24-0.27 in the elastic region and 0.44-1.0 in the plastic region, and for slow loading, it ranges from 0.24-0.27 in the elastic region and 0.49-0.74 in the plastic region, while for intermediate loading, the range is from 0.23-0.30 for elastic region and 0.28-0.75 in the plastic region.

Table 4.5.1 Stress paths at the different regions with different loading rates

Stress Paths		
Core	**Elastic region**	**Plastic region**
E2 [R]	0.27	1
E3 [S]	0.24	0.49
E4 [R]	0.27	0.67
E8 [I]	0.30	0.29
E11 [I]	0.26	0.71
E12 [I]	0.29	0.75
E13 [R]	0.24	0.44
E14 [S]	0.27	0.74
E16 [I]	0.23	0.28

4.5.1 Rapid Loading

From Fig.4.12, considering E2, there appears to be two linear parts of the stress path. Part A-B occurs at the elastic region and into the greater path of the plastic region and part B-C is in the plastic region. The point B marks the start of stiffening of the material, beyond which there is a change in slope as an increasing change in effective lateral stress is required to balance the increase in the effective axial stress. One might say that since the core has yielded and the grains are getting repacked, the porosity has reduced such that the change in the lateral and axial effective stresses tends to become the same as the slope is close to unity.

For sample E2, the value is 0.27 for the elastic range and 1 for the plastic range. For sample E4, the value is 0.27 for the elastic range and 0.67 for the plastic range while for sample E13, the values are 0.24 and 0.44 for the elastic and plastic ranges respectively.

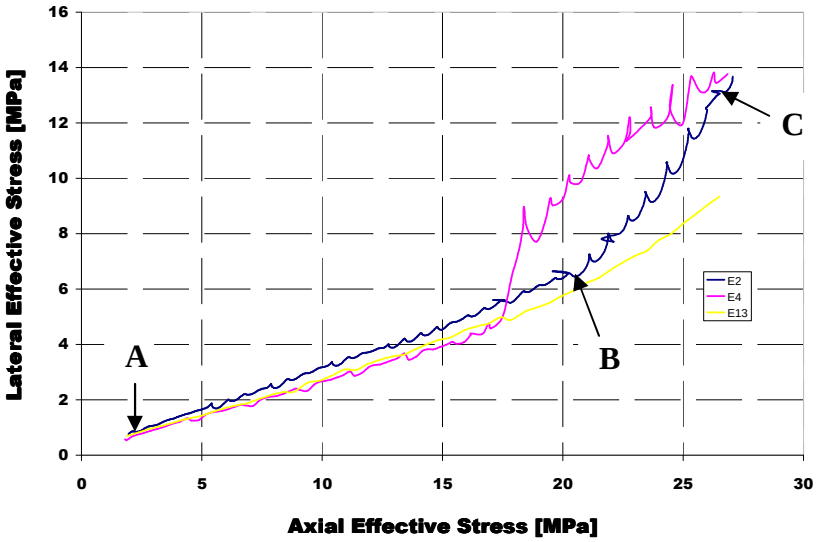

Fig.4.12 Comparison of stress paths for rapid loading samples of core E2, E4 and E13.

4.5.2 Intermediate Loading

Fig.4.13 shows a linear trend from the start of depletion at point A and at point B, there is a slight departure. The departure is sharp and one might say that the response of the material to lateral stresses at point of pore collapse is immediate. Though the trend continued thereafter, the part B-C shows some variations compared to A-B, maybe because it is occurring in the plastic region.

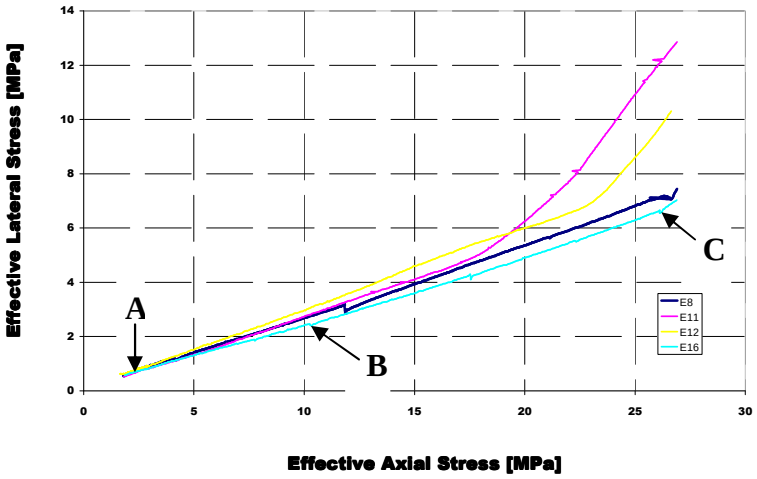

Fig.4.13 Comparison of stress paths for inter mediate loading of cores E8, E11, E12 and E16

4.5.3 Slow Loading

Fig.4.14 shows a departure from linearity from point A mainly at point B when the material yields. Though there is a drop in the lateral effective stress with axial effective stress still increasing around B, the trend did not last for a long time as the $\sigma'_{lateral}$ began to increase once more as seen in the change in the slope. Around point C, the material began to have strain hardening and the slope deepens further until it became linear. Point D marks the end of the loading phase [start of the creep phase].

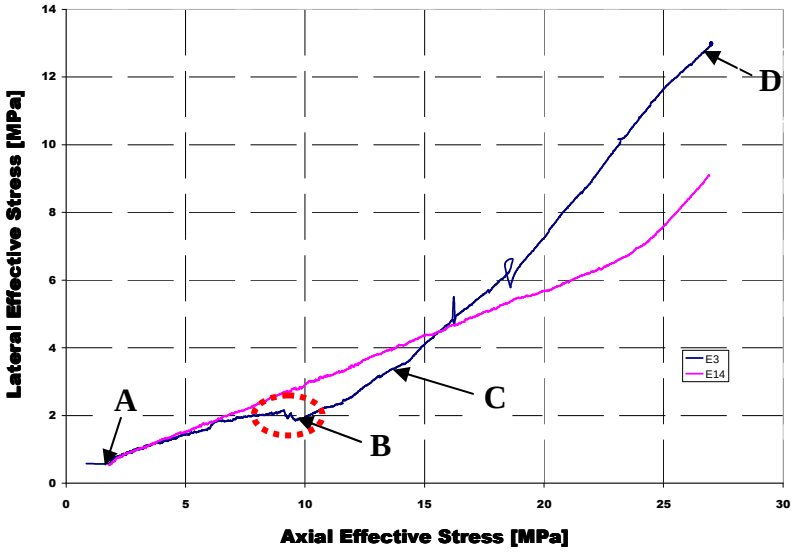

Fig.4.14 Comparison of stress paths for slow loading of core E3 and E14

4.5.4 Comparison of stress paths

From Fig.4.15 below, it appears that the slope of the curve changes once strain hardening begins. The observation is independent of the load rate because the increase was observed for both rapid and slow loading. One might say that the increase in the slope is a function of porosity drop as a result of compaction rather than load rate. The slight change in the curve for intermediate loading from point B to C is more pronounced in slow loading from B to D.

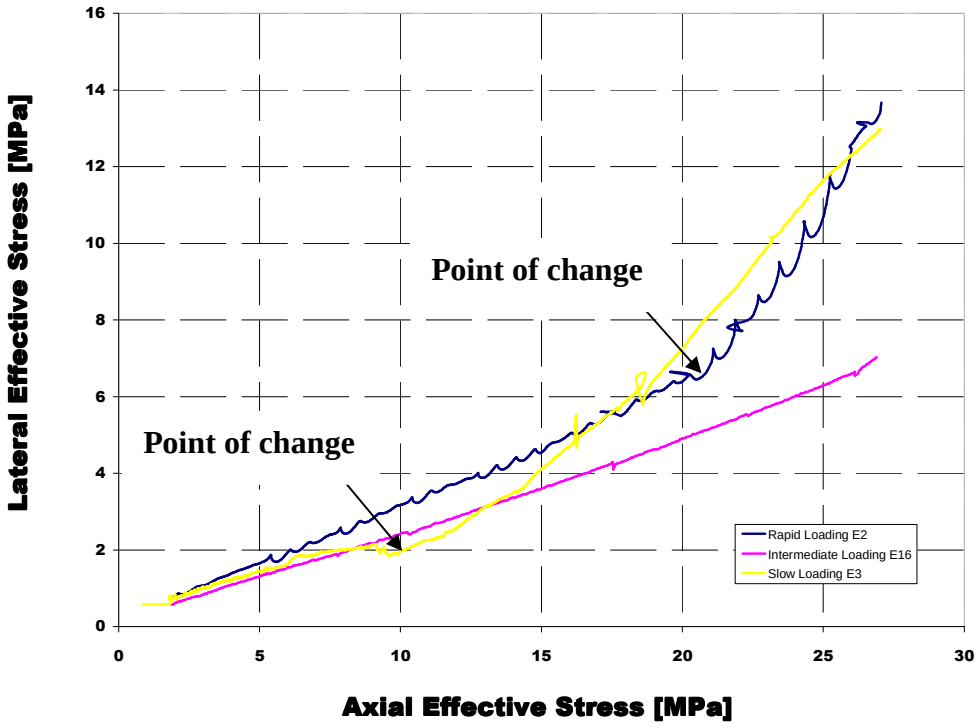

Fig.4.15 Comparison of stress paths for the different loading scenarios

4.6 Porosity versus Mean Effective Stress

The porosity versus mean effective stress follows the path as shown in the figures below. The curves for rapid, intermediate and slow loadings show similar trends during the depletion of a reservoir. The point B in Fig.4.16 is the onset of yield and plastic deformation occurs, followed by a change in the slope . The increase in slope corresponds to a large drop in the porosity of the sample per mean effective stress. This is because the inter-granular bonds have been broken leading to compaction of the materials. It has been shown that the porosity change of chalk is very close to the total plastic volumetric strain [axial strain for uniaxial strain test]. It means that the plastic volumetric strain is mainly contributed by the pore collapse and the compressibility of the chalk is negligible [Dahou, A. *et al.* (1995)].

4.6.1 Rapid Loading

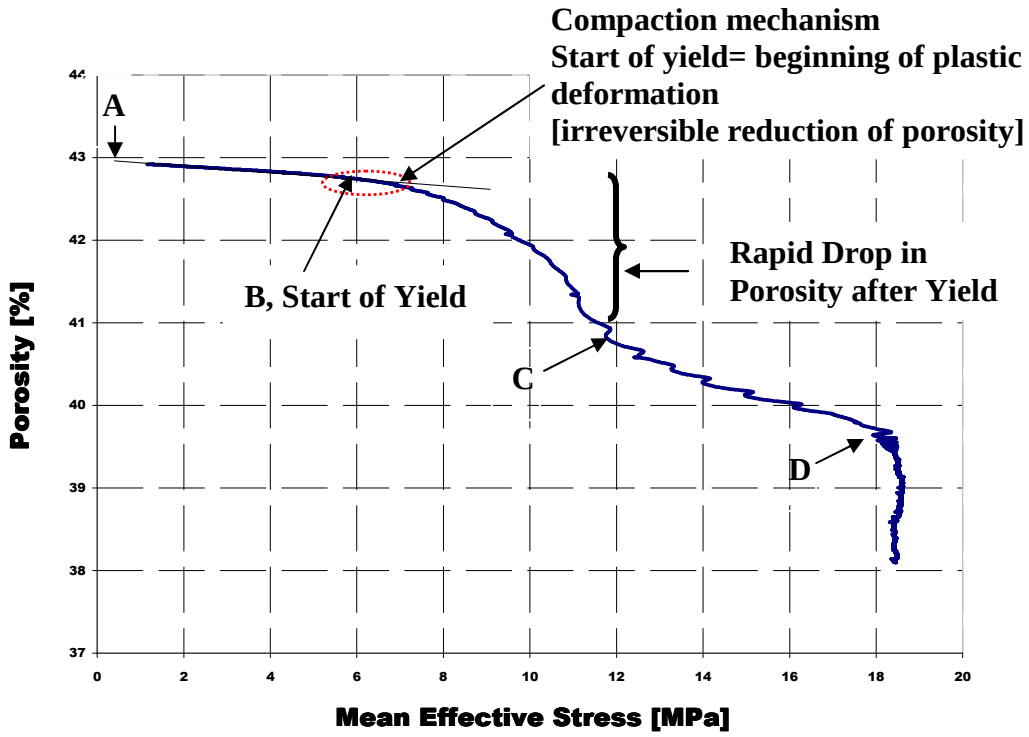

Fig.4.16 Change of porosity with mean effective stress of sample E2

From Fig.4.16 above, one can observe that the drop in porosity was linear with increase in mean effective stress from A-B. However after yield at point B, the drop in porosity became very sharp [B-C], and later stabilized with linear drop from point C-D. Point D marks the start of creep and there is little variation of porosity at constant mean stress.

4.6.2 Slow Loading

The difference between the Fig.4.16 above for rapid loading and Fig.4.17 below for slow loading is the introduction of loading cycles. As seen in the curves, the porosity drop trends are similar but in sections B-C, one would observe that the curve is steeper in slow loading than in rapid loading. It could be concluded that the rate of porosity drop in slow loading after yield is more that the drop after yield for rapid loading. Hence, porosity change during compaction is load rate dependent. This might not be conclusive because the initial porosity difference between the two samples is not much with E2 of 42.92% and E3 of 41.38%, but the pore volume of core E3 is less than E2 with 37.25 cm^3 and 39.08 cm^3 PVs respectively.

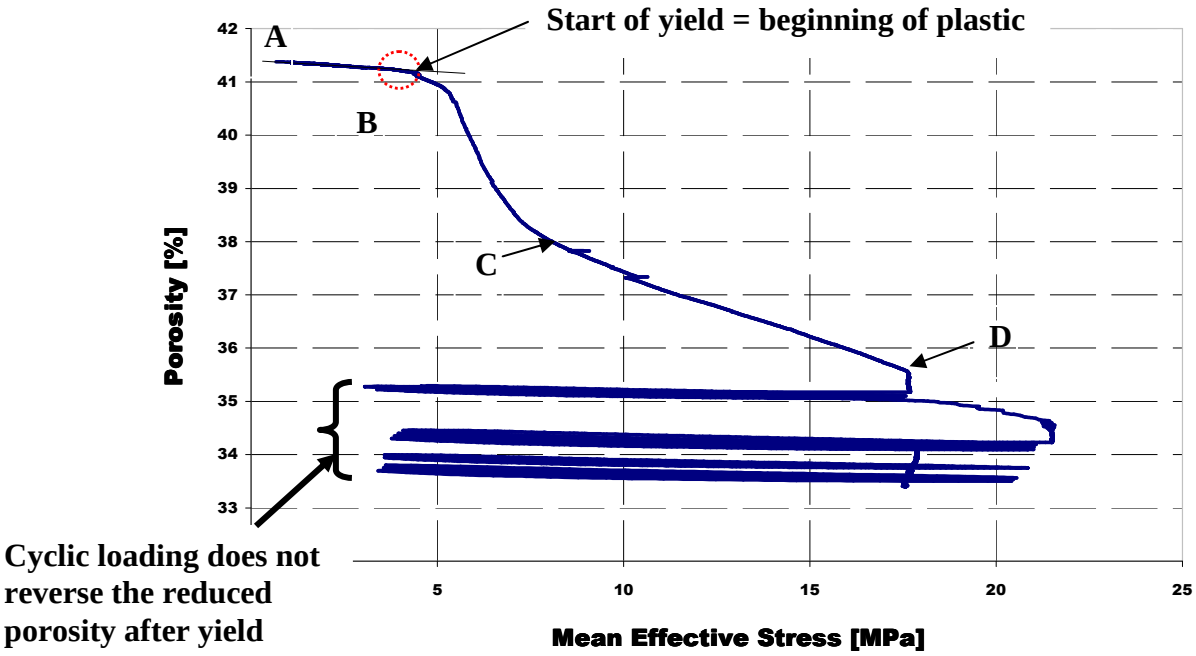

Fig.4.17 Change of porosity with mean effective stress of sample E3 with cyclic loading introduced during the creep phase

4.6.3 Intermediate Loading

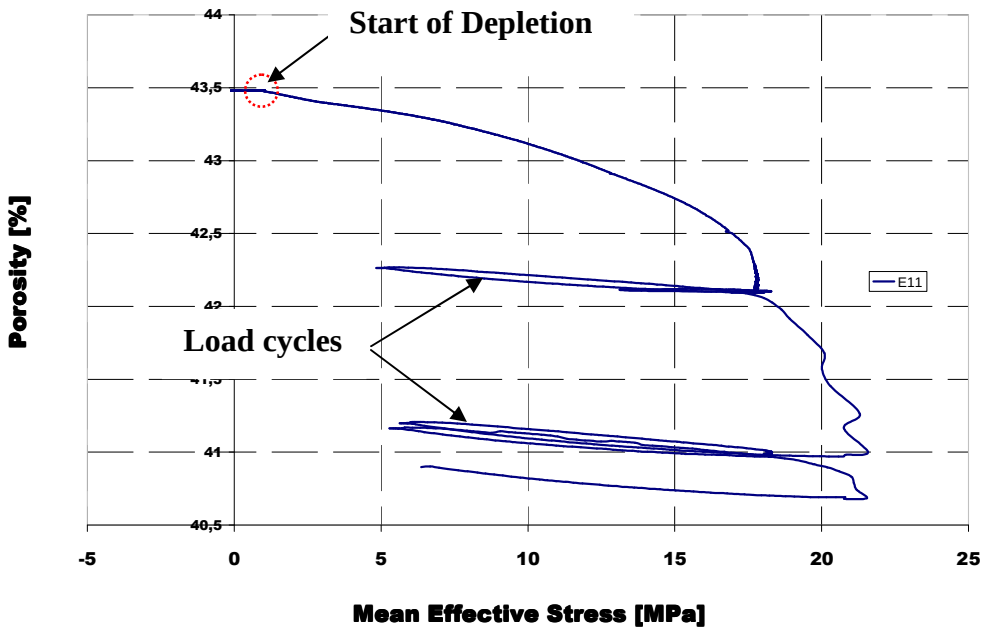

Fig.4.18 Change of porosity with mean effective stress of sample E11 with cyclic loading introduced during the creep phase

For Fig.4.18 of intermediate loading, it is difficult to detect the exact point of yield but one could see the effect of the mean stress on the loading cycles. The irreversible reduction in porosity is still maintained during the load cycles. The outcome is expected since the material has already deformed [strained] and it becomes difficult to regain the lost porosity. This observation is irrespective of the loading rate used.

4.7 Porosity versus Mean Effective Stress [Pore Pressure]

Expectedly, there is decrease of porosity with pore pressure depletion but since a uniform gradient was used for the pore pressure depletion for the different loading rates, one would ordinarily expect the porosity to decrease uniformly as well. But this is not the actual case because the pore pressure reduction which increases the effective stress on the grains governs the behavior of the materials [Terzaghi (1936)], especially when a material has got to the point of yield. As stated in previous sections, increases in the effective stress gets to a point where the material yields and the material's response to stress changes from elastic to plastic and as the material continues to compact. It is believed that the zone of deviation from the initial trend testifies to response in the chalk grains to effective stresses upon yield. It is a

zone of transition of plastic yield behavior. The trends are similar for the loading scenarios. From Fig.4.19 below for rapid loading of sample E4, porosity decreases with decrease in pore pressure form A to point B where the material yields and there is a change in the curve pattern from the initial linear to a transition zone of apparently ideal plastic behavior. This stage shows that there is no linear relation between the porosity and pore pressure as the bonding and cementation of the chalk particles are destroyed. This is equivalent to yielding in shear between the grains. This stage is followed by another linear curve C-D where the rate of reduction in porosity is directly proportional to the rate of pore pressure reduction. Though this part is linear, the slope is steeper compared to the earlier part. That could account for the fact that the chalk became stiffer after yield. The rate of decrease in porosity is then very high compared to before the yield [in the order of 0.02% per pore pressure reduction before yield and 0.18% per pore pressure reduction after yield]. In other words a drop in one unit of pore pressure induces as close as nine times a porosity drop in the plastic region than in the elastic region. The point D marks the beginning of creep phase with curves E and F representing loading and unloading respectively.

4.7.1 Rapid Loading

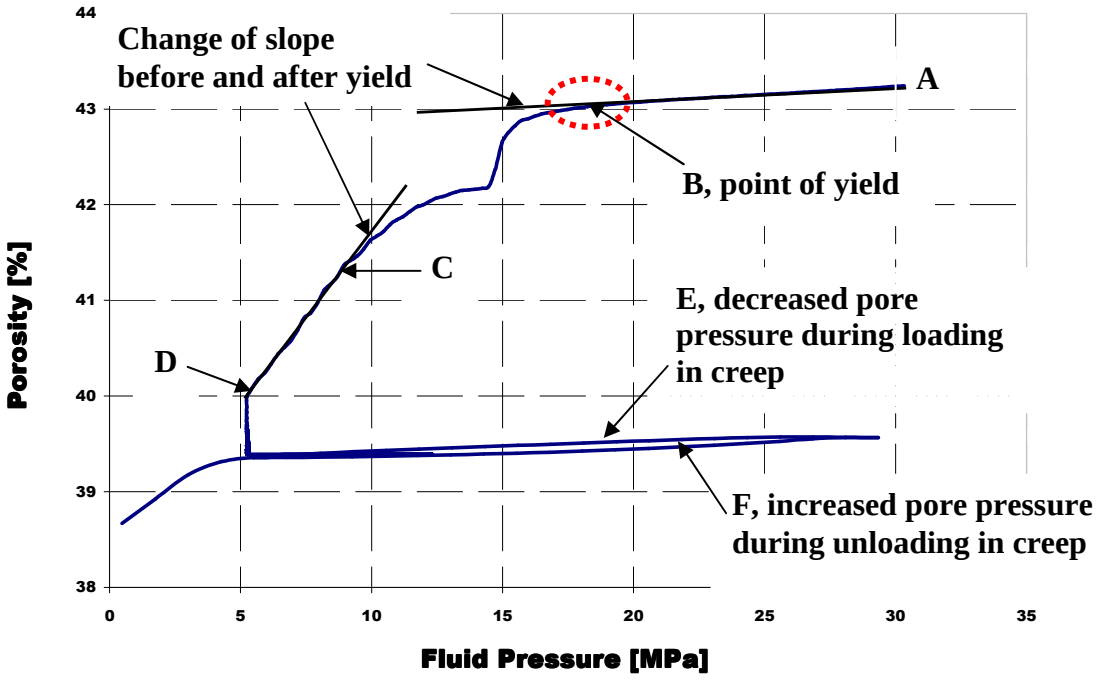

Fig.4.19 Porosity response of sample E4 upon pore pressure decrease during rapid loading with cyclic loading at the creep phase

Core sample E4 above decreased from its initial porosity of 43.24% to about 40% at the start of the creep phase. That is a loss of 3.24 %. Comparatively, core sample E2 decreased in porosity from 42.92% to 39.69% [please see appendix], about the same loss recorded in E4. As seen in the samples, they have different initial porosities but were loaded rapidly during the test but recorded the same amount of porosity drop. This is an interesting observation and if one checks the same change in porosity using mean effective stress, the same value still holds.

4.7.2 Slow Loading

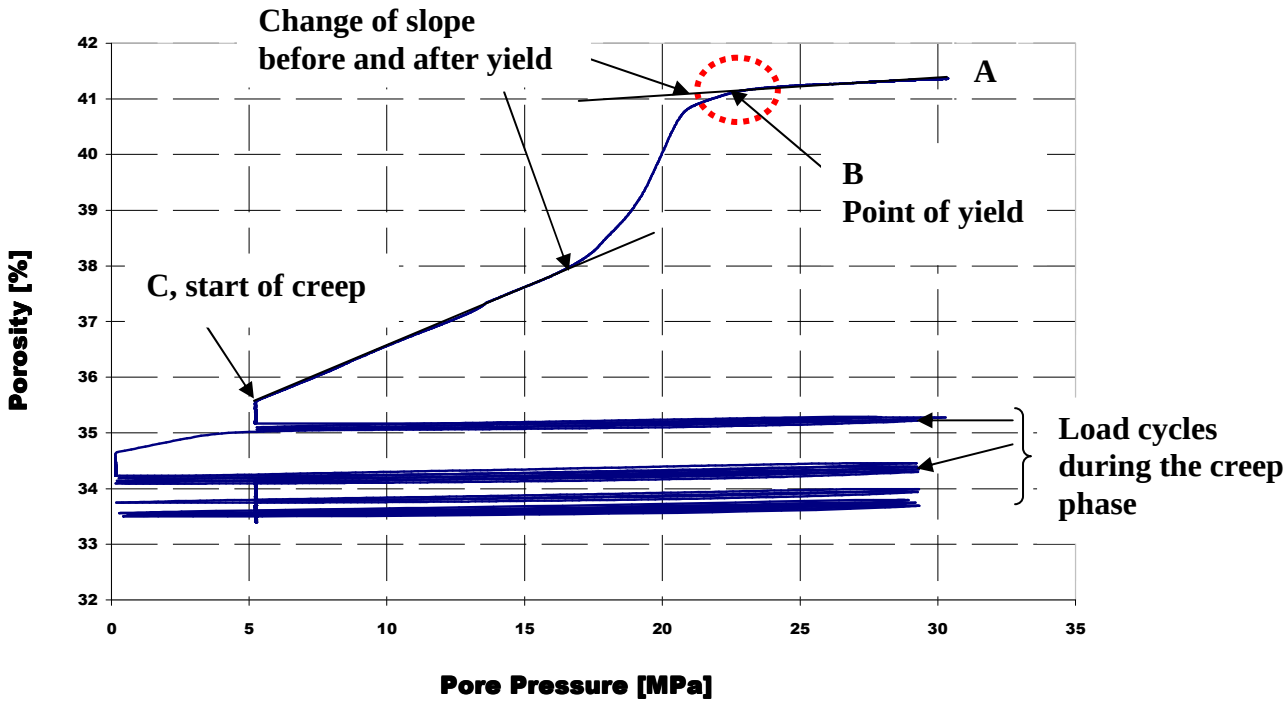

Fig.4.20 Porosity response of sample E3 upon pore pressure decrease during slow loading with cyclic loading at the creep phase

The sample E3 used for slow loading as shown in Fig.4.20 showed a drop in porosity from an initial value of 41.38% to about 35.5% at point C at the start of creep. The loss of 5.88% is larger than that recorded in the rapid loading cases of cores E2 and E4. One might then conclude that if porosity is a factor that influences creep, then creep behavior is loading rate

dependent. Hence, the behavior of the chalk core samples depends on the remaining porosity from the start of creep and coupled with the delay in pressure response of the grains [viscoelastic property], there is a variation in the creep response at different load rates.

4.8 Yield Stress

The yield stress in chalks marks the onset of pore collapse. This mechanism is a volumetric failure mainly activated where lateral displacement is either zero or small. It is a situation where shear failure cannot take place; hence the only mechanism for material disaggregation would be pore collapse through material failure.

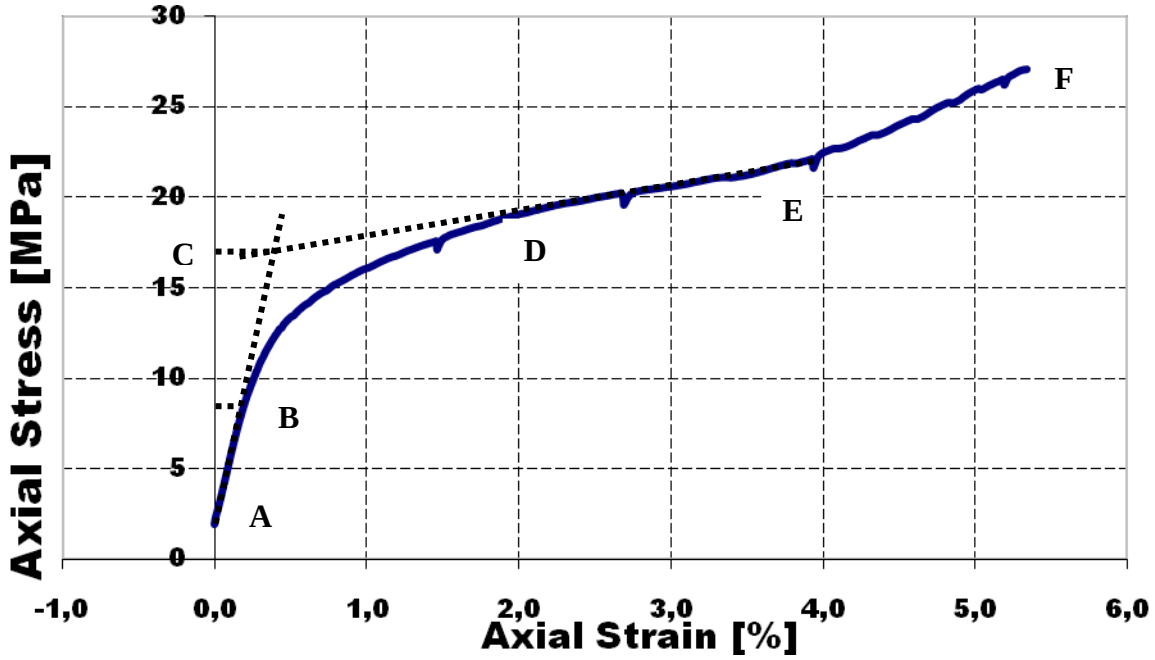

Fig.4.21 Method of determination of the yield stress

The yield stresses of the core samples were estimated from departure from linearity of the curve from the origin as indicated by the point B in Fig.4.21. The yield stress for the different loading scenarios varies and shows marked increase from slow to rapid loading. Though the yield stress [Havmøller and Foged] formula is a function of porosity; comparison is made to check for a trend.

$$\sigma_{yield}^{K_o} = 363e^{-7.36\phi} \qquad \text{[Eq.4.3]}$$

Table 4.8.1 Yield stress for rapid loading

Core name [rapid loading]	Yield stress [MPa]
E2	8.5
E4	11.5
E13	x

Table 4.8.2 Yield stress for intermediate loading

Core name [intermediate loading]	Yield stress [MPa]
E8	7
E11	10
E12	11
E16	11

Table 4.8.3 Yield stress for slow loading

Core name [slow loading]	Yield stress [MPa]
E3	6.5
E14	12

The yield stress from the formula gives a better comparison at high porosities with that from the test as the spread became closer, Fig.4.22. This shows that the porosity calculated from the measurements in the laboratory are far much less than the true porosity of Stevns Klint chalk as predicted from the formula. The formula was made from a best curve fit from the yield stresses of data from various samples. The difference could also be due to laboratory effects or maybe the database from which the relationship was proposed does not take the best of matches at several points. Otherwise, if the matching was done properly and the porosity measured in the laboratory is the same, then the formula should give a closer value with the yield stress estimated from the stress-strain curve.

However, there appears to be higher yield stresses for rapid loading compared to slow loading irrespective of the porosity of the samples as could be observed from the Table 4.8.4 below. The yield stresses for the intermediate loading tests show some inconsistencies relative to the rapid and slow loading scenarios as they could not be said to fall between the two. If porosity

is used as a basis to determine the yield stresses, one would observe that the samples with higher porosity values have low yield stresses. For instance, for samples E4, E11 and E12 whose porosities are greater than 43%, their yield stresses are much closer with less spread compared to samples E2, E3 and E8 whose porosities are less than 43% and their yield stresses are much closer. There then seems to be a grouping of the samples with those whose porosities are above 43% and those below 43 % behaving similarly in terms of yield. That seems to be irrespective of the loading rate used during the test, though samples E14 and E16 show some departure.

The yield stress of sample E13 could not be easily determined from the curve due to the irregularity in the deviation from the linear part. One then observes that the sample has the lowest porosity of all. It could then be concluded that the yield stress of a core sample of chalk is more predictable if the porosity is high enough. This needs to be confirmed by running more tests on core samples of similar or lower porosities.

Table 4.8.4 Comparison of the yield stresses at the various loading rates

Core	Porosity (ϕ)	Yield Stress $\left[\sigma_{yield}^{K_o}\right]$, MPa	Yield Stress $\left[\sigma_{yield}^{Test}\right]$, MPa
E2 [R]	0.4292	15.42	8.5
E3 [S]	0.4138	17.27	6.5
E4 [R]	0.4324	15.06	11.5
E8 [I]	0.4284	15.51	7.0
E11 [I]	0.4348	14.80	10.0
E12 [I]	0.4320	15.10	11.0
E13 [R]	0.4053	18.38	x
E14 [S]	0.4280	15.55	12.0
E15	0.4323	15.07	No test
E16 [I]	0.4117	17.54	11.0
E17	0.4328	15.01	No test

LEGEND	
R:	Rapid Loading
I:	Intermediate Loading
S:	Slow Loading

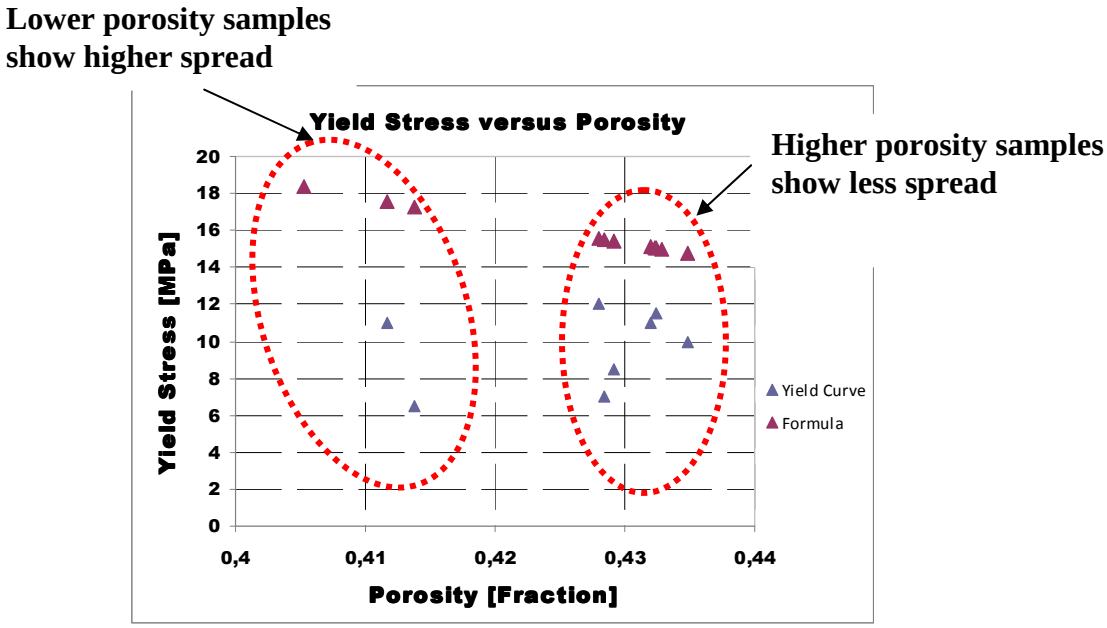

Fig.4.22 Comparison of the yield stresses of the various load rates from test with formula

One would also observe that a closer look at the yield stresses for the loading scenarios show that they yielded at the same level of stress if a deviation from the linear trend at the elastic region of the yield curve is chosen as the proper way to decide the yield stress. That does not mean that good and enough quality data points does not show varying yield stresses using the same criteria.

One could also choose the yield point by projecting a line from the linear portion of the yield region [D-E] and upwards from the elastic region [A-B] and using the point of intersection as the yield stress of the sample as shown in point C of Fig.4.21. Evidently, the value obtained with this method is higher than the value for the earlier method. However, the proper way to decide the point of yield and hence the yield stress remains an issue that needs proper and more attention in the chalk research.

4.9 Creep Strains

There are clear differences between the strains observed at the creep phases under the different loading scenarios. There appears to be a connection between the strain at the loading phase and the strain at the creep phases. When higher strain is exhibited at the loading phase, there tends to be a lower strain at the creep phases and vice versa.

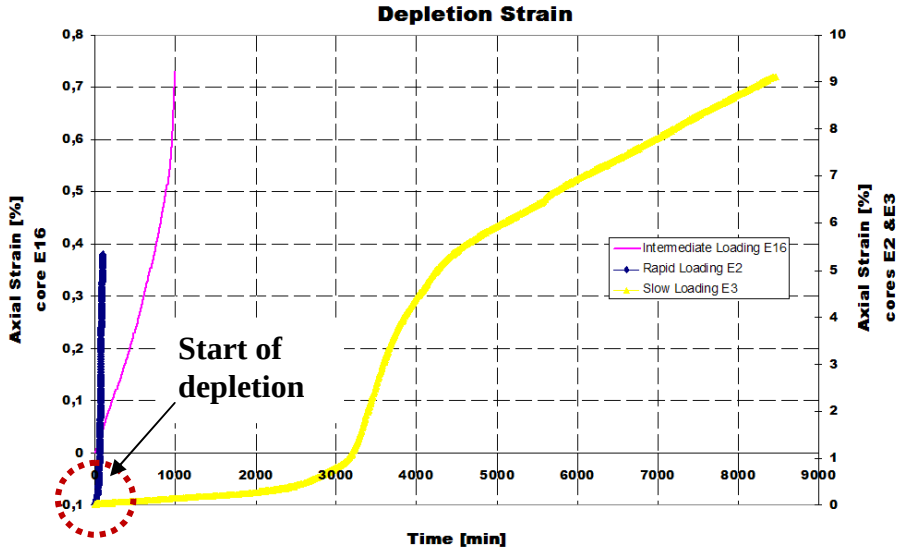

Fig.4.23 Comparison of the strains observed for slow [E3], rapid [E2] and intermediate [E16] loading scenarios during pore pressure depletion.

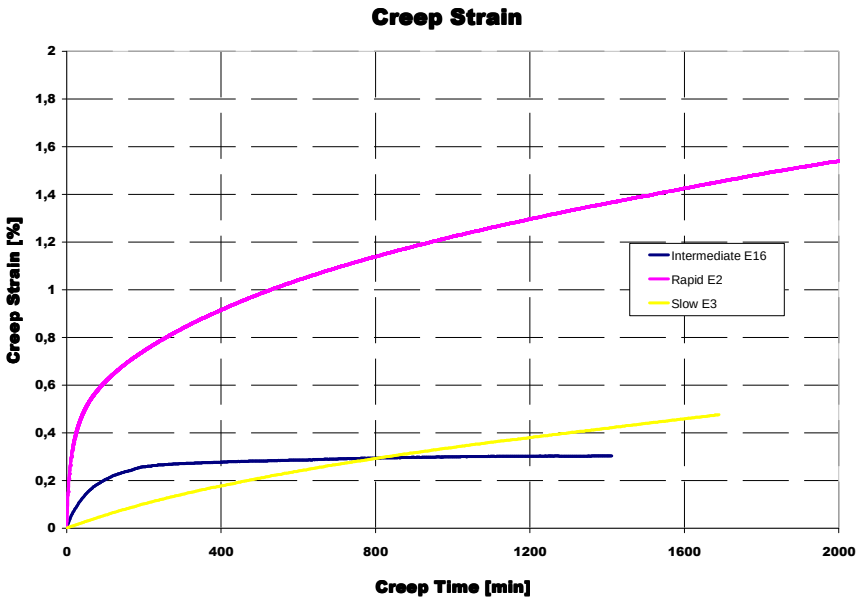

Fig.4.24 Comparison of the creep strains observed for slow, rapid and intermediate loading scenarios.

From Fig.4.23, for rapid loading [core E2], the strain observed during the loading [when the effective stress was increased by depleting the pore pressure] was lower compared to that observed during the slow loading. But at the creep phase, as seen in Fig.4.24, there was a significant difference in the strains on both scenarios. The rapid loading showed a rapid strain especially in the transient [primary] creep phase, followed by a reduced strain at the region described as the steady state or [secondary] creep stage.

Table 4.9.1 Creep strains for rapid loading

Core name [rapid loading]	Creep strain [%]		
	500 min.	1000 min.	2000 min.
E2	1.00	1.23	1.55
E4	0.74	0.78	0.82
E13	0.15	0.16	0.17

Table 4.9.2 Creep strains for intermediate loading

Core name [intermediate loading]	Creep strain [%]		
	500 min.	1000 min.	2000 min.
E8	0.38	0.41	0.48
E11	0.31	0.36	0.40
E12	0.28	0.29	0.31
E16	0.28	0.30	0.31

Table 4.9.3 Creep strains for slow loading

Core name [slow loading]	Creep strain [%]		
	500 min.	1000 min.	2000 min.
E3	0.21	0.33	x
E14	0.068	0.085	0.096

At about 500 minutes of normalized creep time into the creep phases, the strain in the rapid loading is 1% as shown in Fig.4.25 below for rapid loading. There was no accelerating [tertiary] creep stage observed in the creep strains.

For slow loading [core E3] in Fig.4.26, there appeared to be a lower strain and also a less rapid change in strain in the transient creep stage compared to the rapid loading. At about 500 minutes of normalized creep time into the creep phases, the strain in the slow loading is 0.20%. If this is compared with the strain in the rapid loading test, one could see a factor of 1:5. Though the ratio reduces as we get into the next stage [secondary phase], it shows that the creep strain, under different loading conditions is significantly high to be given some due considerations.

Within the same period, the strain observed in the core used for intermediate loading in this case [core E16] seems to have stabilized at a value of 0.3% when compared with the others, though a closer look by zooming into the plot shows that the material still creeps at a low rate. The creep strain observed in this case expectedly falls between the rapid and slow loading scenarios. The high creep was observed in the transient phase while the stabilization could be said to represent a state of low creep strain rate.

One would then ask the factors that contribute to this variation in the creep behavior of chalk under different loading rates. The porosities fall within the same range and hence might not be the differentiating factor. The effect of porosity could be investigated if the same load rate is used to test the cores so that variations could be accounted for by maybe also including the pore volumes.

As it is obvious that the cores had already yielded before the start of this creep period, one should then look at the behavior of chalk after yield together with the behavior before yield [elastic] to account for this observation. Though compaction has been defined as the irreversible reduction of porosity after compressive strength has been exceeded, the additional deformation and maybe reversible reduction in porosity before yield is taken into account [Settari, A. (2002)]. This is done by calculating the strain from the start of depletion where loading of the cores are started [increase in effective stress]. Since yield stress is higher for rapid loading than for slow loading, an onset of yield earlier in slow loading is accompanied by a sharp decrease in porosity and hence strains in the depletion phase that occur after yield begins earlier in slow loading. The material then deforms more in the longer time spent in the loading phase. This leads to a less strain observed during the creep phase.

Whereas for the rapid loading, the higher yield stress and short time does not permit strain enough to be seen in the depletion phase rather this is observed in the creep phase mainly at

the transient creep stage, due to the viscoelastic properties of the chalk grains. There appears to be a delayed response in the stress [pressure] changes during depletion. The delayed response is exhibited in the creep stage resulting in higher creep. Although this phenomenon happens also in the slow loading, the extra time allowed in this test for the loading allows for the viscoelastic behavior to be exhibited. Then more strain is observed during the loading phase, and in the creep phase, a lower value of strain then results. As explained in the discussion section, the strain is a combination of several factors.

One might also see creep strain from another perspective in that the yield of chalk causes a mobilization of the grains as the cementation is broken, and materials begins to re-orient in position. The dislodged particles then migrate through the porous, fluid filled medium, though facing some resistance from the fluids, unto other locations until they come to a point of rest. This point of rest prohibits further movement unless the bounding particles are themselves shifted. That would often be the case as loading continues. Then there tends to be an ever continuous migration of particles a far as there remains a porous [and permeable] medium. This particle movement happens through the matrix permeability and even enhanced by the presence of micro-cracks which are developed as strain continues. One might then say that creep is an ‘everlasting phenomenon’ especially in high porosity materials [chalk] which still retains high porosities, for instance 38.10 % at 5 MPa pore pressure after some creep period. From Fig.4.25 and Fig.4.26 below, one could see that the trend already established from the start of the creep signals continuous creep strains with time, though for slow loading, the curve is more linear [E3] from the beginning which shows less variation of strain at the various stages. This observation has been reported by several authors and several models exist that tend to predict how the curve would behave over a long period of time.

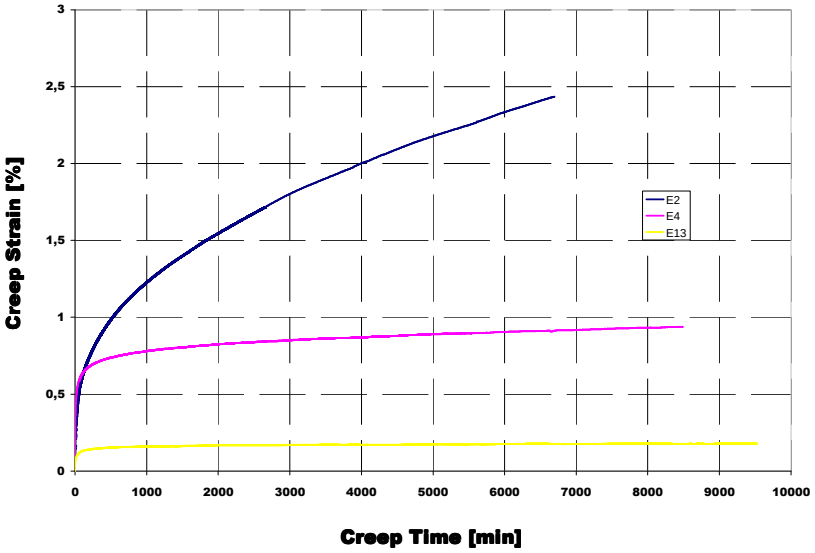

Fig.4.25 Creep strain for rapid loading of E2, E4 and E13

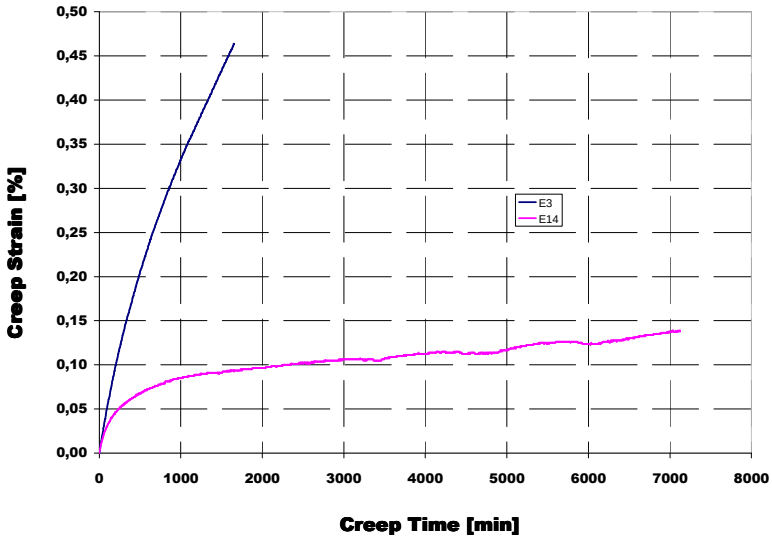

Fig.4.26 Creep strain for slow loading of E3 and E14

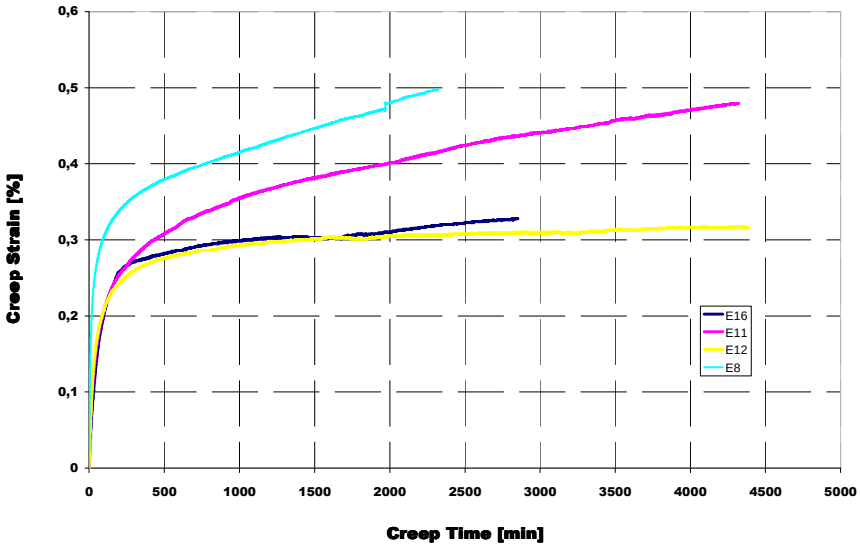

Fig.4.27 Creep strain for intermediate loading with cores E8, E11, E12 and E16

The Fig.4.28 below shows the comparison of the creep strain of some cores which shows that for intermediate loading, the creep strains falls between rapid and slow loading cases as was originally expected. Though core E14 seems not to show any strains after about 1000 minutes of creep time from the plot, one might conclude that creep does not last for slow loading. That is not exactly so since re-scaling of the plot would show the similar trend with the others. Conclusively, creep behavior of chalk is load rate dependent and the degree of variation of different samples at a particular load rate, example rapid loading depends on the peculiar properties of the sample used. If one tries to separate the plot into transient and steady-state phases of creep, it would be observed that the curves are more comparable in the transient than in the steady-state where it seems like some cores have stabilized and begins to creep alike in terms of trend. Models have been used to predict the persistence of the trends with time [Omdal, E. *et al.* (2009)].

If we assume that cores E4 [rapid loading], E11 [intermediate loading] and E14 [slow loading] are comparable, then after about 500 minutes of normalized creep time which observably falls within the transient phase, the creep observed are 0.74125%, 0.31019% and 0.06875% respectively; hence the core loaded rapidly had creeped in excess of 10 times that loaded slowly and 2 times that of intermediate.

After 1000 minutes of normalized creep time, it had creeped about 9 times as much as that in slow loading and 2 times that in intermediate and after 2000 minutes, about 8 times as much as slow loading and 2 times that of intermediate. If the intermediate and slow loadings are

compared at the different times as done above, one finds that the intermediate has the same excess strain of 4. The conclusion might be that the loading rate has to be widely different for variations in accumulated strains to differ with time.

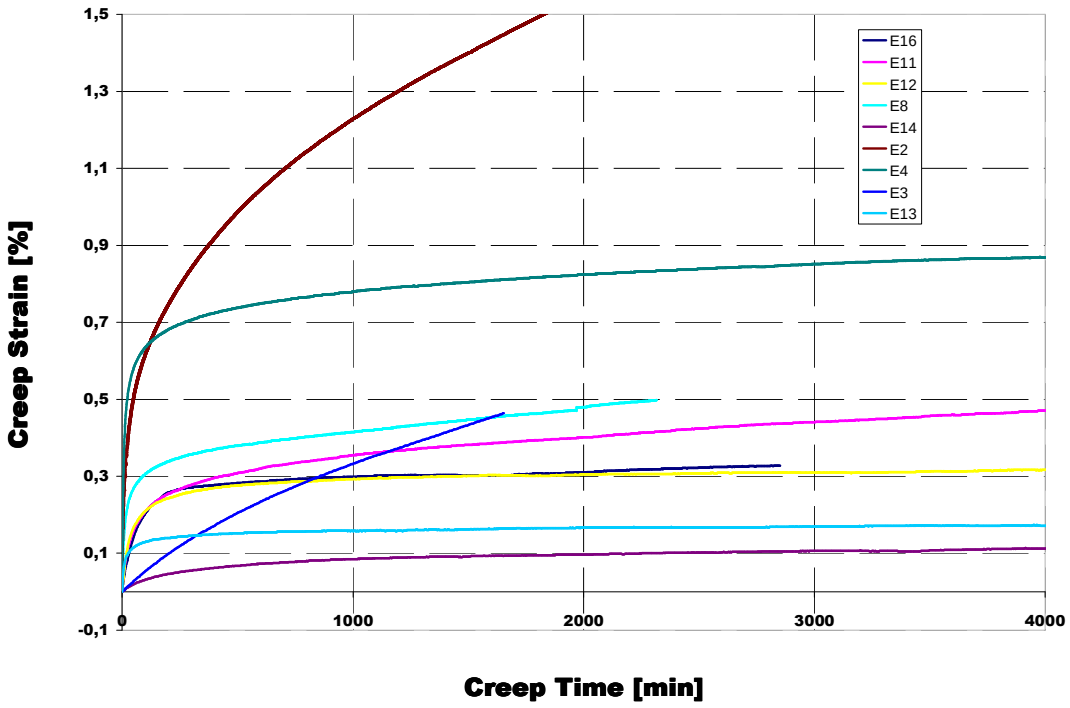

Fig.4.28 Creep strain for different loading rates used in the test; rapid loading [E2, E4 and E13], intermediate loading [E8, E11, E12 and E16] and slow loading [E3, E14]

4.10 Creep Rates

This is the observed rate of creeping over a time interval. It is extracted from the creep strain versus time plot and could be presented as strain [%] per hour, minute and decade.

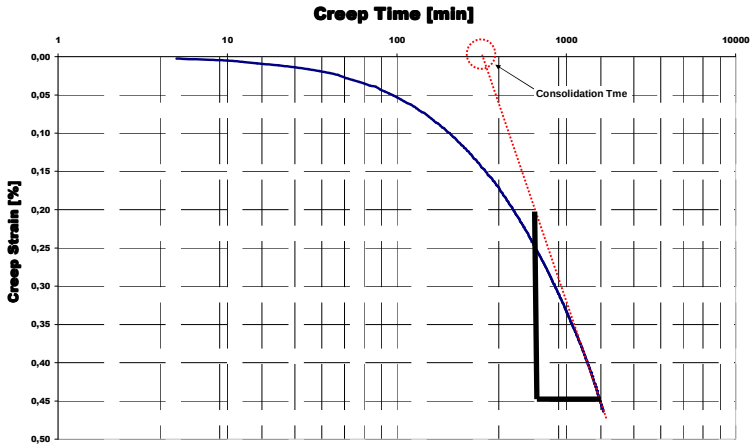

Fig.4.29 Determination of creep rate using method of Pattillo, P.D. *et al*. (1989)

One approach as shown in Fig.4.29 is by making a plot of the creep strain and the logarithm of time and obtaining the slope of the linear part [usually end] of the curve. It then becomes evident that enough data needs to be logged to be able to have a good curve to produce the linear side of the curve. Inadequate data points produces a continuous curve that never converges due to consolidation, hence no linear part might be seen. A projection of this linear part of the curve unto the time axis yields the consolidation time, which is the time used for the pore pressure equilibrium to re-equilibrate. One observes that this consolidation time decreases with the various creep periods introduced after each cyclic phase as shown in Fig. C11 in the appendix. These cycles serves to agitate and repack the chalk grains, though without re-establishment of the initial porosities.

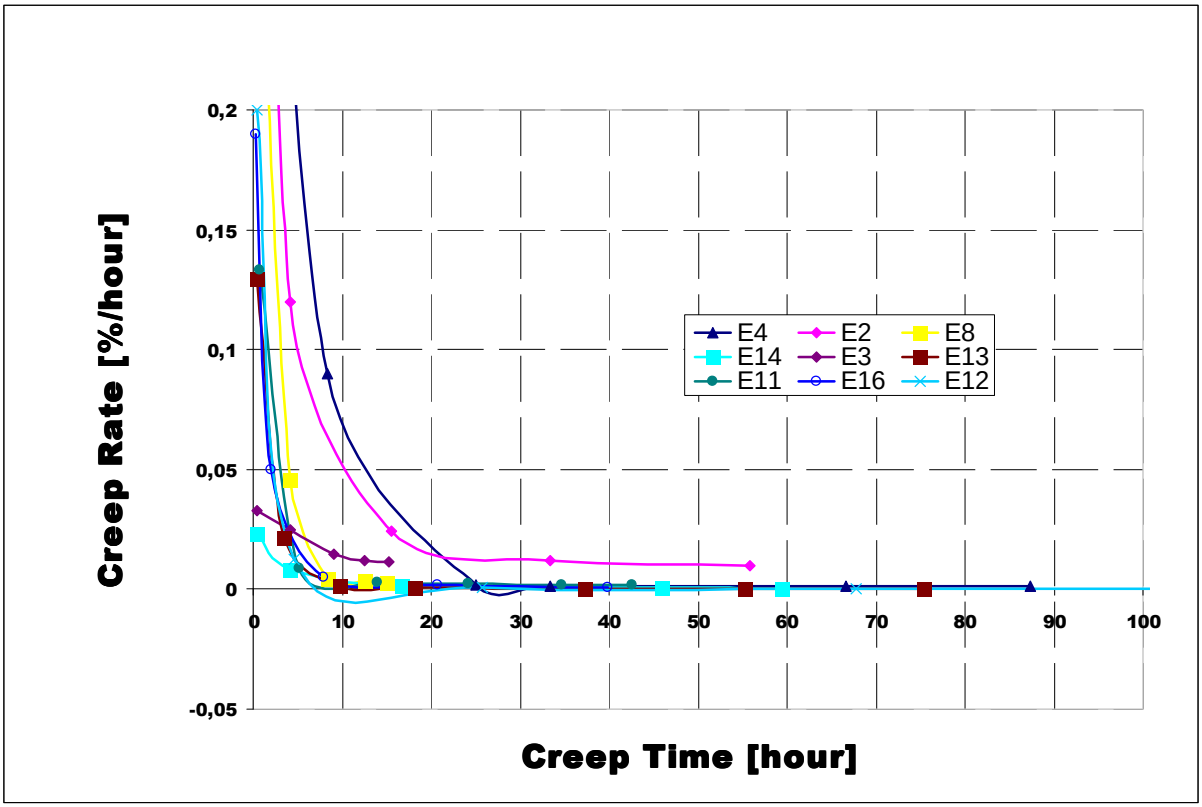

Fig.4.30 Plot of creep rate versus time

Another approach is to choose points from the normalized creep strain versus time curve and find the slopes and make plots as desired as shown if Fig.4.30 above. One observes that core samples E2 and E4 used for rapid loading has the highest creep rates before stabilizing at nearly constant creep rate, though E13 behaved differently; while samples E3 and E14 used in slow loading has the lowest creep rates prior to stabilization. Samples E8, E11, E12 and E16 are used for intermediate loading all fall between those of rapid and slow loading. One should also note that stabilization in this context means close to constant creep rate. Also, all the three curves for intermediate loading later intersected those of slow loading before stabilization and the rate curves for slow loading showed signs of stabilization earliest.

Generally, creep rate decreases with time at a very high rate at the start of the creep and then stabilizes after a time. One might say that the creep rate becomes constant after some time. It then follows that a material creeps as far as there is porosity and none of the samples stopped creeping as long as the tests were kept running.

From Fig.4.31 below, the creep rate is plotted against the log of time. It is observed that the rates tend to converge after some time irrespective of the load rate with the slow and intermediate loading converging earlier than that of rapid loading. One could then say that the intermediate load rate [0.025 MPa/min] used in the test results in behaviors of the sample that

tend towards the behavior of slow loaded materials in terms of creep rate. If another intermediate rate closer to rapid loading is used, the result should confirm if the rate should clearly separate or tend towards rapid loading.

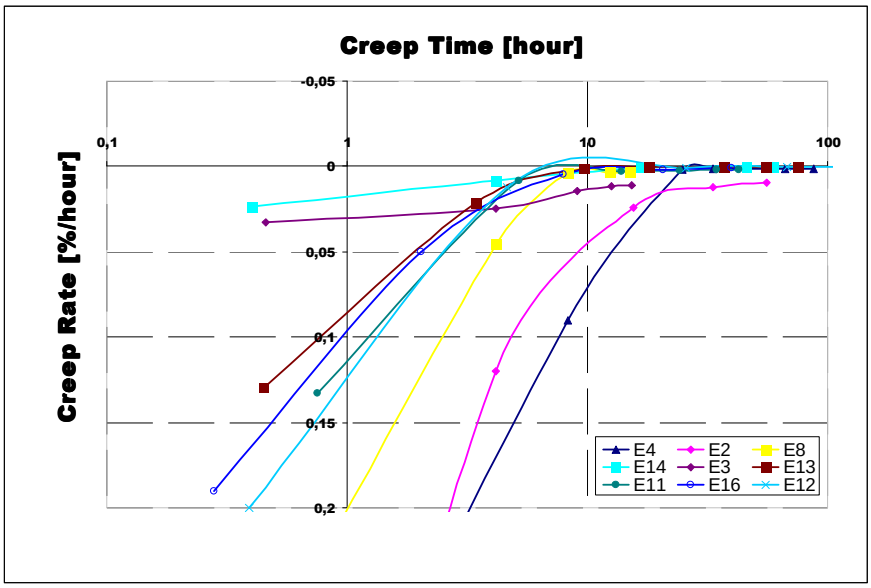

Fig.4.31 Plot of creep rate versus log of time for rapid loading [E2, E4 and E13], intermediate loading [E8, E11, E12 and E16], and slow loading [E3, E14].

Chapter 5: Discussion [Part B]

Deformations associated with those phases in the tests were examined to ascertain which ones affected the samples most or whether the strain will be the same. Physically, we are not in control of the lateral and overburden stresses in a reservoir but we can determine how the pore pressure will be depleted based on economic considerations, enhanced recovery capabilities, etc. All these would determine the rate of strain or deformation in chalk reservoirs that result from production of hydrocarbon. The tests give us an insight into what is expected.

It has been observed that when rapid loading was performed on the samples, the strain observed in the creep stage is more compared to the slow loading rate. However, this higher strain seems to occur very rapidly at the primary (transient) phase and then disappears gradually into the secondary phase with no strain at all in the tertiary phase. Conversely, the strain occurs slowly at the creep stage for the slow loading as evidently shown by the creep rates already discussed in section 4.10

It could be said that the total strain [compaction] experienced by a core sample is a combination of the elastic strain, plastic strain and visco strain, i.e,

$$\varepsilon_{TOTAL} = \varepsilon_{ELASTIC} + \varepsilon_{PLASTIC} + \varepsilon_{VISCO} + \varepsilon_{OTHERS}$$

The elastic strain is seen at pore pressure depletion stage of the test. It is a stage where any applied axial stress instantly results in an axial strain. The strain would varnish if the applied stress is removed from the sample. But because the pore pressure depletion continues up to the point of yield, the sample continues to compact and even if the stress is removed, a permanent deformation is left on the sample. At the start of creep, where the material would have yielded, the material skeleton continues to deform due to the viscoelastic properties. This deformation could be said to occur as a result of delayed pressure response of the chalk grains. This deformation (creep) then continues at a constant stress state after the pore pressure depletion had stopped. This is the contribution to the entire strain and hence could be said to be a visco strain.

Also crushing of the chalk grains and rearrangement under high effective stresses could result in another additional strain which seems to continue as long as the chalk sample has porosity. These crushed and smaller particles continue to settle and occupy spaces in the core sample. This crushing could be said to precede yielding when the bonds would have been broken and could be classified as ‘other’ strain. Other authors have discussed this same cause of creep. Andersen, M. A. *et al.* discussed that while a material is under constant loading, the support

structures continue to fail and happens at increasing rates as the load becomes higher due to lower values of pore pressure. When the forced load stops, the *cascade* resulting from the loading continues, usually noticed at the transient creep phase which is the first phase of the creep with highest strain and creep rate, indicating the time period during which the compaction continues at about the same rate before falling off.

For core E3, 3 cycles and 4 stages of creep was analyzed to examine the effect of the cycles on the creep behavior, Figs.C10 and C11 in the appendix. Increasing the pore pressure from an initial value of 5 MPa to 29 MPa, down to 0.07 MPa and so on is termed cycle. Load cycles were also introduced in core E4 and each of the materials creeped after application of the loads. These cycles load and unload stresses on the chalk grains. As a result, they are repacked tightly and the sample is expected to become stiffer. The strain observed after the cycles became smaller as expected if allowed to creep.

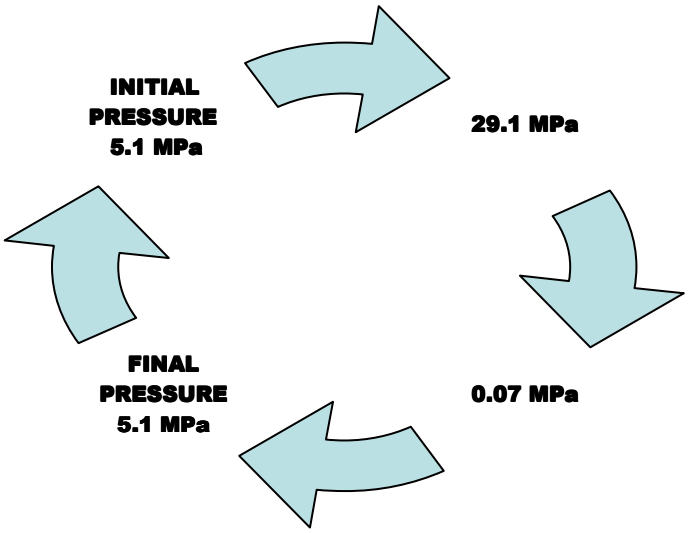

Fig 5.1 Load cycle phase

The cycle was performed to achieve certain levels of reorganization of the grains in the chalk. The results are seen as variations in consolidation times for the creep strains observed after the cycles. Trends were observed in the consolidation times as later stages of creep resulted in lesser consolidation times compared with earlier stages. Reduction in porosity of the samples after the cycles was observed as expected.

Chapter 6: Conclusions

[1] A change of load rate from lower to higher pressure gradient for different tests results in an apparently higher stiffness, yield stress, and elastic modulus [uniaxial compaction modulus] etc, hence the mechanical properties of chalk are loading rate dependent.

[2] Application of loading cycles in the creep phase affects the compaction behavior. This loading cycle involves increasing [unloading] and decreasing [loading] the pore pressure, as the effective stress is decreased and increased respectively. The grains are agitated, re-oriented and re-packed and as a result, they become stiffer and strain less. It was observed that the introduction of the cycles did not reverse the porosity already lost during the depletion phases.

[3] Consolidation time changes with application of more load cycles, the result showing a downward trend or decrease in consolidation time with more load cycles. This is because the material becomes stiffer as stated previously after every cycle phase. It therefore takes lesser time for the pore pressure equilibrium to re-equilibrate [consolidation].

[4] There is more loss of porosity during pore pressure depletion in slow loading compared with rapid loading from the start of depletion to the end [beginning of creep]. Hence, if creep is porosity dependent, one might say that it is load rate dependent.

[5] Creep rate is highest for rapid loading and lowest for slow loading, while that for intermediate loading are between the two.

[6] Since yield stress for rapid loading is higher, one can say that chalks can withstand more loads before yield if loaded rapidly than when loaded slowly.

Nomenclatures:

σ' - effective stress [MPa]
σ_T - overburden stress [MPa]
P_p - pore pressure [MPa]
α - Biot's constant [dimensionless]
E - elastic modulus [MPa]
H_e - uniaxial compaction modulus in the elastic region [GPa]
H_p - uniaxial compaction modulus in the plastic region [GPa]
$\varepsilon_{1,2,3}$ - change in strains, where subscripts 1, 2 and 3 denotes the principal directions
$\Delta\sigma'_{1,2,3}$ - change in effective principal stresses [MPa]
ν - Poisson's ratio [dimensionless]
m - matrix
b -bulk
c - compressibility [MPa^{-1}]
K -K-modulus (stiffness) [GPa^{-1}]
ϕ -porosity [%]

Assumptions:

- Uniaxial compaction
- Elastic rock behavior
- Biot's factor of 1 for chalk
- No lateral deformation [constant core diameter]

References:

[1] Fjær, E., Holt, R.M., Horsrud, P., Raaen, A.M., and Risnes, R.: 'Petroleum Related Rock Mechanics, 2nd Edition (2008) ', Developments in Petroleum Science 53. Elsevier Radarweg 29, PO Box 211, 1000 AE Amsterdam, The Netherlands; The Boulevard, Langford Lane, Kidlington, Oxford OX5 1GB, UK, (2008).

[2] Alex Maltman,: 'The Geological Deformation of Sediments', Chapman & Hall, 2-6 Boundary Row, London SE1 8HN, UK, (1994).

[3] Charlez, P.A.: 'Rock Mechanics (Volume 2) Petroleum Applications', Editions Technip, 27 Rue Ginoux 75737, Paris, (1997), pp. 1-71.

[4] Aadnøy, B.S.: 'An Introduction to Petroleum Rock Mechanics', (1997), Rock Mechanics Compendium, Revised 2 August, (2003).

[5] Risnes, R.: 'Deformation and yield in high porosity outcrop chalk'. Physics and Chemistry of the Earth, Part A: Solid Earth and Geodesy 26, 53–57, (2001)

[6] Flugel, E.: 'Microfacies of Carbonate Rocks; Analysis, Interpretation and Application', Springer-Verlag Berlin Heidelberg, (2004).

[7] Selley, R.C.: 'Elements of Petroleum Geology', San Diego-Academic Press, (1998).

[8] Zolotuchin, A.B., Ursin J.R.: 'Introduction to Reservoir Engineering', (2000).

[9] Monjoi, A., Shroeder, C., Prignon, C., da Silva, F., and Debande, G.: 'Establishment of Constitutive Laws of Chalk and Long Term Tests', Third North Sea Chalk Symposium, Copenhagen Denmark, June 11-12, (1990).

[10] Osborne, M.J., Swarbrick, R.E.: 'Mechanisms for generating overpressure in sedimentary basins: A re-evaluation', AAPG Bull. 81, 1023-1041, (1997).

[11] Yassir, N., Addis, M.A.: 'Relationships between pore pressure and stress in different tectonic settings"'. In: Huffman, A.R., Bowers, G.L. (Eds.), Pressure Regimes in Sedimentary Basins and their Prediction: AAPG Memoir, pp. 79–88, (2002).

[12] Chang, C.T., Zoback, M.D.: 'Viscous Rheology and State of Stress in Unconsolidated Sands', SPE/ISRM 47401, Trondheim Norway, 8-10 July, 1998.

[13] Cole, K.S., Cole, R.H.: 'Dispersion and Absorption in Dielectrics', *Journal of Chemical Physics*, (1941) 9, 341-351.

[14] Gross, B.: 'On Creep and relaxation', *Journal of applied physics* (1947) 18, 212-20.

[15] Tucker, M.E.: 'Sedimentary Petrology An Introduction', Geoscience Texts Volume 3, pages 96-157.

[16] Leeder, M.R.: 'Sedimentrology Process and Product', pages 15-29, 285-302.

[17] Seright, R.S., Laing, J., and Seldal, M.: 'Sizing Gelant Treatments in hydraulically Fractured production Wells', SPE 52398, SPE Production Facilities November (1998), pp 223-229.

[18] Settari, A.: 'Reservoir Compaction', SPE 76805, University of Calgary, August (2002).

[19] Liingaard, M., Augustesen, A., Poul V. Lade.: 'Characterization of models for Time-Dependent Behavior of Soils', 10.1061/(ASCE) 1532-3641 (2004) 4:3 (157)

[20] Santarelli, F.J., Tronvoll, J. T., Svennekjaer, M., Skeie, H., Henriksen, R., Bratli, R. A.: 'Reservoir Stress Path: The Depletion and the Rebound'', SPE/ISRM Eurock '98 Trondheim, Norway, 8-10 July (1998).

[21] de Waal, J.A., Smits, R.M.M.: 'Prediction of Reservoir Compaction and Surface Subsidence: Field Application of a New Model', SPE 14214, June (1988).

[22] Sulak, R.M.: 'Ekofisk Field: The First 20 Years', JPT (October 1991), 1265, Trans., **291**.

[23] Havmøller, O. and Foged, N. 1996. "Review of Rock Mechanics Data for Chalk," Proc. 5th North Sea Chalk Symposium, Reims, France, 7.-9. October

[24] Ruddy, I., Andersen, M. A., Pattillo, P. D., Bishlawl, M., Foged, N.: 'Rock Compressibility, Compaction, and Subsidence in a High-Porosity Chalk Reservoir: A Case Study of Valhall Field', SPE 18278, (1989).

[25] Shafer, J.L., Boitnott, G.N., Ewy, R.T.: 'Effective Stress Laws for Petrophysical Rock properties', Society of Petrophysicists and Well Log Analysts (SPWLA), Edinburgh, Scotland, May 25-28, (2008).

[26] Leddra, M.J., Jones, M.E., Goldsmith, A.S.: 'Laboratory Investigation of the Compaction of Chalk under Conditions of Increasing Effective Stress', Sediment Deformation Research, Department of Geological Sciences, University College London.

[27] Johnson, J.P., Rhett, D.W., Slemers, W.T.: 'Rock Mechanics of the Ekofisk Reservoir in the Evaluation of Subsidence', SPE 17854, Offshore Technology Conference, July, (1989).

[28] Teufel, L.W., Rhett, D.W.: 'Geomechanical Evidence for Shear Failure of Chalk During Production of the Ekofisk Field', SPE 22755, Dallas Texas, October 6-9, (1991).

[29] Hjuler, M.L.: 'Silica and Clay Mineralogy and Distribution in Reservoir Chalk (Valhall) and Outcrop Chalks (Stevns, Aalborg and Liege)', Technical University of Denmark, (2006).

[30] ''Quizix Pump-works User's Manual''.

[31] Geertsma, J.: 'Land Subsidence Above Compacting Oil and Gas Reservoirs', SPE 3730, June, (1973).

[32] Jones, M.E., Leddra, M.J.,: 'Compaction and Flow of Porous Rock at Depth', Rock at Great Depth Symposium, (eds. Maury, V. and Fourmaintraux, D.), Pau, France, August, 1989, A. A. Balkema, Rotterdam, pp 891-898.

[33] de Waal, J. A.: 'On the Rate Type Compaction Behavior of Sandstone Reservoir Rock', Thesis at The University of Delft, (1986).

[34] de Waal, J. A., Smits, R. M. M., van Kooten, J. F. C.: 'Prediction of Abrupt Reservoir Compaction and Surface Subsidence Due to Pore Collapse in Carbonates', SPE 15642, June, (1988).

[35] Holt, R. M.: 'Mechanics in Earth Science and Petroleum Engineering', TKT4125 Lecture Notes, NTNU, (2003).

[36] Dahou, A., Shao, J. F., Bederiat, M.: 'Experimental and Numerical Investigation on Transient Creep of Porous Chalk', Laboratoire de Mecanique de Lille, URA 1441 CNRS, Villeneuve d'Ascq cedex, France, Elsevier Science B.V., (1995).

[37] Thomas Lindsay Blanton III.: 'Deformation of Chalk Under Confining Pressure and Pore Pressure', SPE of AIME, February, (1981).

[38] Andersen, M. A., Foged, N., Pedersen, H. F.: 'The Link Between Waterflood-Induced Compaction and Rate-Sensitive Behavior in a Weak North Sea Chalk',

[39] Hadi, B., Alireza N.: 'Reservoir Rock Behavior pre and Post Pore Collapse during Production', International Petroleum Technology Conference, IPTC 11657, Dubai, 4-6 December (2007).

[40] Omdal, E., Madland, M.V., Korsnes, R.I., Hiorth, A., Nagel, N.B.[CoP] and Kristiansen, T.G. [BP]: 'Deformation Behavior of Chalk studied close to In-Situ Reservoir Conditions', University of Stavanger, (2009).

Websites Visited

[a] www.wikipedia.org

[b] www.slb.com

[c] http://www.rdpe.com/displacement/lvdt/lvdt-principles.htm

[d] http://www.welltec.com/dictionary.aspx

[e] http://www.chalk.no

[f] http://www.singletonbirch.co.uk/

[g] http://www.geologyshop.co.uk/chalk.htm

Appendices:

Part A

Pressure History

Rapid Loading

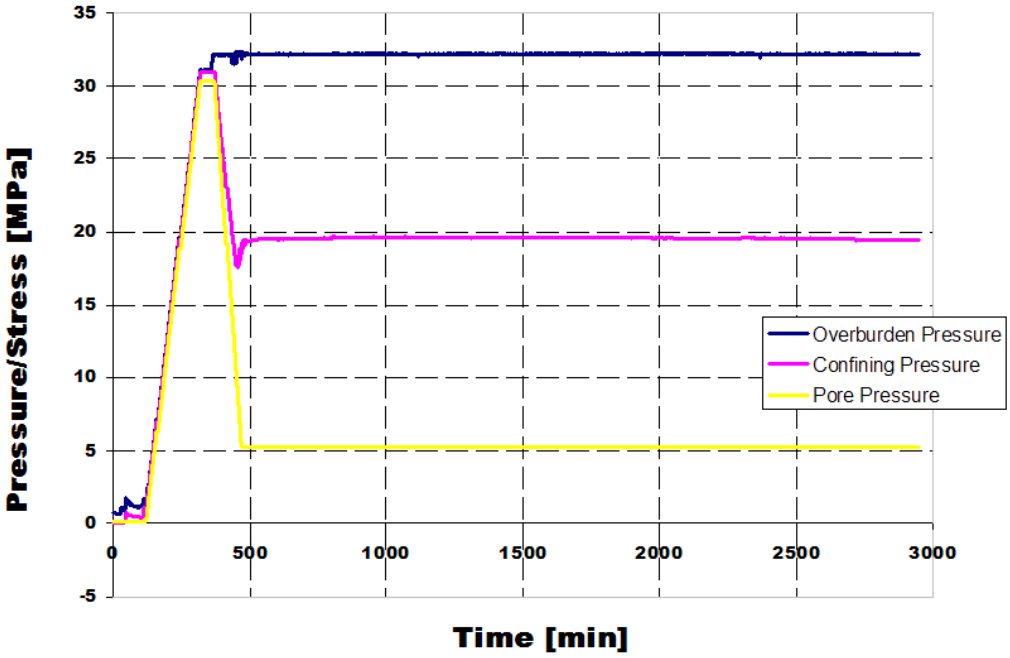

Fig.A1 Pressure history of core E2 from ramping to pore pressure depletion followed by creep phase

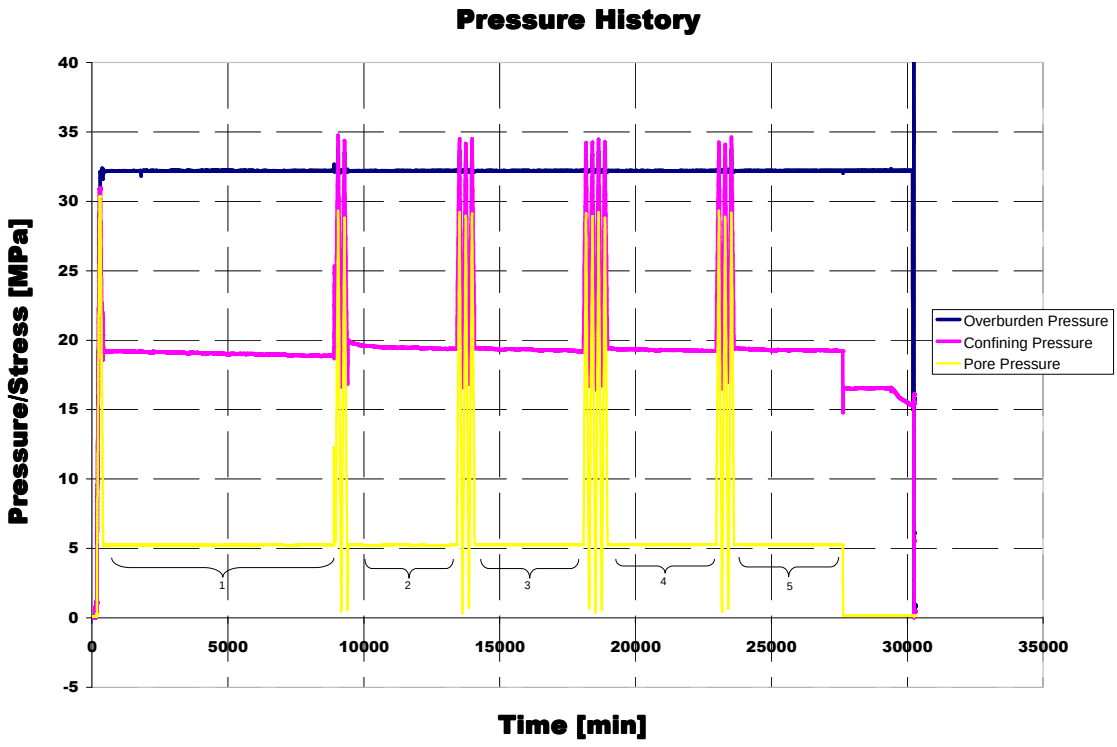

Fig.A2 Pressure history of core E4 showing ramping, pore pressure depletion and load cycles introduced at the creep stage

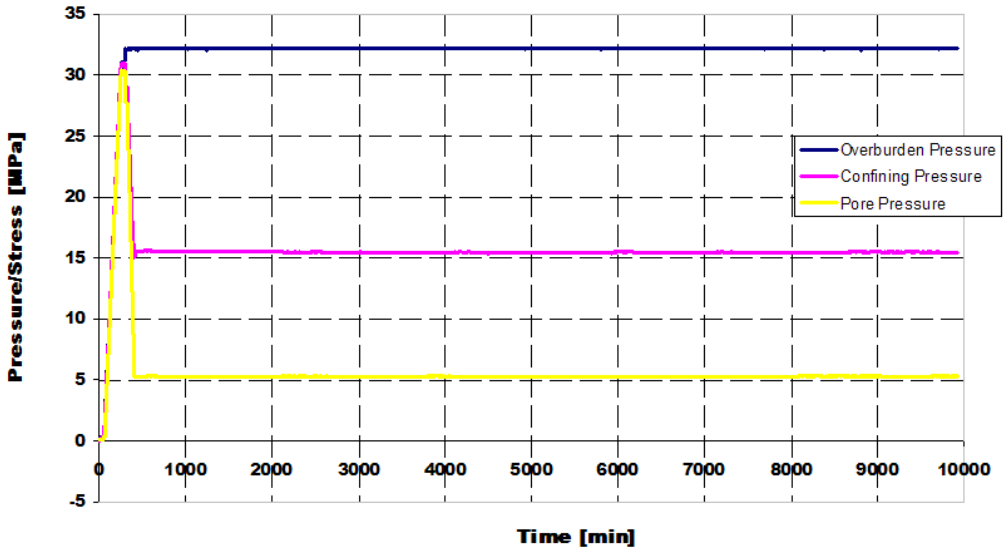

Fig.A3 Pressure history of core E13 without load cycles

Intermediate Loading

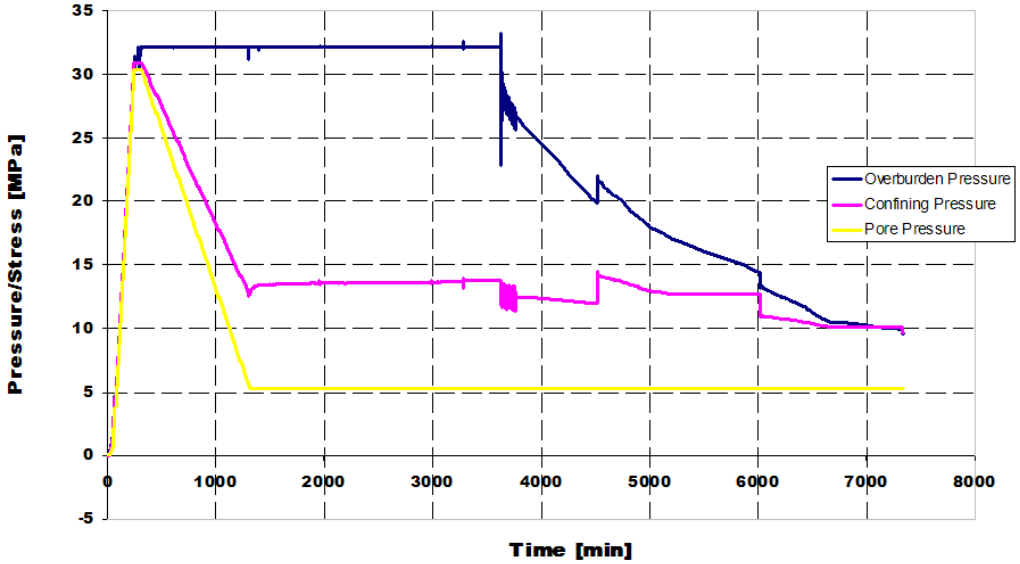

Fig.A4 Pressure history of core E8 showing ramping, pore pressure depletion and creep with the point of failure when the overburden dropped and the confining fluctuated

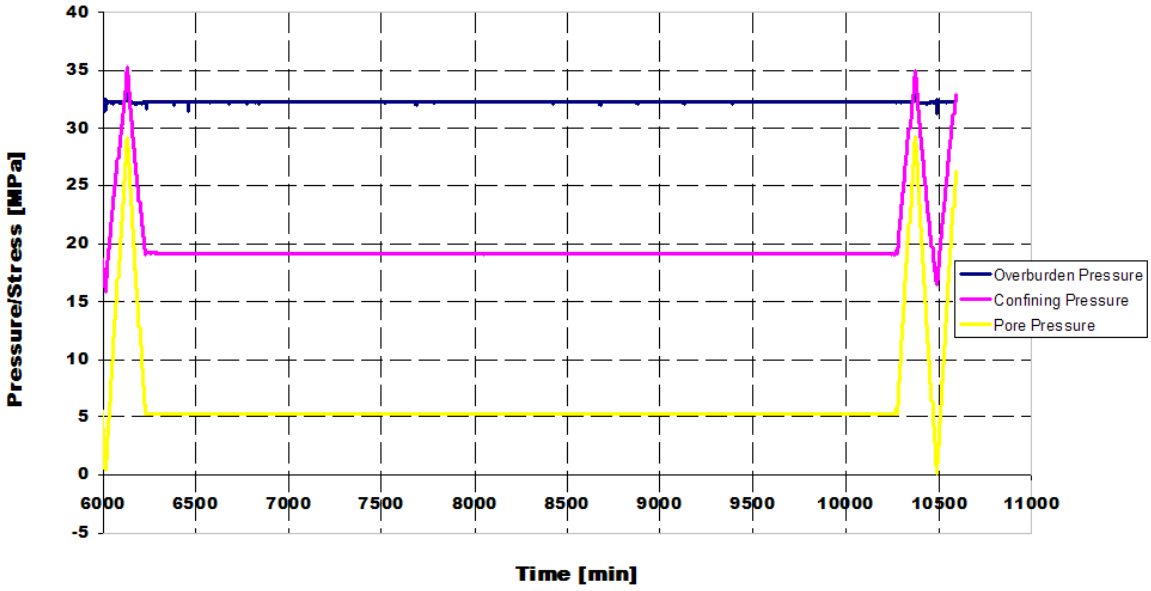

Fig.A5 Pressure history of core E11 with one load cycle before the end of test

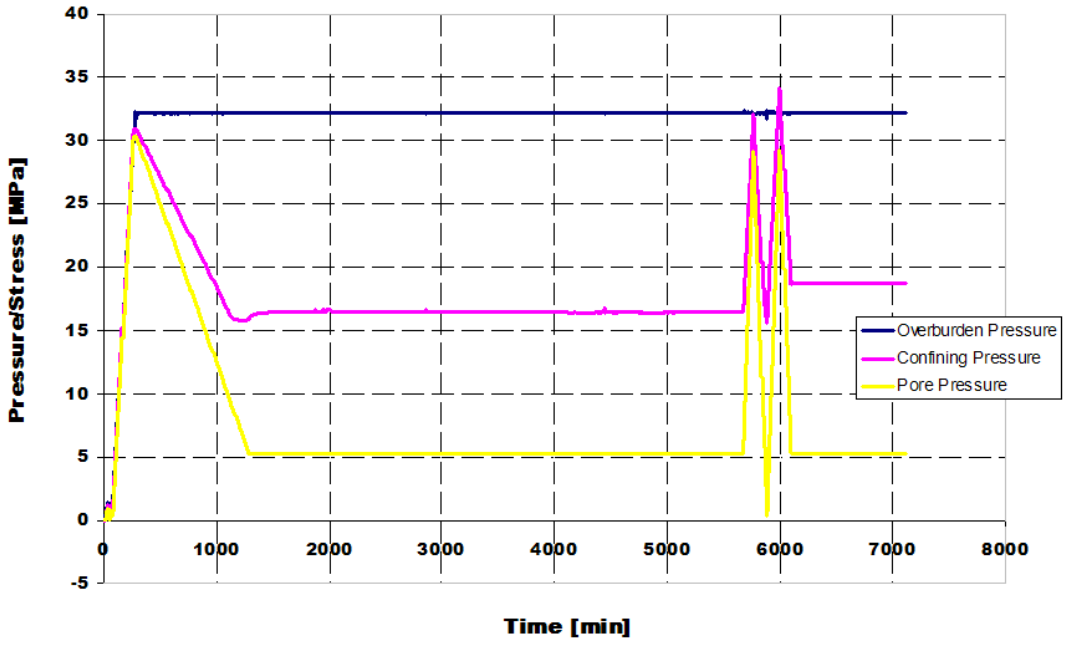

Fig.A6 Pressure history of core E12 with one load cycle and a short creep period before the end of test

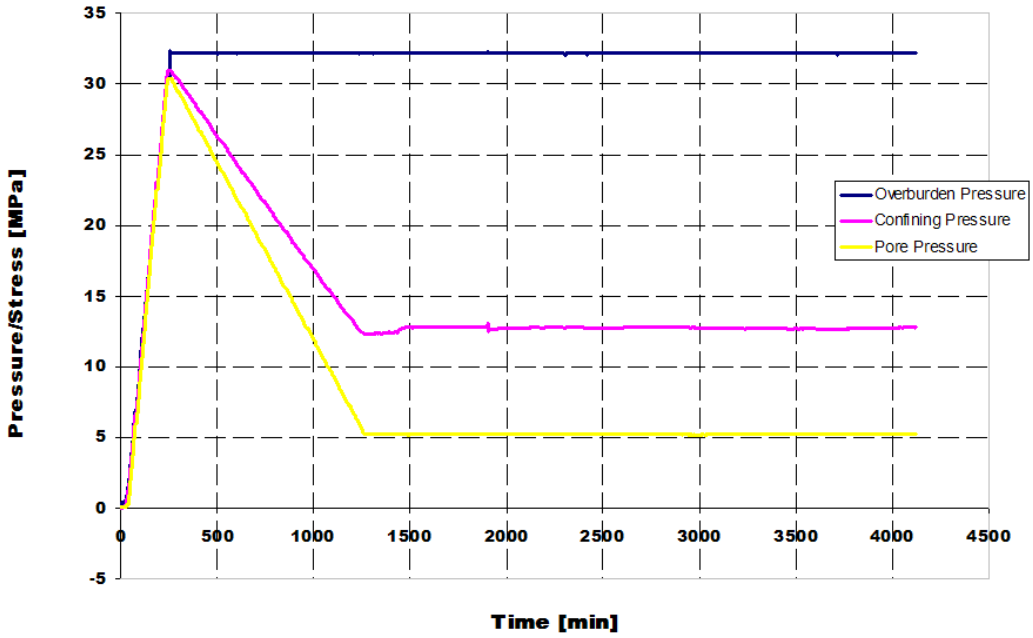

Fig.A7 Pressure history of core E16 from ramping to pore pressure depletion to creep without any cyclic load

Slow Loading

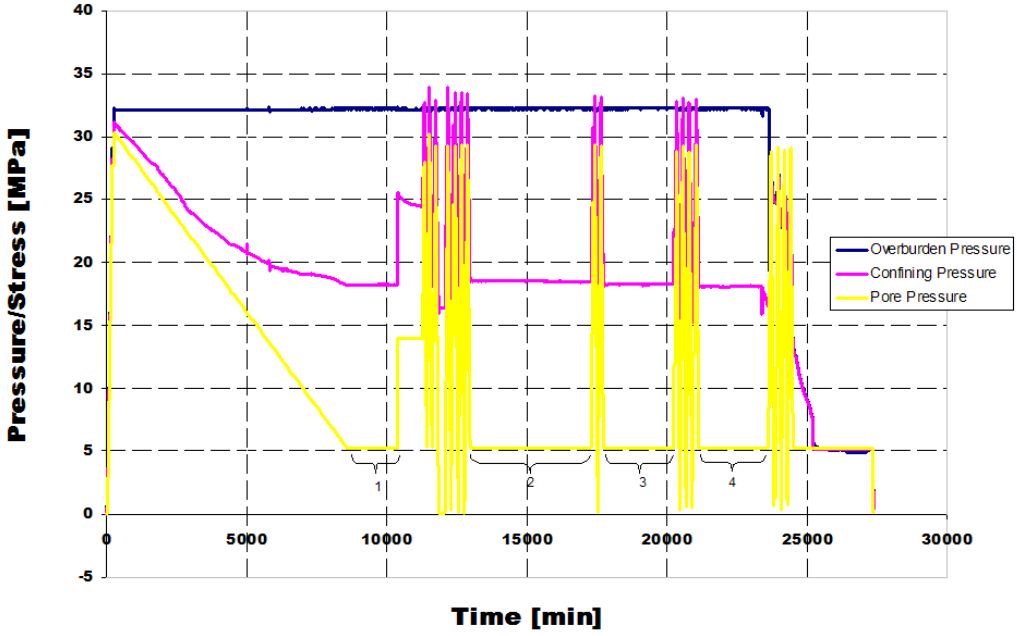

Fig.A8 Pressure history of core E3 with load cycles during the creep phase with overburden pressure drop when the test was stopped

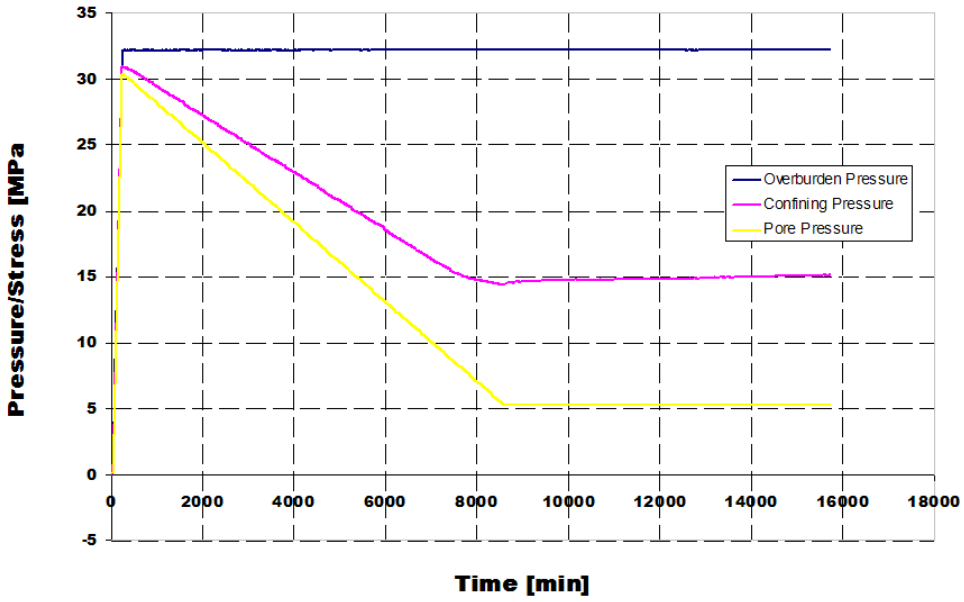

Fig.A9 Pressure history of core E14 from ramping to pore pressure depletion and a very long creep period. This test was the longest of the creep phases

Part B

Stress-Strain Curve

Rapid Loading

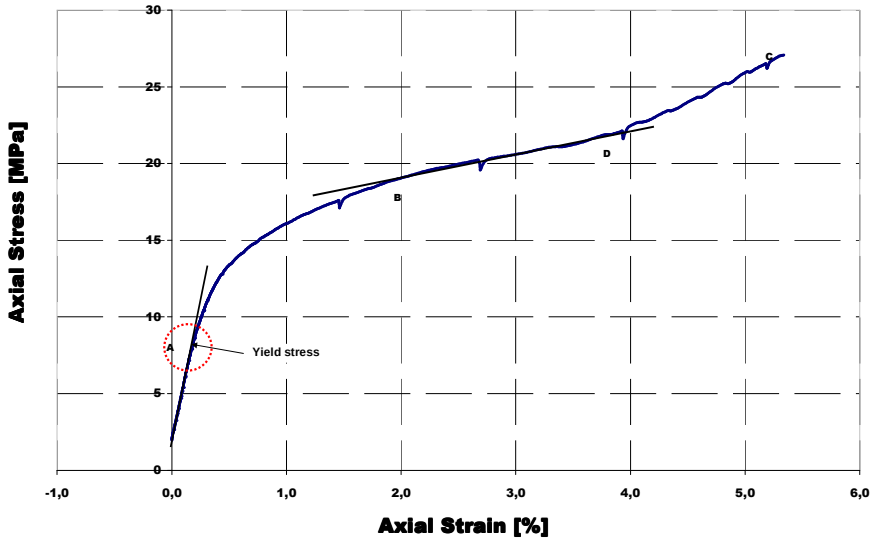

Fig. B1 Stress-strain curve of core E2 showing the yield point, strain softening and strain hardening

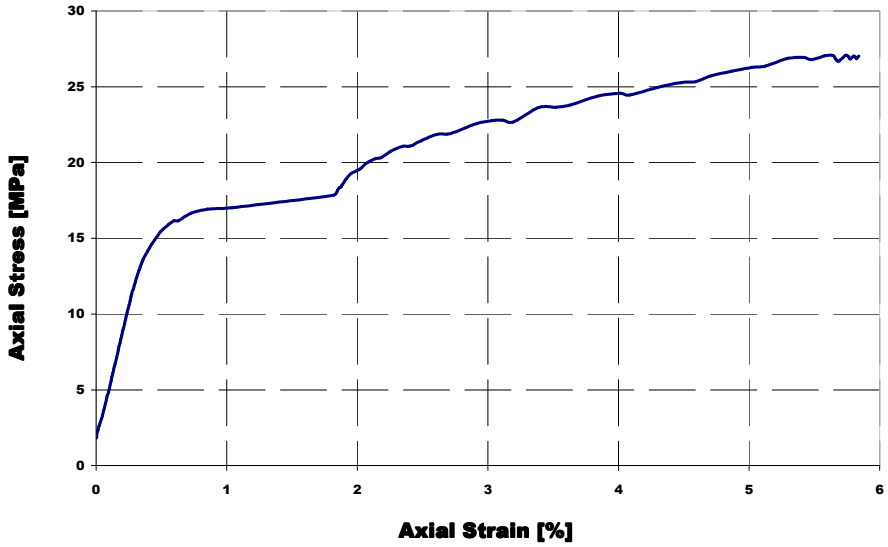

Fig. B2 Stress-strain curve of core E4

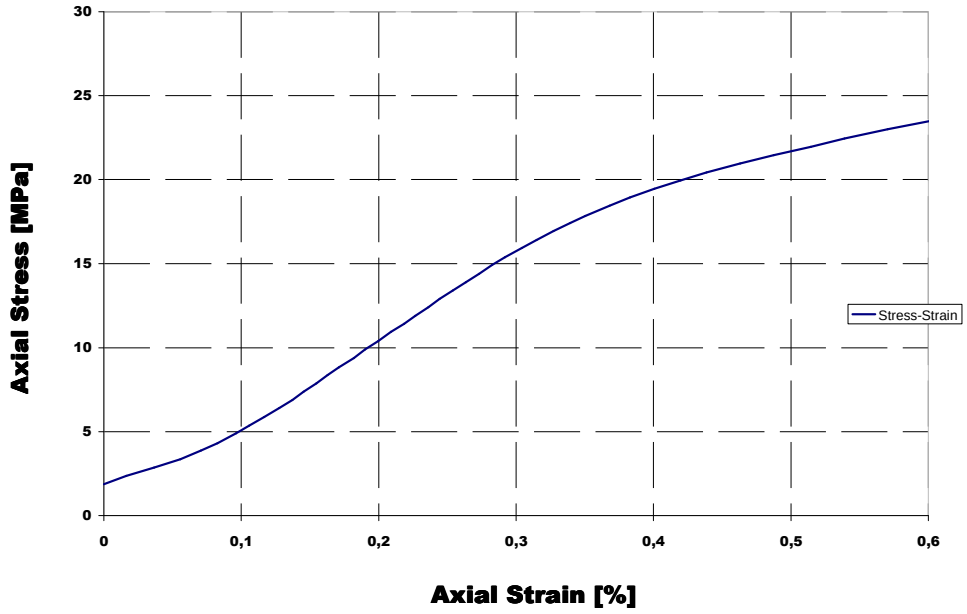

Fig. B3 Stress-strain curve of core E13

Intermediate Loading

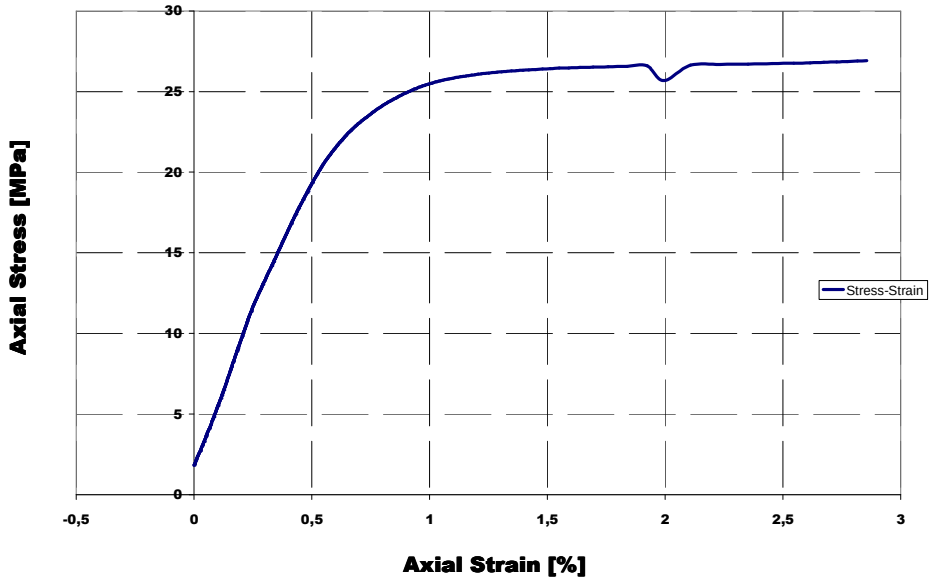

Fig. B4 Stress-strain curve of core E8

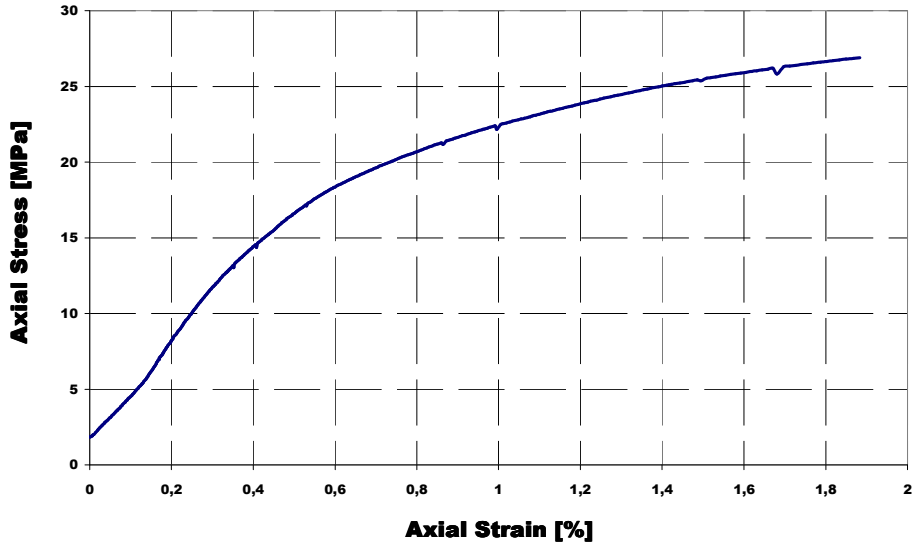

Fig. B5 Stress-strain curve of core E11

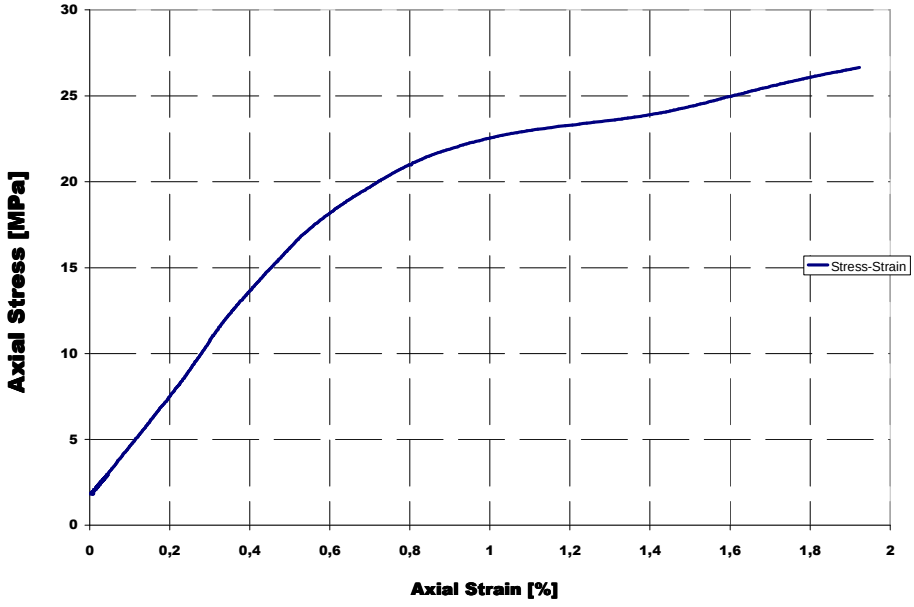

Fig. B6 Stress-strain curve of core E12

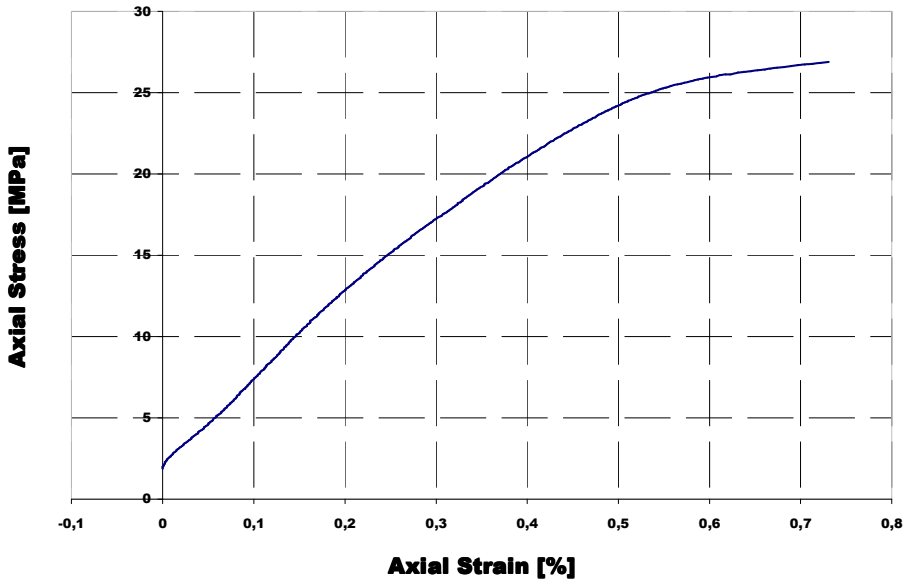

Fig. B7 Stress-strain curve of core E16

Slow Loading

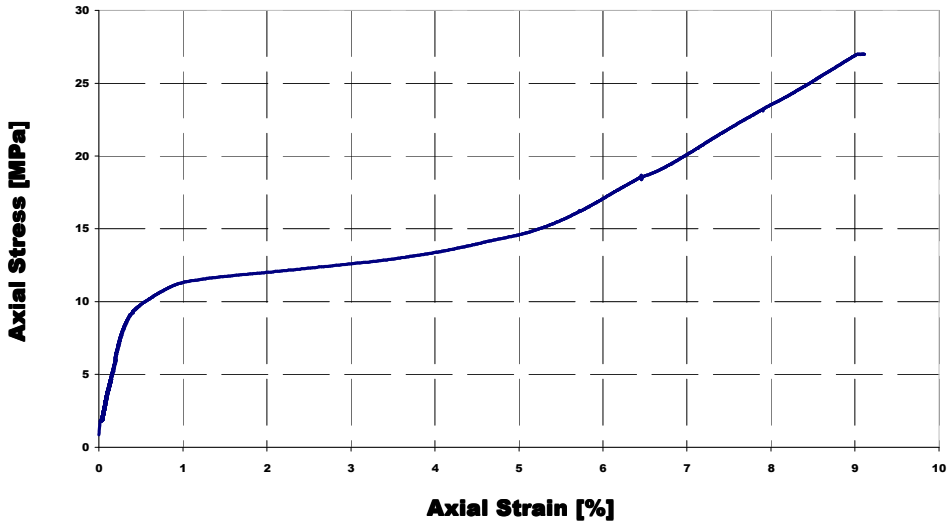

Fig. B8 Stress-strain curve of core E3

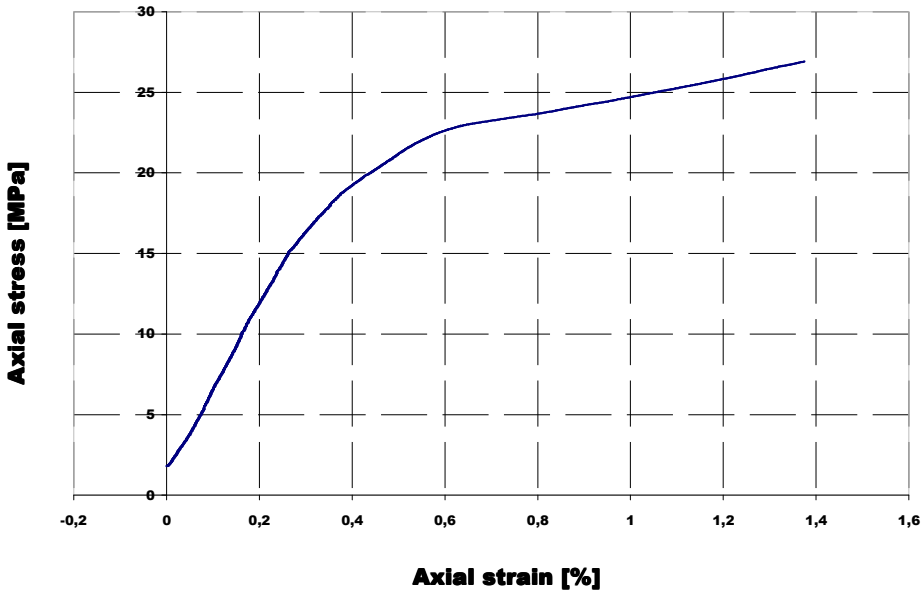

Fig. B9 Stress-strain curve of core E14

Part C

Creep Strain

Rapid Loading:

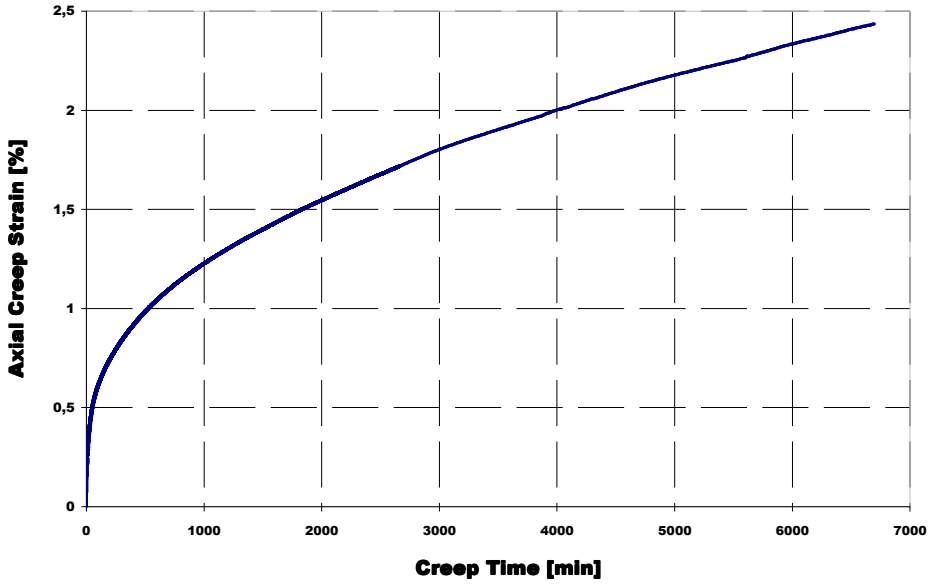

Fig.C1 Creep strain of core E2 showing that the strain recorded during the creep phase was the highest

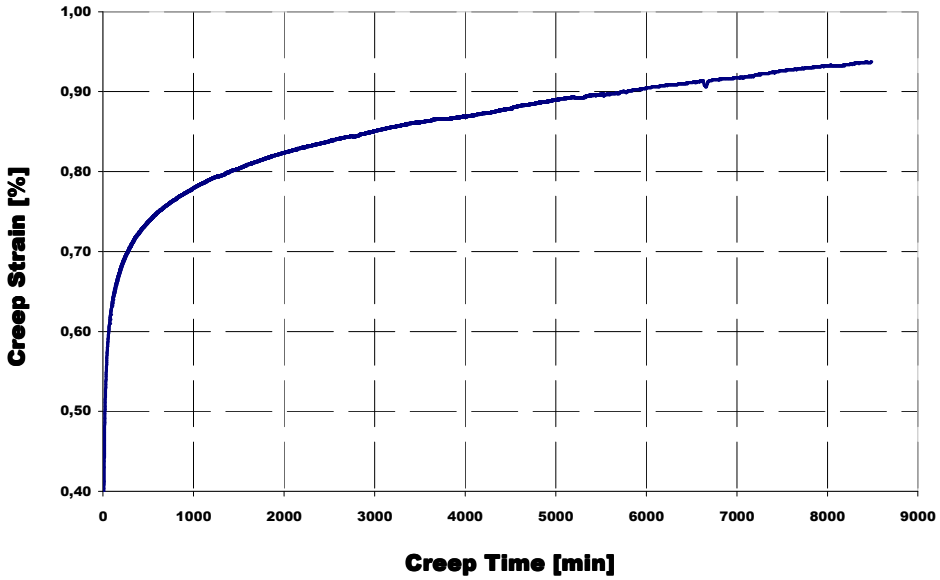

Fig.C2a Creep strain core E4 at the start of creep

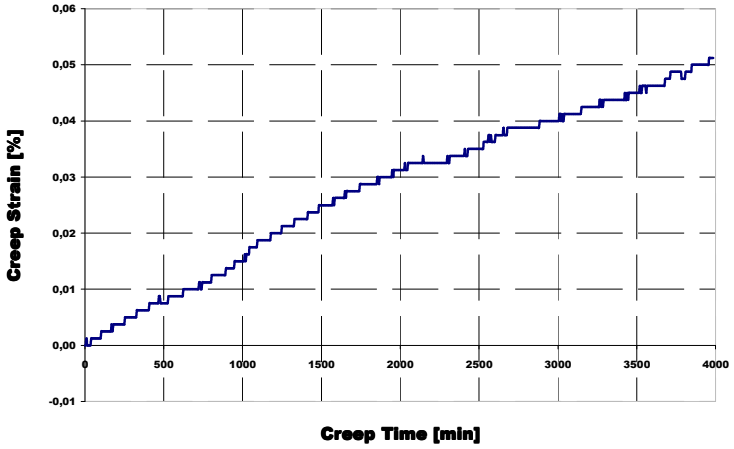

Fig.C2b Creep strain of core E4 after the first cyclic loading

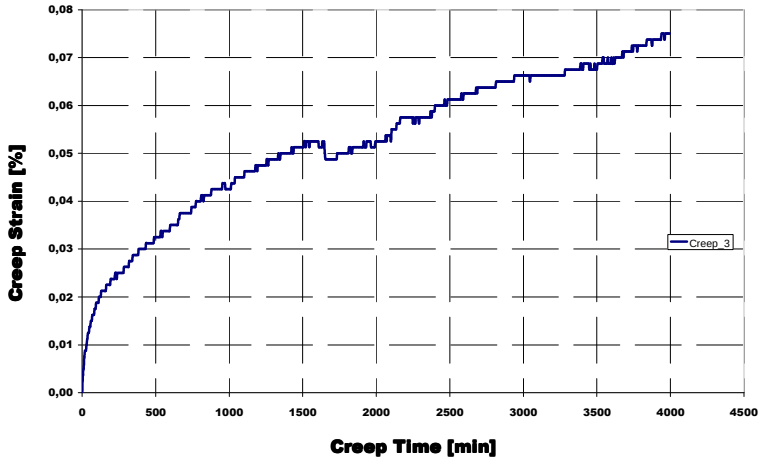

Fig.C2c Creep strain of core E4 after the second cyclic loading

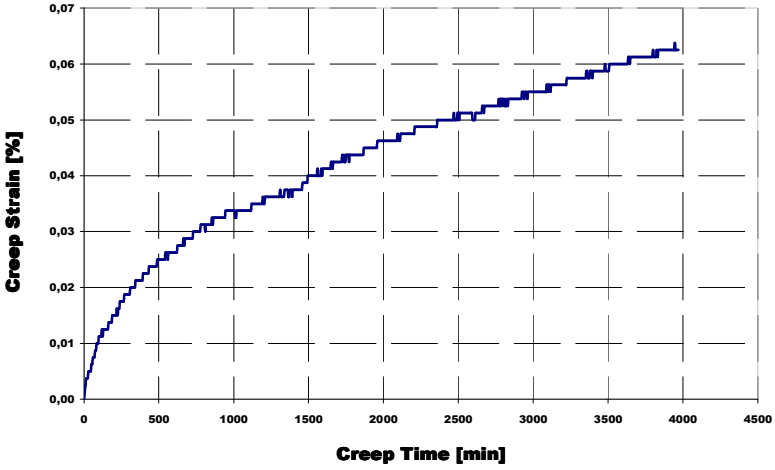

Fig.C2d Creep strain of core E4 after the third load cycle

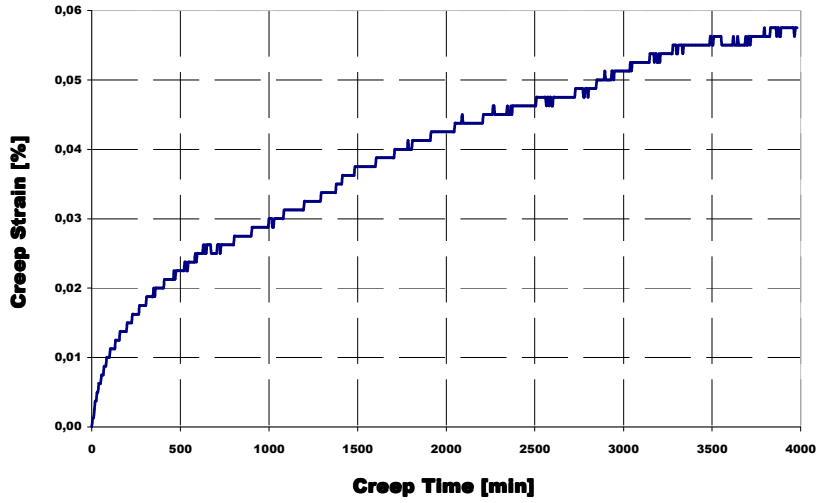

Fig.C2e Creep strain of core E4 after the fourth load cycle

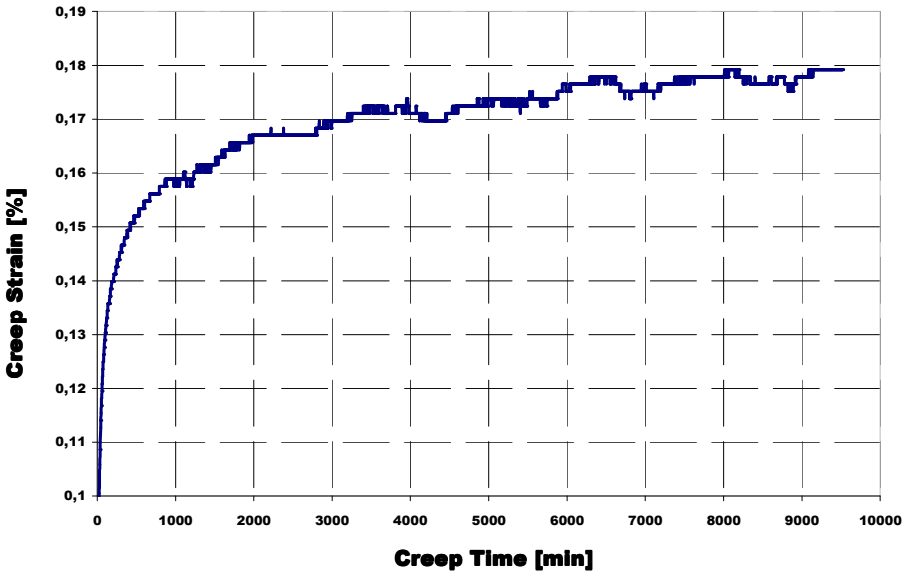

Fig.C3 Creep strain core E13

Intermediate Loading

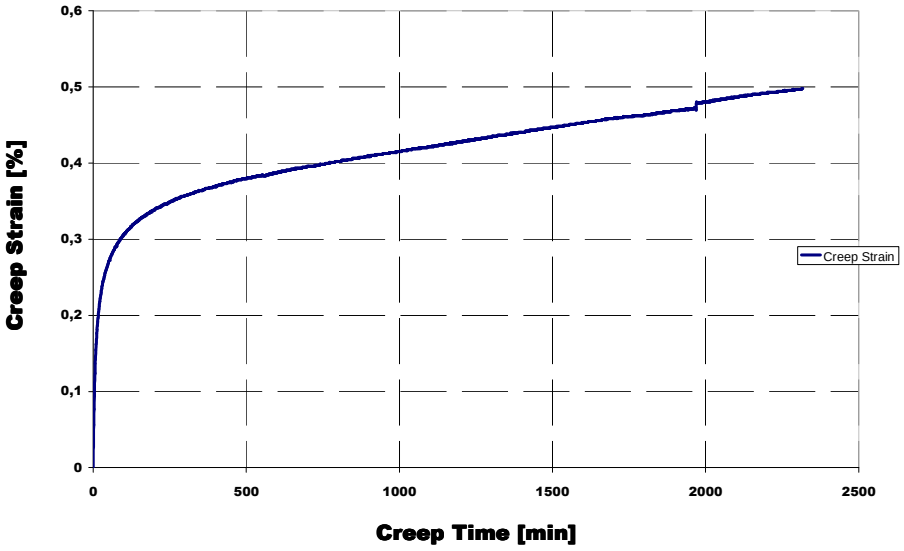

Fig.C4 Creep strain core E8

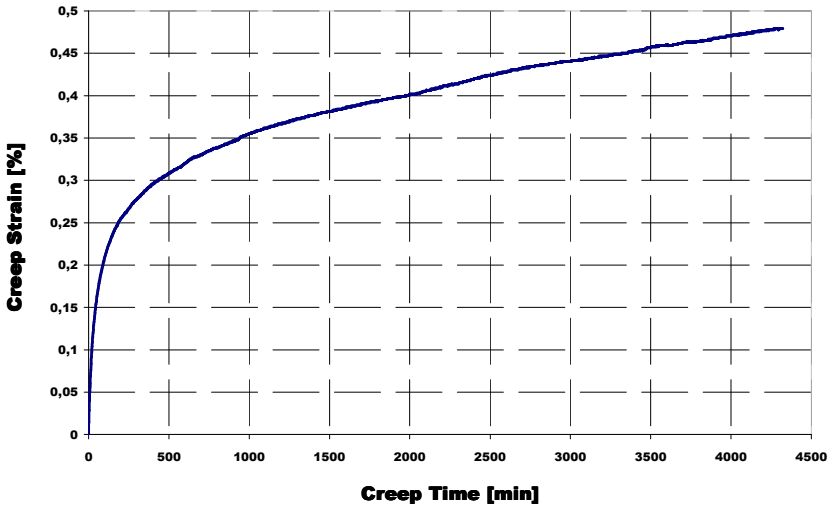

Fig.C5 Creep strain core E11

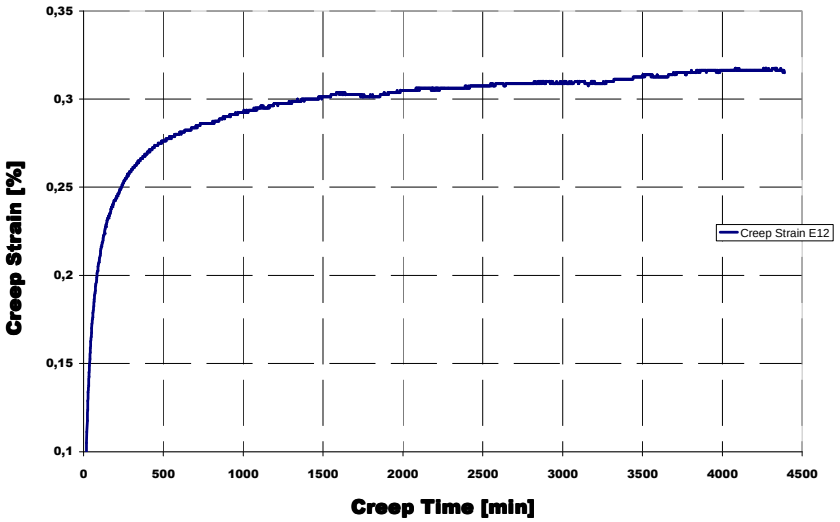

Fig.C6 Creep strain core E12

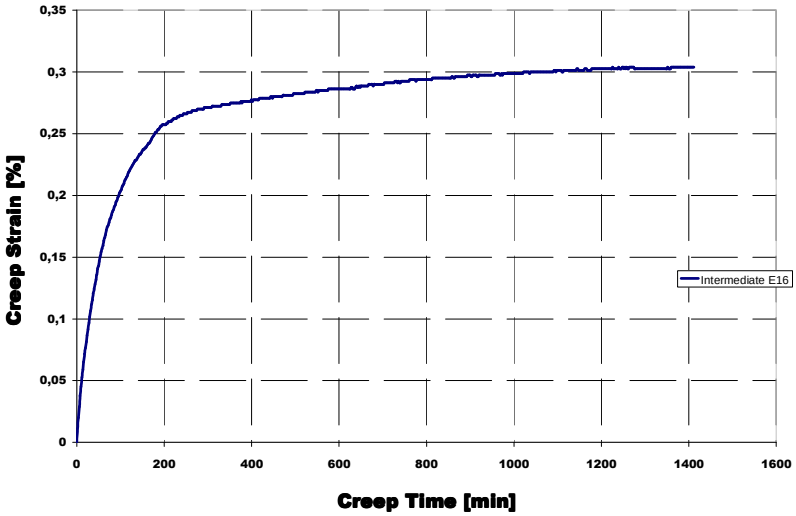

Fig.C7 Creep strain core E16

Slow Loading:

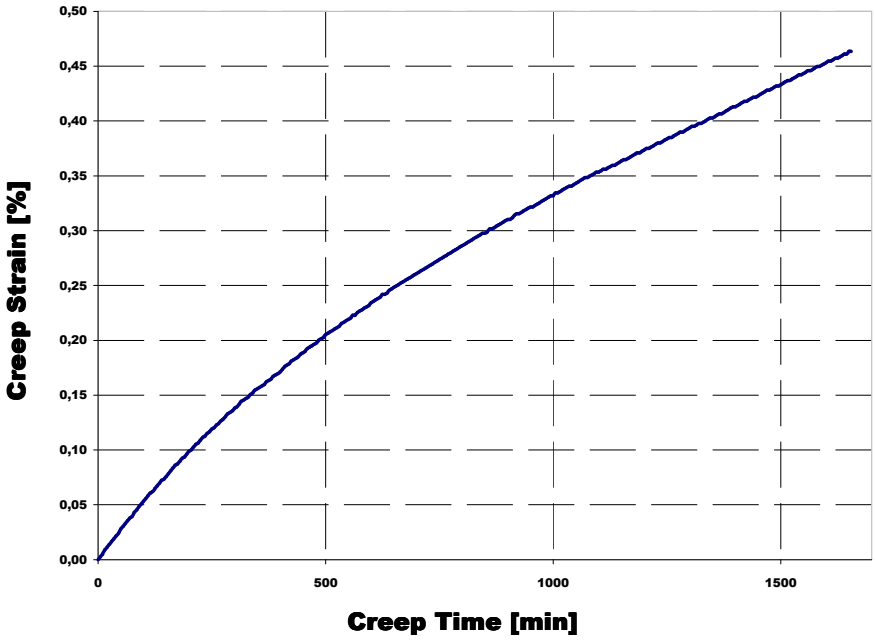

Fig.C8 Creep strain core E3

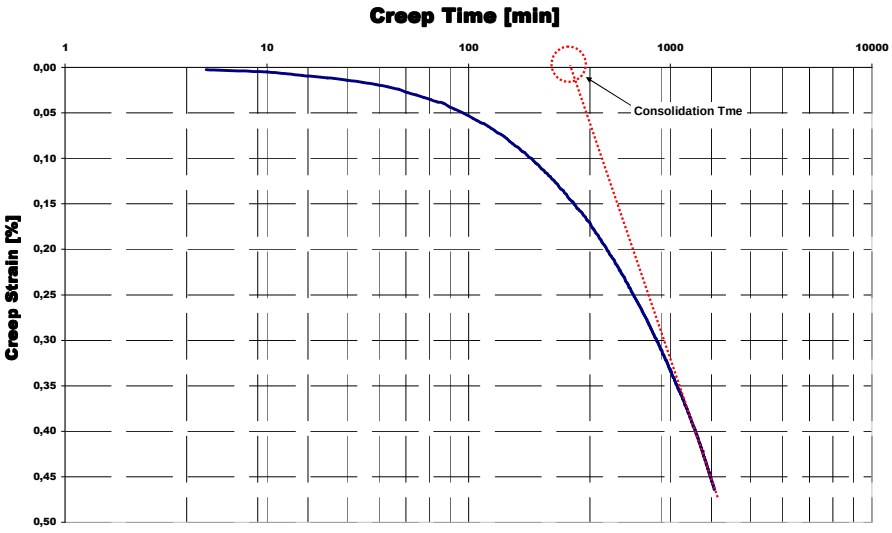

Fig.C9 Consolidation time for core E3 using the method of Pattillo, P.D. et al (1989)

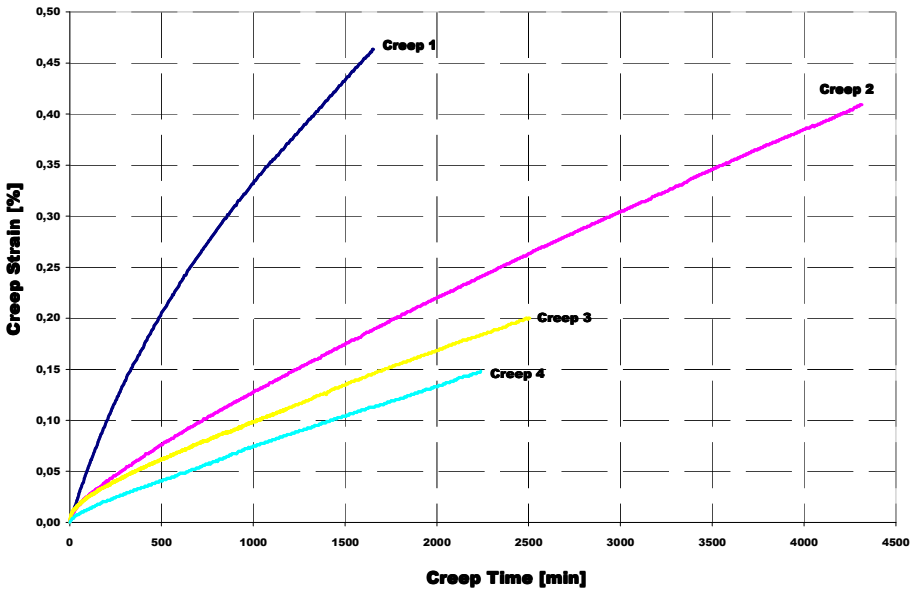

Fig.C10 Creep strains of E3 after various stages of cycles as shown in the pressure history

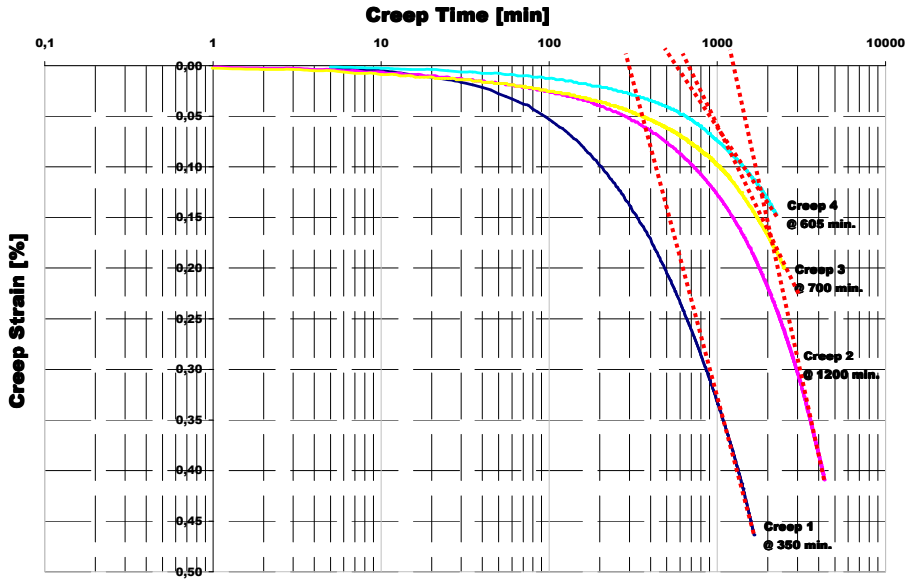

Fig.C11 Consolidation times of E3 after various stages of cycles as shown in the pressure history

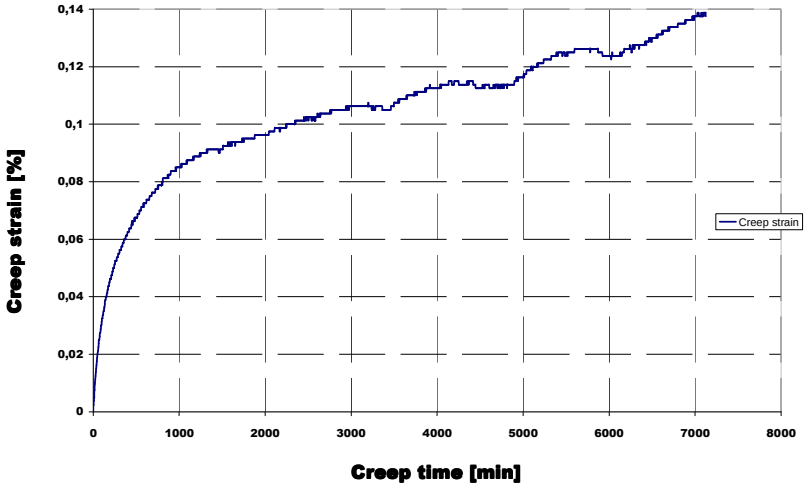

Fig.C12 Creep strain of C14 showing the continuous creep after a very long time

Part D

q-p Plot

Rapid loading

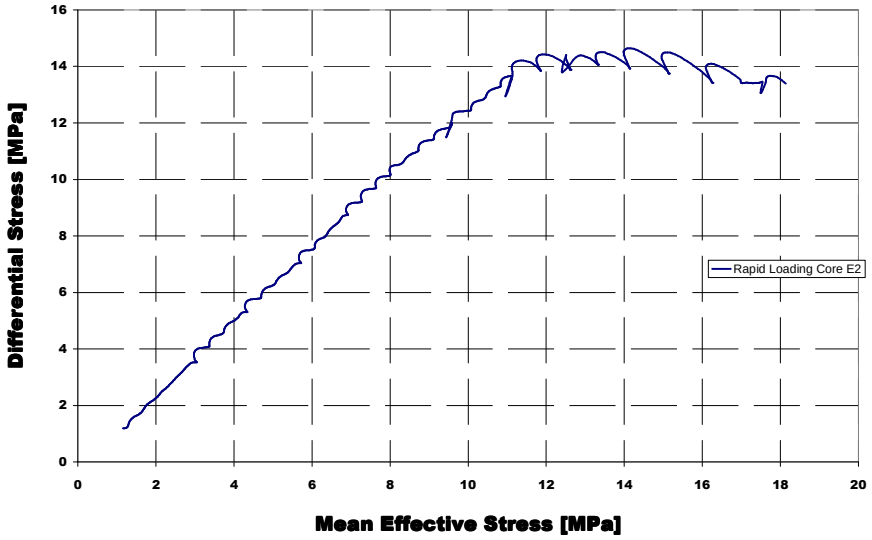

Fig.D1 q-p plot of E2 during depletion

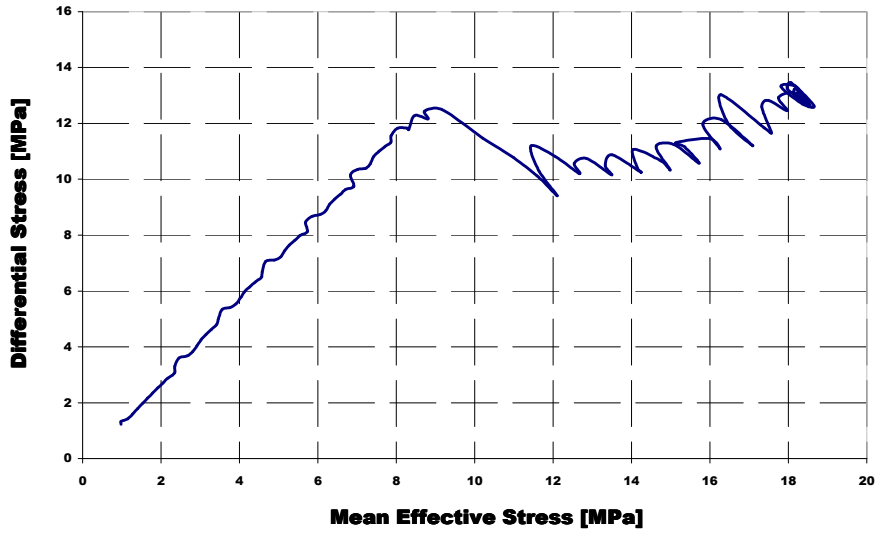

Fig.D2 q-p plot of E4

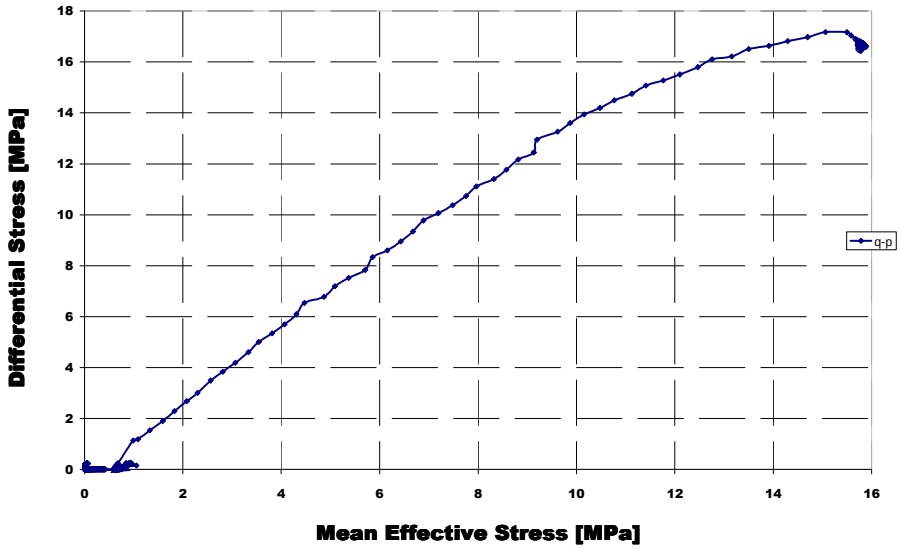

Fig.D3 plot of E13

Intermediate Loading

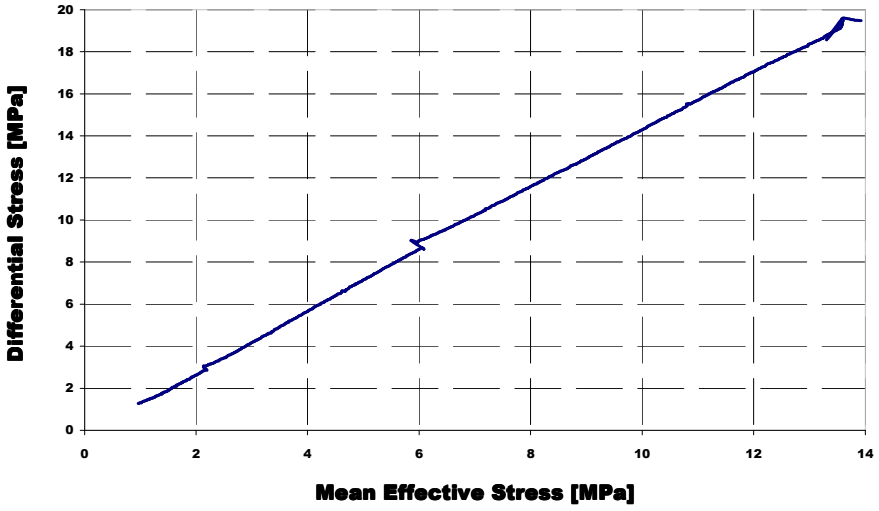

Fig.D4 q-p plot of E8

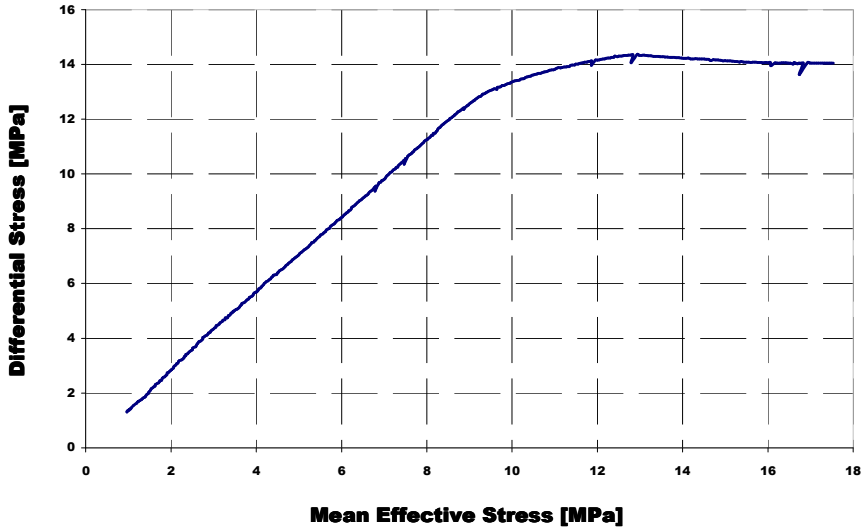

Fig.D5 q-p plot of E11

Fig.D6 q-p plot of E12

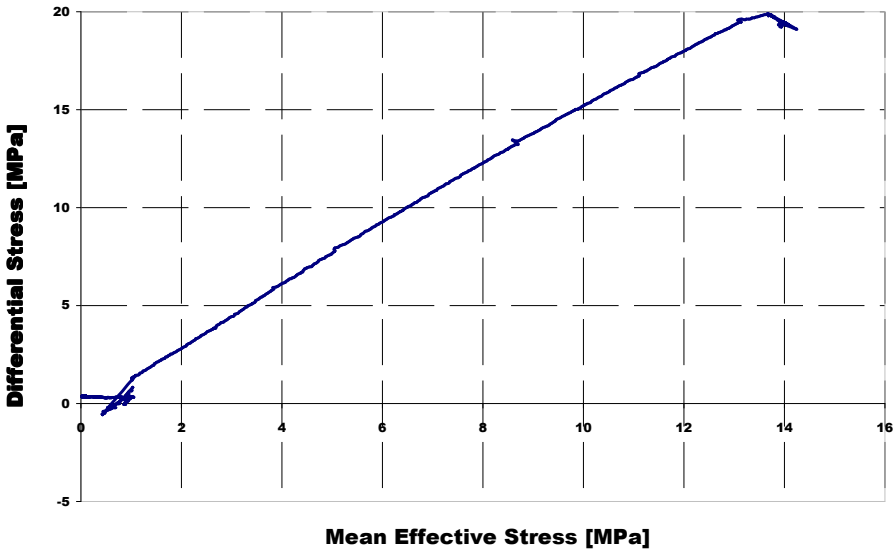

Fig.D7 plot of E16

Slow Loading

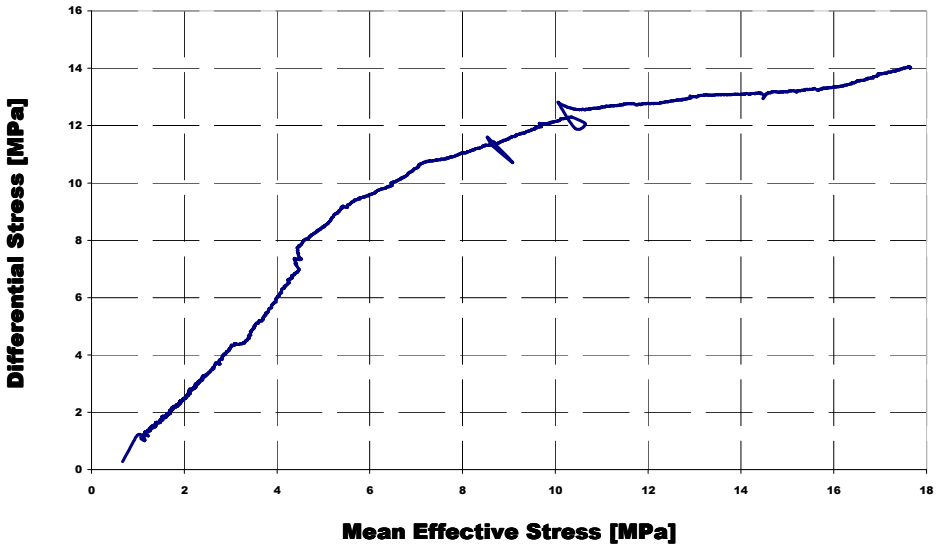

Fig.D8 plot of E3

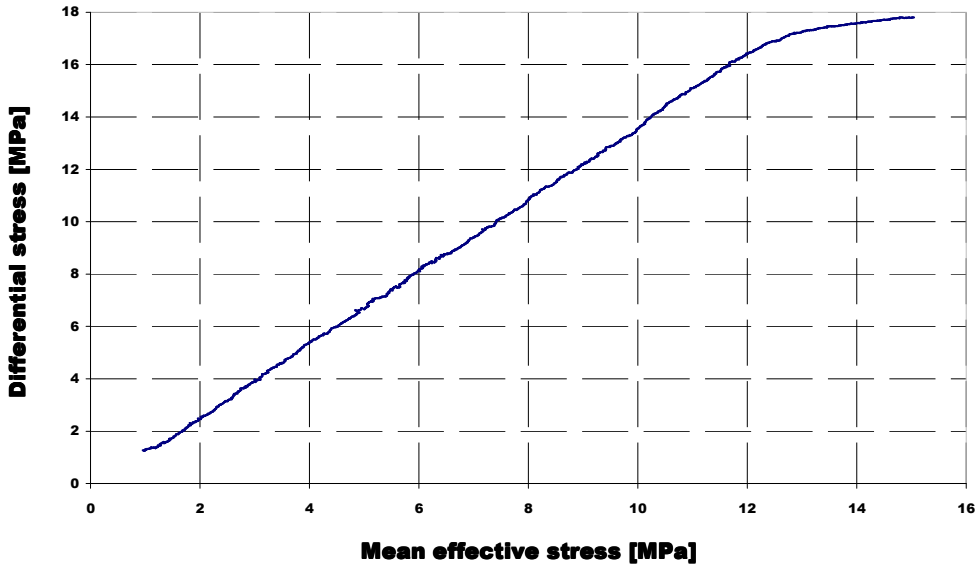

Fig.D9 plot of E14

Part E

Stress Path

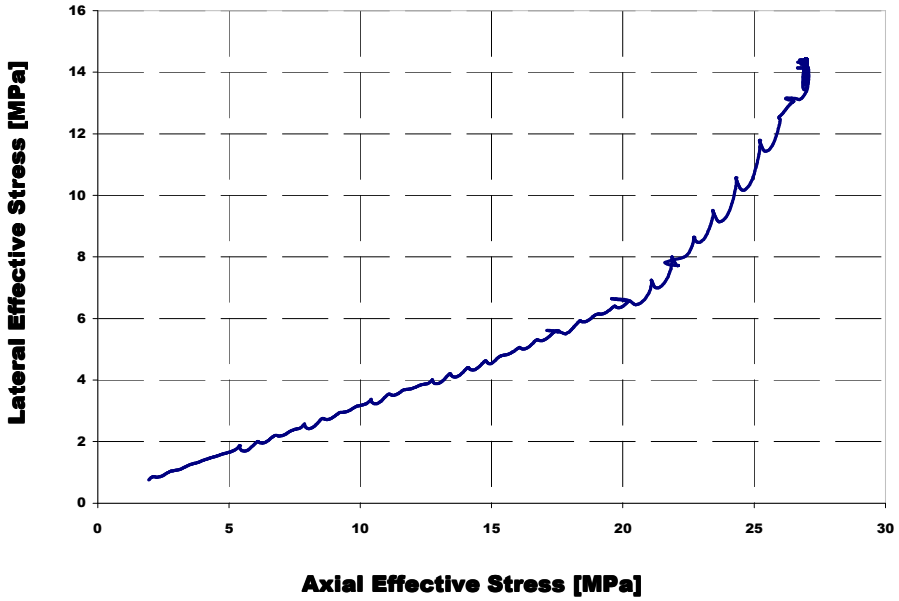

Fig.E1 Stress path of E2 during depletion

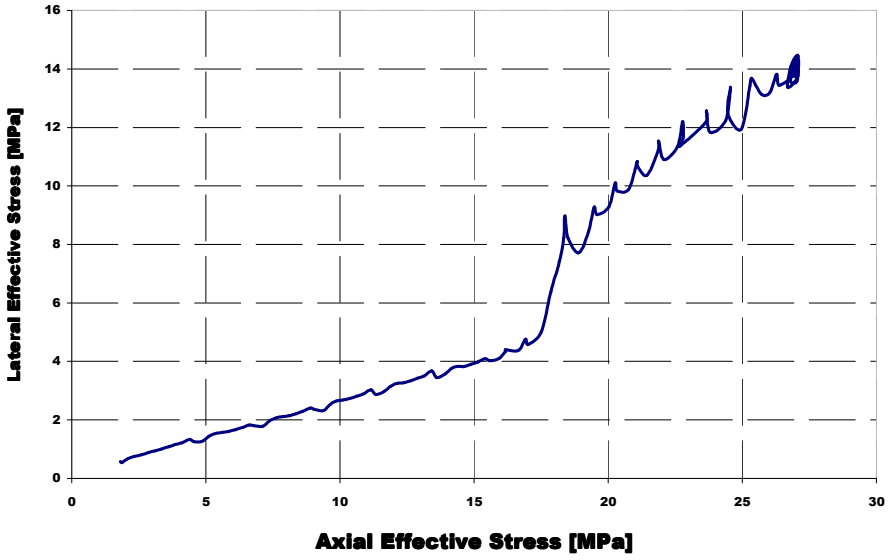

Fig.E2 Stress path of E4

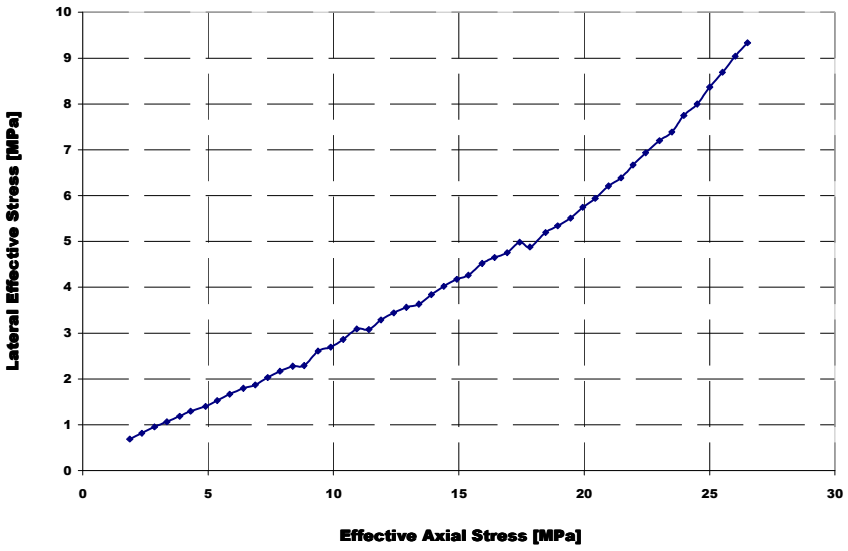

Fig.E3 Stress path of E13

Intermediate Loading

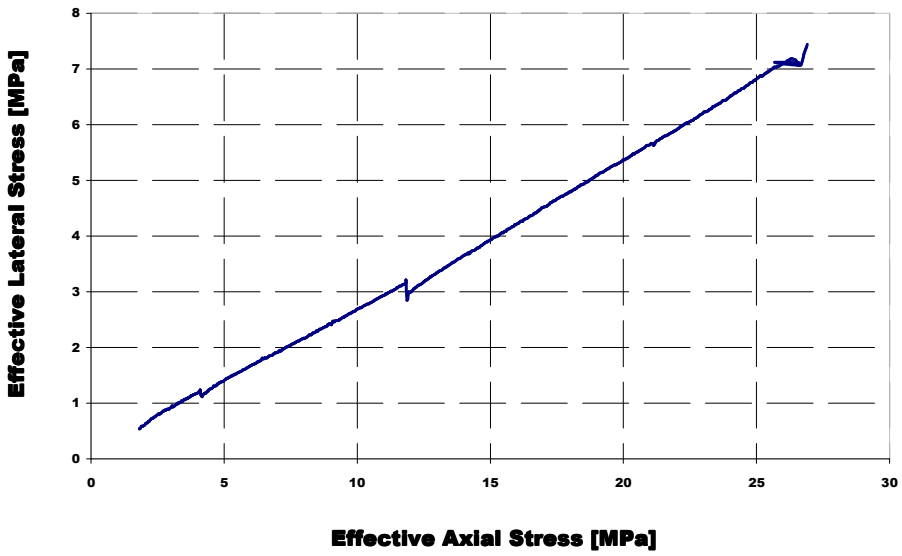

Fig.E4 Stress path of E8 during depletion

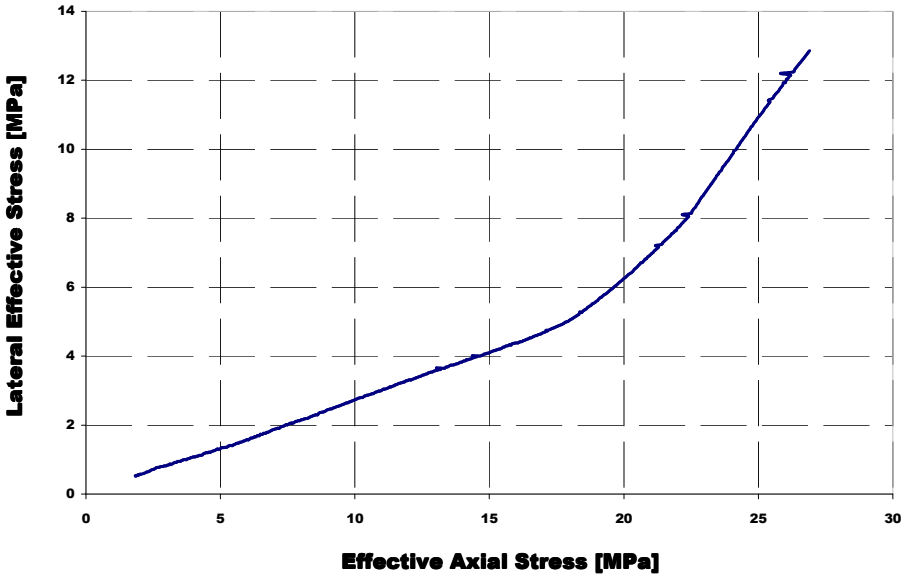

Fig.E5 Stress path of E11 during depletion

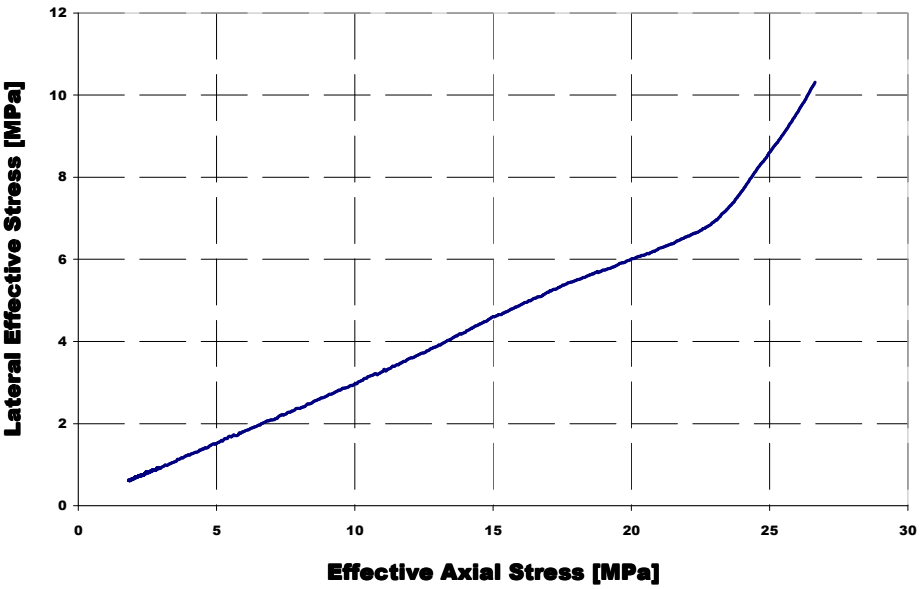

Fig.E6 Stress path of E12

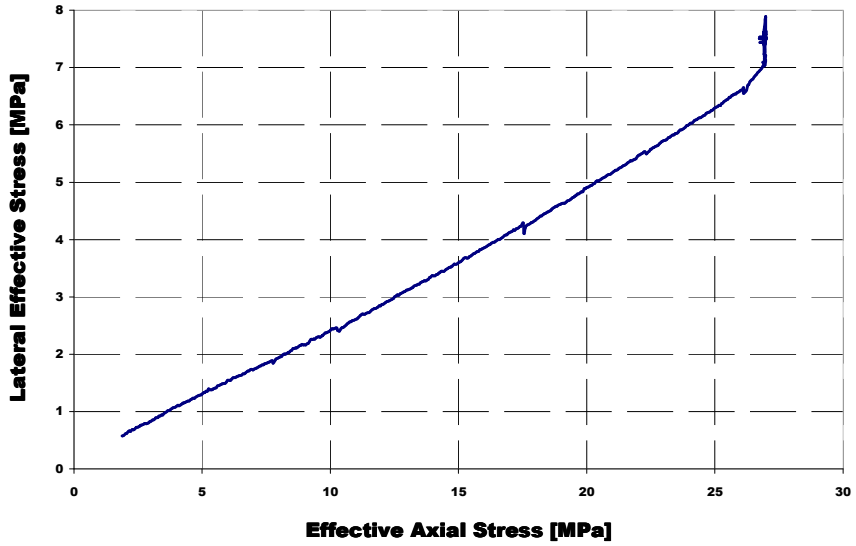

Fig.E7 Stress path of E16

Slow Loading

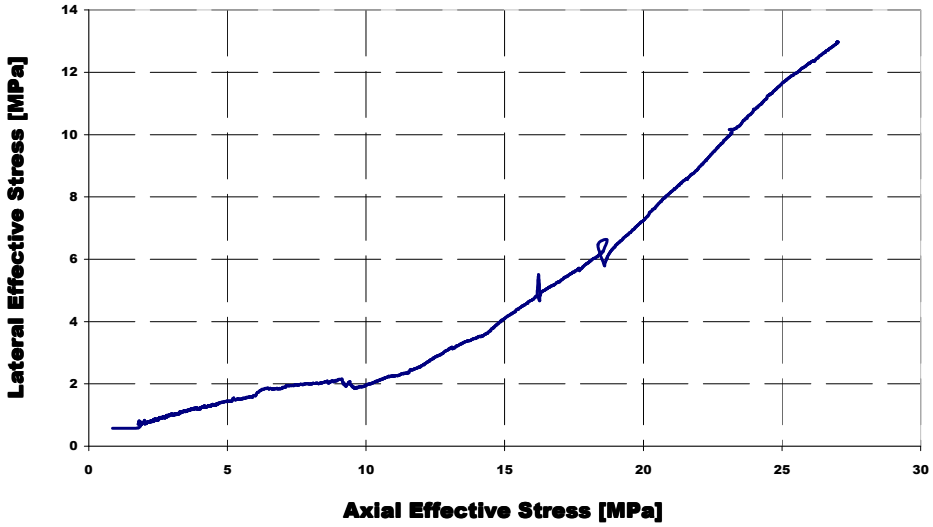

Fig.E8 Stress path of E3

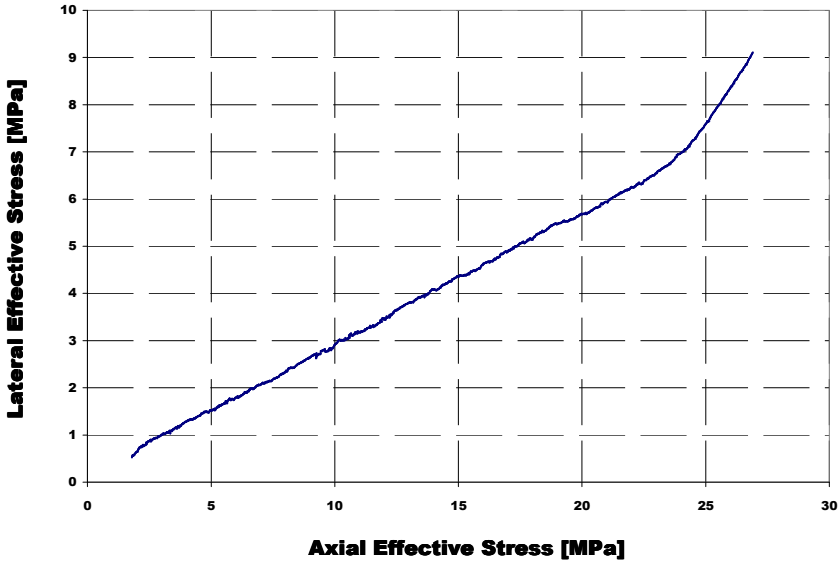

Fig.E9 Stress path of E14

Part F

Porosity versus Mean Effective Stress

Rapid Loading

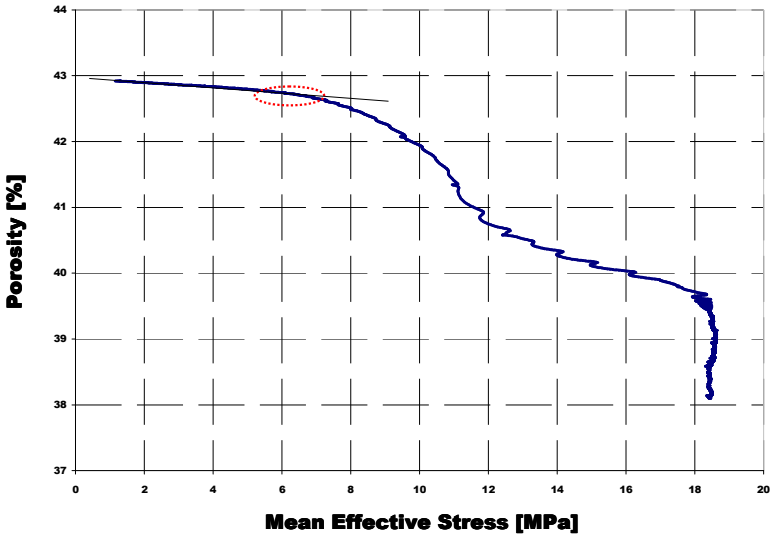

Fig.F1 Porosity variation with mean effective stress during depletion of the pore pressure of core E2

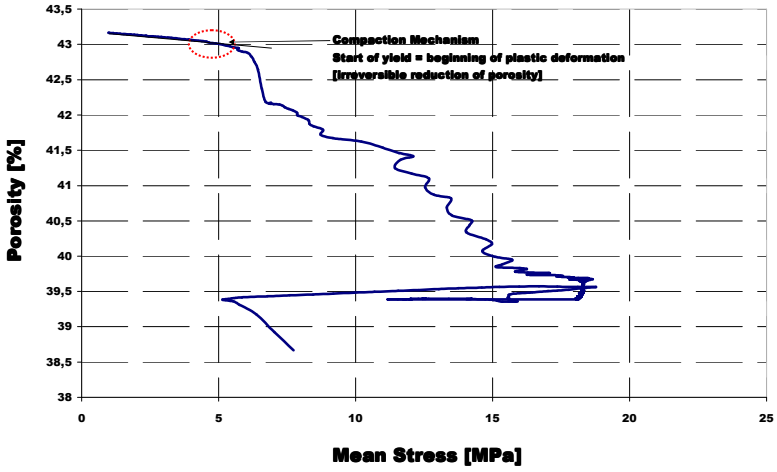

Fig.F2 Porosity variation with mean effective stress during depletion of the pore pressure of core E4

Fig.F3 Porosity variation of core E13

Intermediate Loading

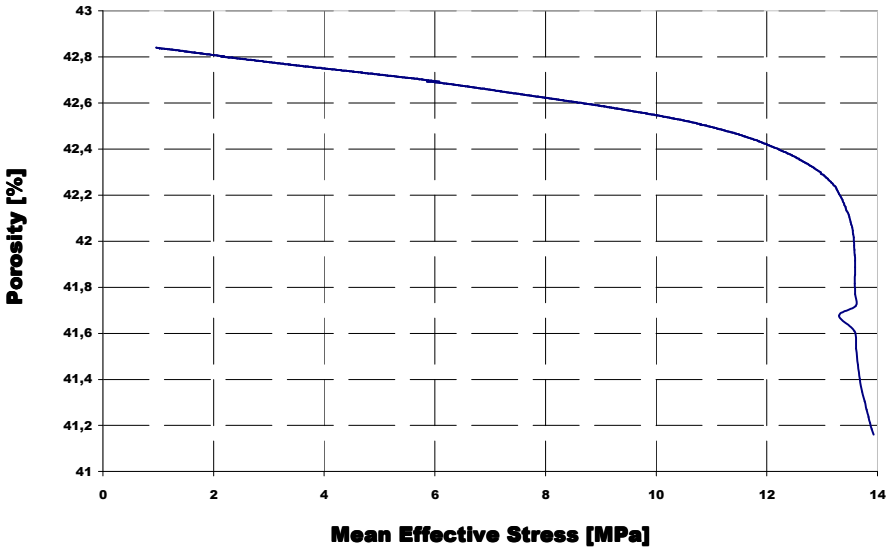

Fig.F4 Porosity variation of core E8

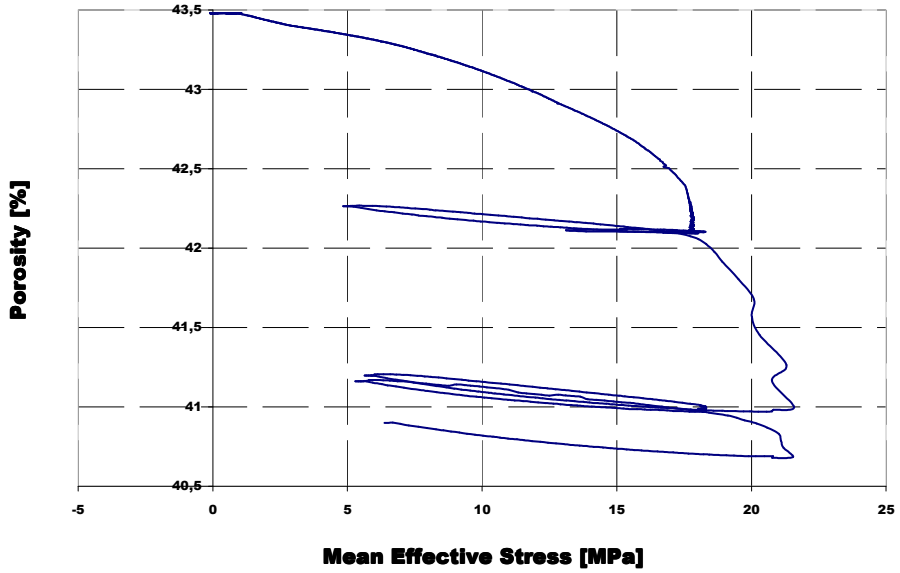

Fig.F5 Porosity variation of core E11

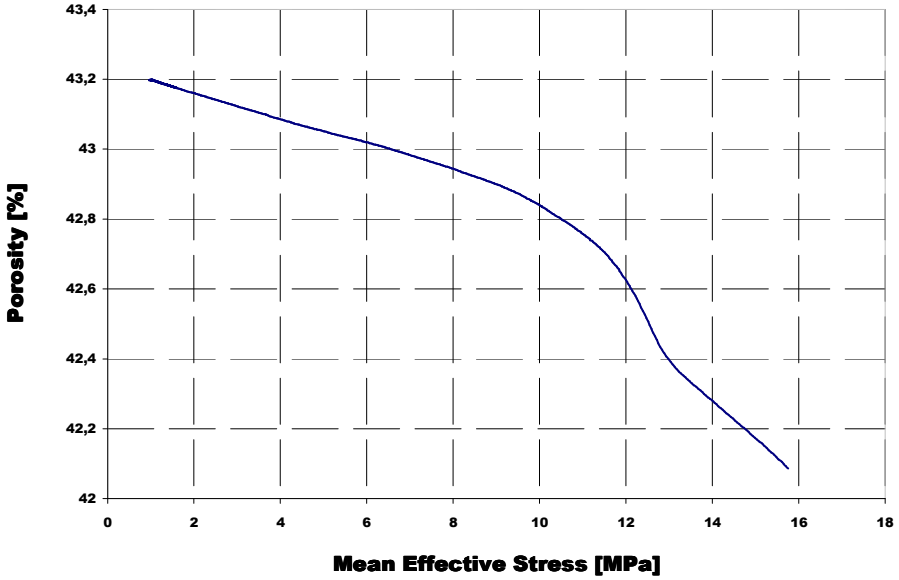

Fig.F6 Porosity variation of core E12

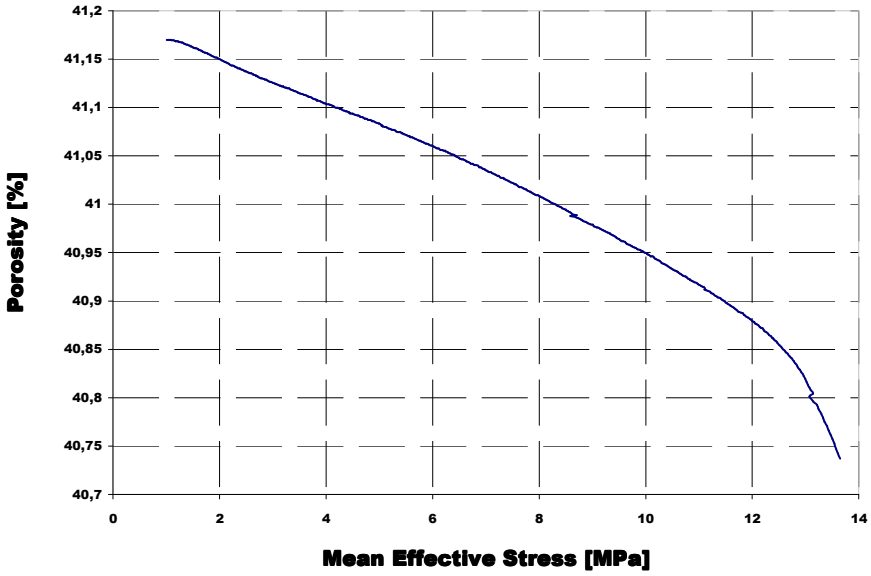

Fig.F7 Porosity variation of core E16

Slow Loading

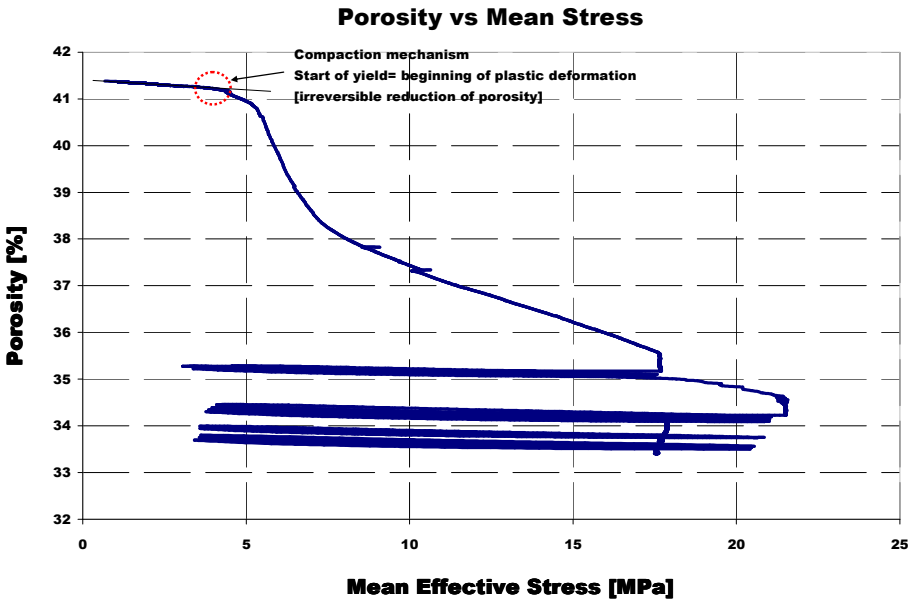

Fig.F8 Porosity variation of core E3

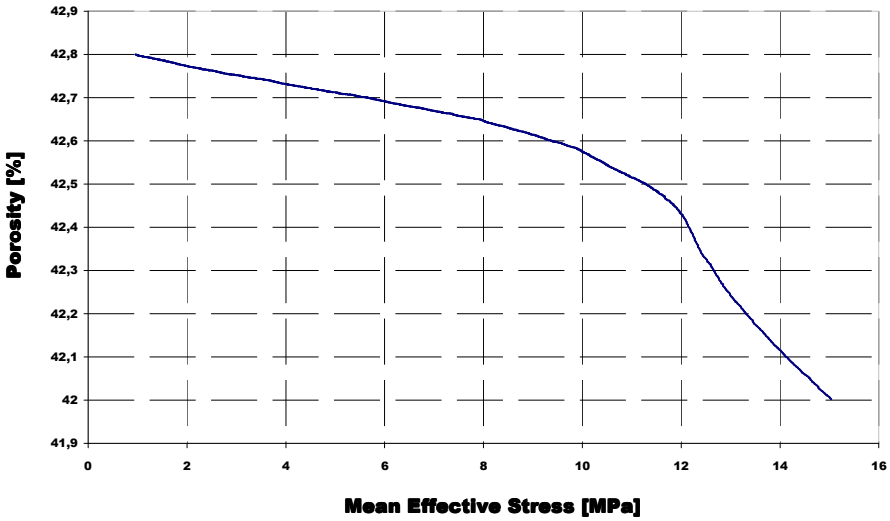

Fig.F9 Porosity variation of core E14

Part G

Porosity versus Pore Pressure

Rapid Loading

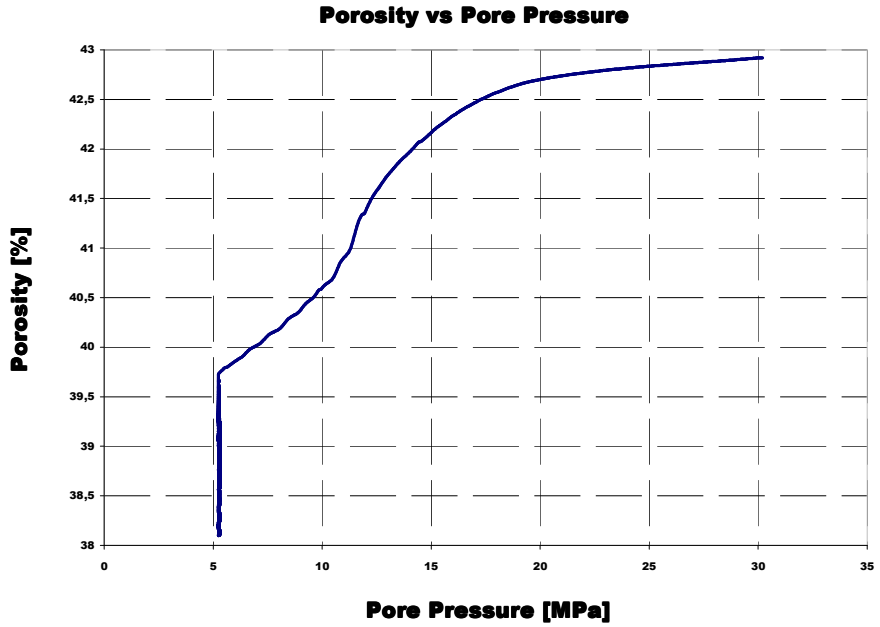

Fig.G1 Variation of porosity with fluid pressure in core E2

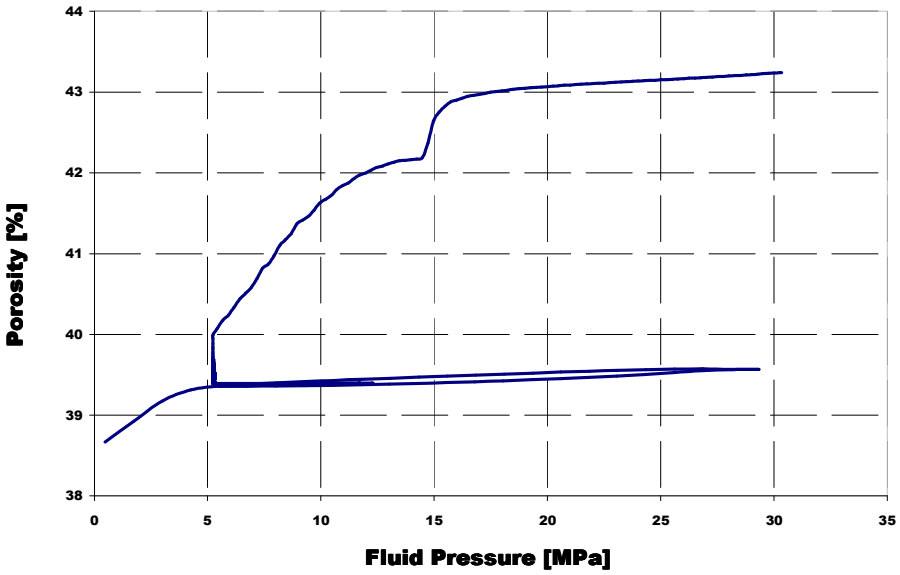

Fig.G2 Variation of porosity with fluid pressure in core E4

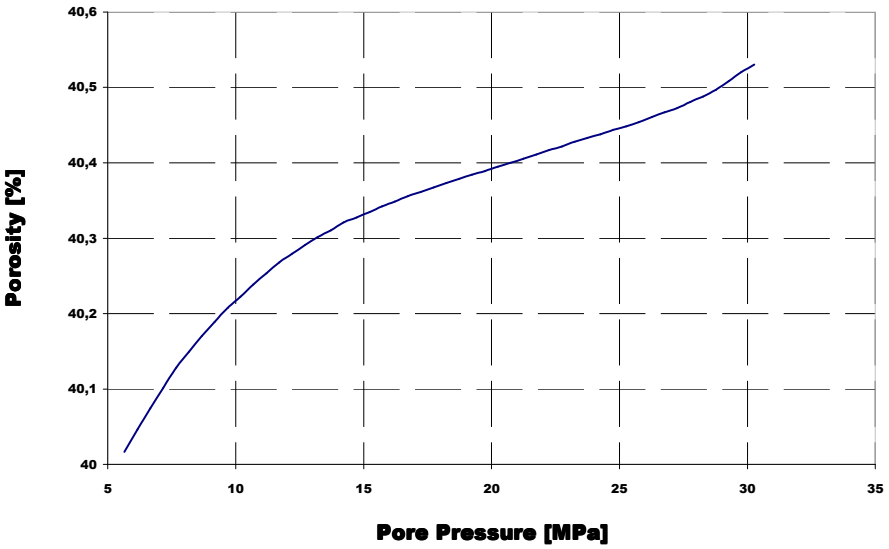

Fig.G3 Variation of porosity with fluid pressure in core E13

Intermediate Loading

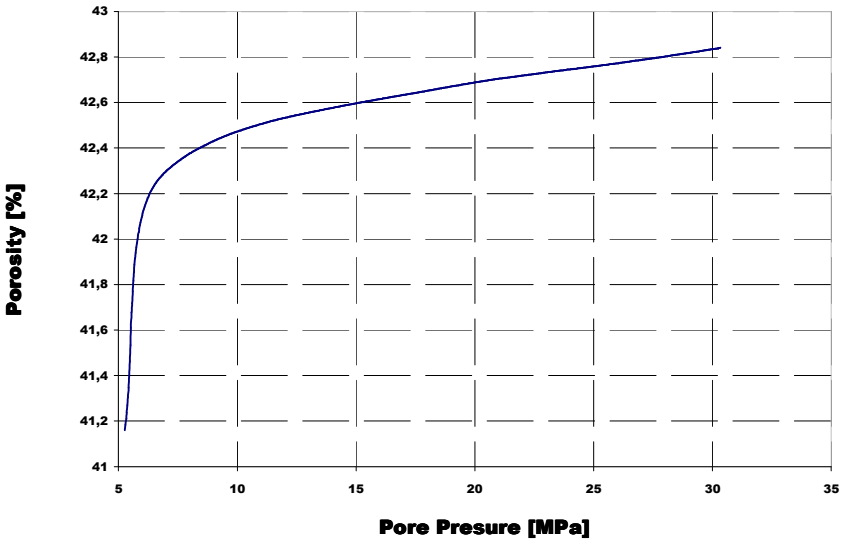

Fig.G4 Core E8

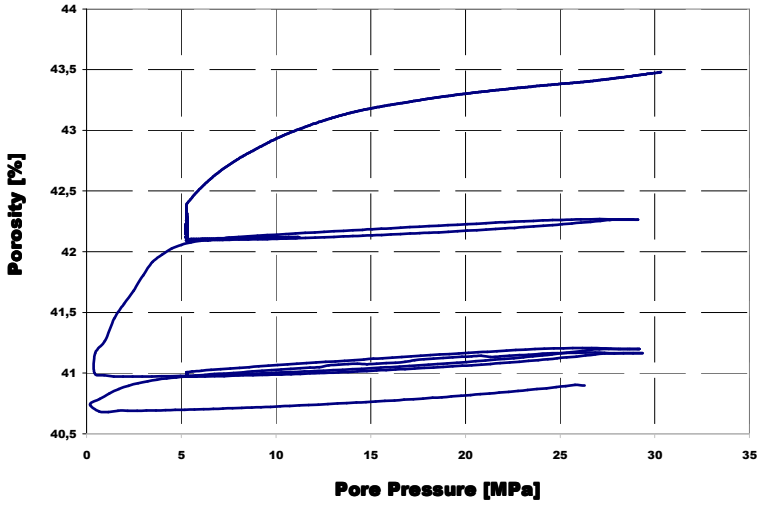

Fig.G5 Core E11

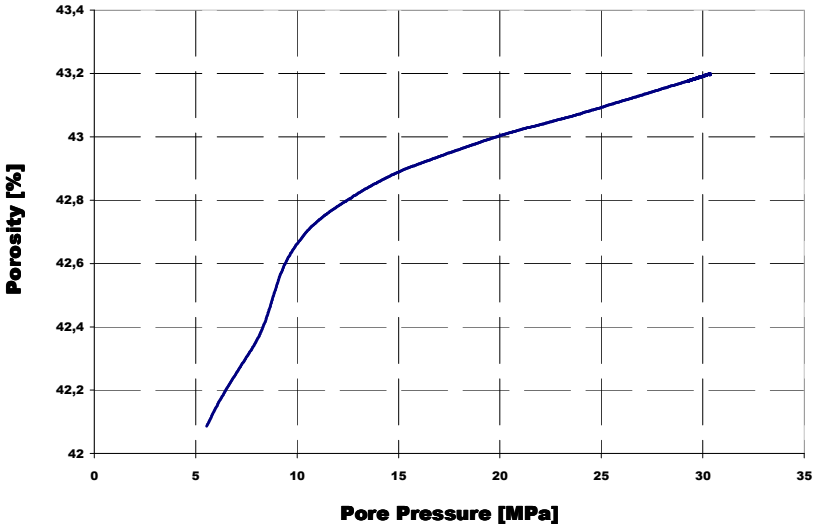

Fig.G6 Core E12

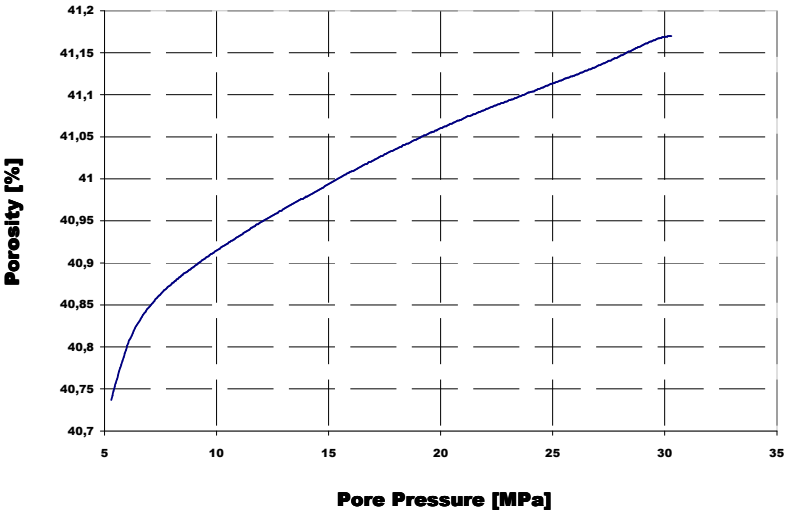

Fig.G7 Core E16

Slow Loading

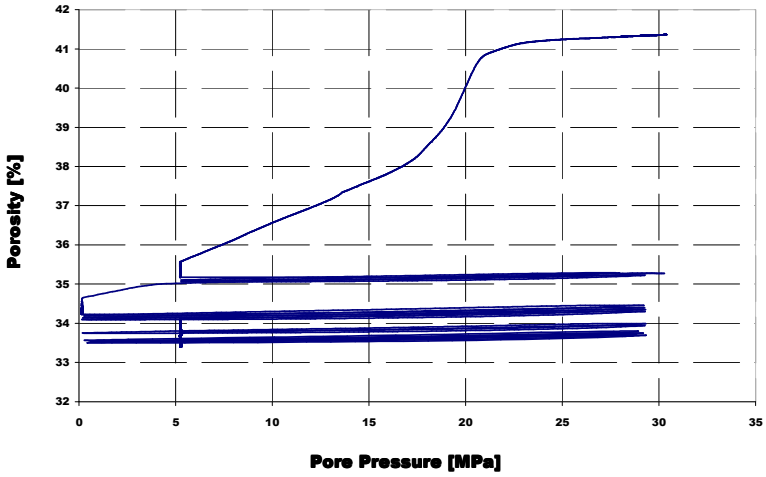

Fig.G8 Core E2

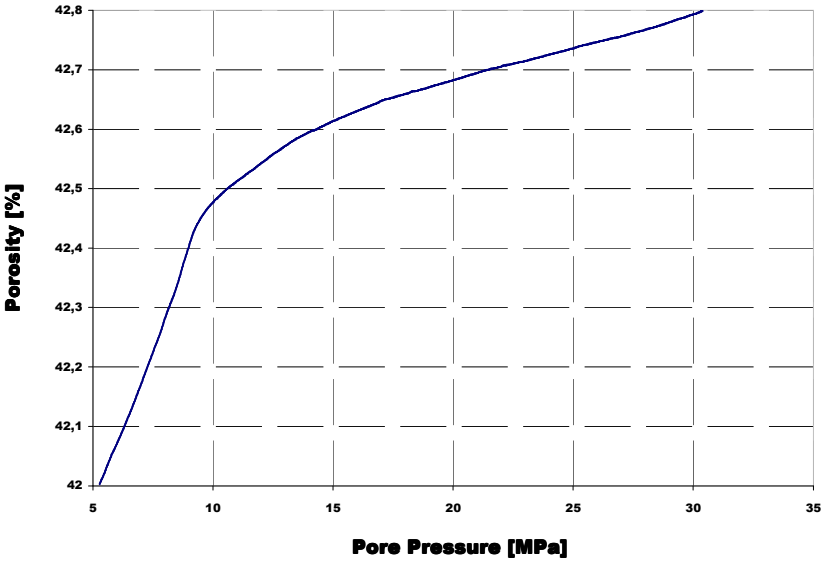

Fig.G9 Variation of porosity with fluid pressure during depletion of Core E14